# INFORMATION TO USERS

This manuscript has been reproduced from the microfilm master. UMI films the text directly from the original or copy submitted. Thus, some thesis and dissertation copies are in typewriter face, while others may be from any type of computer printer.

**The quality of this reproduction is dependent upon the quality of the copy submitted.** Broken or indistinct print, colored or poor quality illustrations and photographs, print bleedthrough, substandard margins, and improper alignment can adversely affect reproduction.

In the unlikely event that the author did not send UMI a complete manuscript and there are missing pages, these will be noted. Also, if unauthorized copyright material had to be removed, a note will indicate the deletion.

Oversize materials (e.g., maps, drawings, charts) are reproduced by sectioning the original, beginning at the upper left-hand corner and continuing from left to right in equal sections with small overlaps.

Photographs included in the original manuscript have been reproduced xerographically in this copy. Higher quality 6" x 9" black and white photographic prints are available for any photographs or illustrations appearing in this copy for an additional charge. Contact UMI directly to order.

ProQuest Information and Learning
300 North Zeeb Road, Ann Arbor, MI 48106-1346 USA
800-521-0600

UMI®

# NOTE TO USERS

**This reproduction is the best copy available.**

UMI

DISSERTATION

# IMAGE QUALITY, DOSE, AND QUALITY CONTROL IN SCREEN-FILM AND FULL-FIELD DIGITAL MAMMOGRAPHY

Submitted by

Eric A. Berns

Department of Radiological Health Sciences

In partial fulfillment of the requirements

For the Degree of Doctor of Philosophy

Colorado State University

Fort Collins, Colorado

Fall 2001

UMI Number: 3038621

UMI Microform 3038621



ProQuest Information and Learning Company
300 North Zeeb Road
P.O. Box 1346
Ann Arbor, MI 48106-1346

COLORADO STATE UNIVERSITY

October 30, 2001

WE HEREBY RECOMMEND THAT THE DISSERTATION PREPARED UNDER OUR SUPERVISION BY ERIC A. BERNS ENTITLED IMAGE QUALITY, DOSE, AND QUALITY CONTROL IN SCREEN-FILM AND FULL-FIELD DIGITAL MAMMOGRAPHY BE ACCEPTED AS FULFILLING IN PART REQUIREMENTS FOR THE DEGREE OF DOCTOR OF PHILOSOPHY.

Committee on Graduate Work

Adviser

Department Head

## ABSTRACT OF DISSERTATION

## IMAGE QUALITY, DOSE, AND QUALITY CONTROL IN SCREEN-FILM AND FULL-FIELD DIGITAL MAMMOGRAPHY

The purpose of this work is to measure and compare the current state of equipment performance of screen-film mammography (SFM) and full-field digital mammography (FFDM). There are three distinct projects including: 1) the evaluation of screen-film systems in Colorado, 2) optimizing technique factors for FFDM and comparing them to FSM under the constraint of matched patient dose, and 3) technical comparison of the first clinical FFDM units in the United States to FSM.

Medical physics testing was performed at participating sites in the Colorado Mammography Advocacy Project (CMAP) to assess breast dose, image quality, and trends in equipment performance over the last decade. Between December 1989 and October 1999, 216 on-site physics surveys were performed. In 1989-90, 21 units at 18 CMAP facilities were surveyed. In 1999, 38 units at 25 CMAP facilities were surveyed. Results indicate that mammography image quality has improved significantly over the last decade. Despite significant improvements, however, there are still wide ranges of image quality and dose in the practice of mammography.

Contrast-detail image analysis was performed to optimize technique factors for detection of low-contrast lesions using a silicon diode array FFDM system under the conditions of matched mean glandular dose for a given breast thickness across the full range of compressed breast thicknesses. The FFDM results are then compared to SFM at each breast thickness. The results indicate that low-contrast detection was optimized for FFDM by using a softer x-ray beam for thin breasts and a harder x-ray beam for thick breasts when MGD was kept constant. Under this constraint, optimized FFDM CD scores were superior to SFM CD scores for all but the thinnest breasts.

Results of acceptance testing 18 FFDM systems for clinical use and of conducting annual physics surveys of 38 SFM systems were compared in terms of exposure times, mean glandular breast doses, and image quality. Results indicate that the clinical use of digital mammography may generally improve image quality for equal or lower breast doses, while providing tighter control on exposures and image quality than screen-film mammography.

Eric Arthur Berns
Radiological Health Sciences Department
Colorado State University
Fort Collins, CO 80523
Fall 2001

## ACKNOWLEDGMENTS

I would like to thank Dr. Richard Park for his thoughtful and constant guidance through the course of my graduate study. His advice and support throughout my graduate program have made my time at CSU a pleasant and rewarding experience.

This work could not have been completed without the guidance, support, and contributions of Dr. R. Edward Hendrick. I would like to express my deepest gratitude and respect to Dr. Hendrick. I would like to thank Chuck Ahrens for openly sharing his clinical expertise.

I would like to thank Dr. Susan LaRue for encouraging me to stay the course through my entire graduate career and would also like to thank Dr. Susan Kraft and Dr. Bill Dernell for actively participating in my graduate program.

I would like to thank Dr. Gary Cutter and Dr. Mark Dignan for providing encouragement, sharing their experience in research, and their expertise in data analysis.

## TABLE OF CONTENTS


Chapter 1 - Introduction.....1

Chapter 2 - Mammography Equipment Performance: 10 Years of Clinical Performance Data From the Colorado Mammography Advocacy Project.....12

Chapter 3 - Optimization Of Technique Factors For A Silicon Diode Array Full-Field Digital Mammography System And Comparison To Screen-Film Mammography With Matched Mean Glandular Dose.....49

Chapter 4 - Performance Comparison of Full-Field Digital Mammography to Screen-Film Mammography In Clinical Practice.....83

References.....98

# CHAPTER 1

## INTRODUCTION

This introduction describes the technical history of modern mammography and mammography quality control.

In 1913, German surgeon Albert Salomon was the first to use x-ray imaging to view the gross anatomy of mastectomy specimens and was the first to demonstrate successful visualization of microcalcifications.[1] In 1949, Raoul Leborgne introduced imaging techniques for mammography that included the use of low kVps (20-30 kVp) and light compression during exposure.[2] These ideas resulted in improved image contrast, better patient positioning, and reduced patient motion. Leborgne eventually wrote a classic textbook on breast radiography and ductography.[3] In 1960, Robert L. Egan described a high milliamperage, low kilovoltage technique using a conventional x-ray unit and high-resolution industrial film that resulted in easily reproducible techniques and positioning.[4] This development led to a renewed interest in mammography.

Through the middle of the 1960s, mammography had been performed using general purpose x-ray units with no compression and using industrial grade film. These x-ray units typically had tungsten targets that produced insufficient subject contrast in soft-tissues. In 1965, Charles Gros in cooperation with CGR Company developed the first x-ray unit dedicated to mammography, called the

Senographe.[5] The Senographe had two significant improvements over general purpose x-ray units. The first was a molybdenum target material (0.7 millimeter nominal focal spot size) that provided higher subject contrast when operated in the 22-30 kVp range. The second was a built-in compression device that provided uniformly decreased breast thickness and breast immobilization. This compression device was important because it reduced scatter, reduced patient motion, and spread out overlapping tissues, resulting in improved image quality.

In 1967, the first production Senographe mammography unit became commercially available, but had significant limitations. For instance, the Senographe was designed to have a tube-cone assembly that had the compression device at the base of the cone. This resulted in varying source to image receptor distances from patient to patient, producing different degrees of magnification and image distortion. In the early 1970s, other dedicated mammography units were designed and made available by various manufacturers. Siemens introduced the Mammomat, Philips introduced the Mammodiagnost, and Picker introduced the Mammorex. All of these units employed a molybdenum target, had similar designs of separate compression devices, and had fixed source to image receptor distances.

In 1978, Philips introduced the Diagnost-U mammography unit that was the first to employ a reciprocating grid designed specifically for mammography. The reciprocating grid was made of parallel lead foil strips spaced evenly apart by cardboard interspacing material. The grid was designed to reduce scatter while decreasing the attenuation of the primary x-ray beam compared to

conventional lead foil grids that were interspaced by aluminum. The grid had a significant impact on improving image contrast. The trade-off for this improved contrast was an increase in patient dose compared to non-grid mammography images.

In the late 1970s and early 1980s, new improvements were being added to mammography units. Foot pedal controls to drive the compression paddle were added to allow the technician to use both hands for patient positioning. Automatic exposure control (AEC) systems, also called phototiming systems, were added to produce consistent images from one patient to the next. Microfocal spots were added to allow for magnification mammography. The smaller focal spot size, however, was determined to be useful as a diagnostic tool in geometric magnification mammography, not as a replacement for the larger focal spot used in contact (non-magnification mammography). This was because of the lower x-ray output and higher breast doses that occurred with magnification mammography.[6,7] Magnification mammography was determined to be particularly useful in diagnostic evaluation of small areas that appeared suspicious on a contact mammogram, in particular, areas containing microcalcifications or masses with apparent spiculations.

Mammography image receptors have evolved similarly over the past few decades with the introduction of screen-film systems and xeroradiography systems in the early 1970s. In 1971, Xerox Corporation introduced Xeroradiography as an alternative method for recording the x-ray image. It quickly became the predominant medium for mammography. Xeroradiography

used a selenium-coated aluminum plate inside a cassette. An electostatic charge was applied to the plate immediately before exposure to blank the plate. The plate was then exposed to x-rays forming a latent electrostatic image. The plate was developed in a reading device similar to a Xerox copy machine. A bias voltage was applied to the exposed plate and a charged powder was floated over the plate, collecting on the plate in a manner determined by the prior exposure. An image was formed by fusing the collected particles onto a sheet of paper, forming a reflective image. Initially, xeroradiography produced high-contrast, high-resolution images at doses lower than film mammography. With continuing improvements in screen-film mammography through the 1980s, including lower doses due to the use of faster screen-film cassettes and higher contrast due to improved film and film processing, Xeroxmammography slowly was replaced by screen-film mammography. Production of Xeromammography units was finally discontinued in 1989.

In 1972, DuPont was the first company to introduce a dedicated screen-film system for mammography. This was the result of the work of Price and Butler experimenting with high-definition intensifying screens in contact with industrial film. [8] Ostrum continued with experiments on film-screen combinations to further improve the system.[9] DuPont's system used a single emulsion Cronex LoDose I film in contact with the emulsion of a single Cronex LoDose calcium tungstate intensifying screen. This film-screen combination resulted in shorter exposure times, decreased motion unsharpness, and approximately a 10-20 times lower patient dose.[10]

In 1974, 3M Company introduced a new screen made of gadolinium oxysulfide coupled with orthochromatic film. This screen has higher efficiency in converting x-rays to green light, allowing the use of faster films that provided even lower patient doses without sacrificing image quality.[11,12]

In 1975, Eastman Kodak Company introduced the first systems housed in a special, rigid, low-absorption cassette. The Kodak Min-R film and Min-R screen system held the film firmly in contact with the screen and allowed for elimination of problems associated with the darkroom and vacuum-bag systems of other manufacturers. In 1980, Kodak introduced the Min-R screen – Ortho M film combination that reduced patient dose by half that of Min-R film. In 1996, Kodak introduced Min-R 2000 film and Min-R 2000 cassettes that again improved subject contrast.

By 1988, most facilities in the United States were using film-screen systems and 99% were using dedicated mammography equipment.[13] With an increasing number of film types and manufacturers to choose from, it has become important to have methods to evaluate and compare film performance. Film sensitometry is one method that it used today and has been around since 1890 when Hurter and Driffield developed a way to plot a curve of optical density (OD) versus exposure.[14] This curve is known as an H & D curve or characteristic curve.

Film processors have also evolved over time. Until 1942 all medical x-ray film was developed by hand and image quality depended strongly on the skill and accuracy of personnel following guidelines from the manufacturer. The first

automatic film processor was introduced in 1942 by the Pako Company with processing times of 40 minutes. In 1956, Eastman Kodak introduced the first automatic film processor with a roller transport mechanism that allowed for processing of film of different sizes.[15] This automatic film processor could process films in 6 minutes. In 1965, Kodak improved their processing time to 90 seconds, which is still the standard today.

As mammography equipment developed and improved over the decades, so did quality assurance standards and legislation. In the mid-80s, several studies suggested that large variations from site to site were still present in patient dose, image quality, and film processor performance.[13,16,17] During this time, the American Cancer Society (ACS) was beginning its National Breast Cancer Awareness Screening Programs and was concerned about advising women over the age of 40 to have screening mammograms without some level of confidence that mammography was being performed at a reasonably low dose and reasonably high image quality. It was at this point that the ACS approached the American College of Radiology about testing and designating mammography sites as meeting ACR-established quality standards. As a result, in October 1986, the ACR Mammography Accreditation Program was initiated. Sites began to voluntarily participate in August 1987. The initial program consisted of four parts: a survey questionnaire, the submission of clinical images for assessment of positioning, image quality, and artifacts, the submission of a phantom image for a standardized assessment of image quality, and a measurement of average glandular dose using thermoluminescent dosimeters. In June 1990, a film

processor performance component was added. The goals of the accreditation program were to establish quality standards for mammography, compare performance from site to site, and encourage high quality mammography.

In the fall of 1990, the ACR published quality control manuals for radiologists, technologists, and medical physicists recommending a full quality control program at every mammography site.[18] These manuals provided procedures for quality control tests, frequencies, and recommended action limits. ACR Mammography Quality Control Manuals were revised and updated in 1992, 1994, and 1999.[19,20,21] The mammography quality control manual provides a cookbook for quality control test procedures and provides forms for recordkeeping.

Federal legislation for mammography began with Congress passing the Mammography Quality Standards Act (MQSA) on October 27, 1992 to establish quality standards for mammography. Interim Rules were then published on December 21, 1993.[22] MQSA required by law that all sites providing mammography meet the requirements listed in the Interim Rules by October 1, 1994. The Interim Rules mandated minimum quality control requirements for all facilities and included standards for personnel, facility certification by an approved accrediting body, standards for equipment, standards for record keeping, use of an approved quality assurance program, standards for a medical outcome audit program, and standards for a consumer complaint mechanism. The Interim Rules mandated that all sites perform quality control testing as prescribed by the ACR Mammography QC Manuals (1992 or 1994 versions).[22]

In October 28, 1997, the Food and Drug Administration published the Final MQSA Regulations in the Federal Register; they became effective on April 28, 1999.[23]

In 1986 the National Council on Radiation Protection and Measurements (NCRP) published Report No. 85: Mammography – A User's Guide[24]. This report was intended to be a practical guide to physicians and technologists who perform and interpret mammography. Anatomy, xeromammography equipment, screen-film mammography equipment, dose evaluation, image quality, quality assurance, other modalities used for breast disease diagnosis, and benefits and risks of mammography were presented for clinical application.

In October of 1994, the Agency for Health Care Policy and Research published Clinical Practice Guideline #13: Quality Determinants of Mammography.[25] An expert panel was put together to review and evaluate relevant literature on all aspects of mammography for scientific validity and develop guideline statements on various topics based on the peer-reviewed literature and the panel's expert opinion. The overall purpose of this guideline was to improve the quality and delivery of mammography and provide clinicians a useful resource for use in clinical practice.

In late 1996 and early 1997, the first prototype full-field digital mammography units were installed in the U.S. for clinical evaluation for FDA approval. The first study to comparing screen-film and full-field digital mammography in a clinical study group was published in March 2001.[26] The

study found that there was no difference in cancer detection rate between the two modalities, but found that digital mammography had fewer recalls.[26]

On January 28, 2000 the GE Senographe 2000D was the first full-field digital mammography unit to be approved by the FDA for commercial use. Its initial approval was for image interpretation from printed films (hardcopy). The GE digital detector design uses an amorphous silicon diode array bonded to a cesium iodide (CsI) crystal providing a 100 micron pixel size. This is one of many digital detector designs. On November 13, 2000, the GE Senographe 2000D received approval by the FDA for softcopy interpretation of digital mammograms; that is, digital images could be read and interpreted from the GE review workstation instead of film.

On September 25, 2001 the Fischer Senoscan full-field digital mammography unit received approval by the FDA for commercial use. The Fischer digital detector uses a slot-scanning design where a charge-coupled device (CCD) detector and fan-beam of x-rays scan across the breast to capture the digital image. The slot scanning system currently has a 54-micron pixel size.

With all of these technical improvements in mammography there are still wide variations in image quality, patient doses, film, and film processor performance from one facility to another. Understanding this extent of this variability, along with the comparitive variability of screen-film and digital mammography, may shed light on the solutions needed to keep improving mammography in the future.

For a more detailed account of the history of mammography there are four papers by Gold[27], Bassett[28], Houn[29], and Hendrick[30] that are particularly helpful.

The work in this dissertation is directed toward understanding and measuring the current state of equipment performance in clinical mammography. It is divided into three parts.

The first part evaluates the technical performance of clinical screen-film mammography sites across Colorado over a ten-year period of time. Between 1989 and 1999 over 100 film-screen mammography units and 80 facilities have participated in the Colorado Mammography Advocacy Project (CMAP), a program designed to establish a statewide mammography tracking and reporting system. Each year, each site had a medical physics equipment evaluation to measure image quality, patient dose, and processor performance. Data from these evaluations have been analyzed to determine the range of image quality and dose and to track their variations over time.

The second part of this thesis evaluated and optimized techniques for the recently introduced technology of full-field digital mammography, comparing optimized digital techniques to film-screen mammography under the constraint of matched patient dose. Contrast-detail phantoms at different breast thicknesses were acquired on a film-screen mammography unit and scored. The resulting breast dose was used to calculate matching techniques for the entire range of target-filter combinations, kVps, and mAs settings on a GE Senographe 2000D digital mammography system. Using these techniques, contrast-detail images were acquired and scored on a full-field digital mammography unit. Results of

the contrast-detail imaging were then compared for screen-film and full-field digital mammography.

The third part of this thesis compared the performance of 18 of the first clinically installed full-field digital mammography units in the United States to the performance of 38 clinical film-screen mammography units in Colorado. Medical physics testing was performed on both imaging modalities and was compared in terms of exposure times, mean glandular breast doses, and image quality. Data from these evaluations were analyzed to look for differences and variability between film-screen and full-field digital mammography.

The results of this work provide a snapshot of the technical performance of both screen-film and full-field digital mammography in the United States and provide insight and guidance for improving in the early detection of breast cancer.

# CHAPTER 2

# MAMMOGRAPHY EQUIPMENT PERFORMANCE: 10 YEARS OF CLINICAL PERFORMANCE DATA FROM THE COLORADO MAMMOGRAPHY ADVOCACY PROJECT

## Chapter 2. INTRODUCTION

The Colorado Mammography Advocacy Project (CMAP) was initiated in 1989 to establish a statewide mammography tracking and reminder system. One component of the system was an independent physics evaluation of site performance at participating CMAP facilities, with an emphasis on clinical performance in terms of image quality and breast dose.

This paper summarizes a decade of medical physics testing of CMAP mammography facilities. To assess trends over the last decade, the 1999 medical physics survey results consisting of 38 units at 25 CMAP facilities are compared to the 1989-1995 survey results consisting of 117 units at 73 facilities.

The time period spanned by these physics evaluation data has been an important one in terms of the implementation of quality standards for mammography. In 1989-90 when the first round of CMAP data were collected, the American College of Radiology (ACR) mammography accreditation program had been in place for only two years. There were no national quality control standards and no federal requirements for the performance of screening or diagnostic mammography.

At the time of the first round of CMAP surveys in late 1989 and early 1990, less than 10% of the participating CMAP facilities were ACR-accredited and less than half of CMAP facilities were performing processor sensitometry or phantom image quality tests on a regular basis.[31]

In late 1990, the ACR Standards for the Performance of Screening Mammography and the ACR Mammography Quality Control Manuals were first published.[32,33] The Mammography Quality Standards Act was passed by Congress in late 1992 and went into effect under Interim Final Rules on October 1, 1994.[20,34] Interim Final Rules required each mammography site to perform quality control according to the ACR Mammography Quality Control Manual. On April 28, 1999, MQSA Final Rules went into effect, again requiring QC testing according to more detailed specifications within the rules themselves.[23]

The data collected in these medical physics surveys represent a cross section of predominately private practice facilities serving the Denver metropolitan area during the period of implementation of national quality standards for mammography. The collected data, acquired at CMAP sites using the same test equipment and test procedures over the entire period, serve as an independent measure of the effect of quality standards on a representative sample of mammography facilities.

## Chapter 2. MATERIALS AND METHODS

Medical physics technical surveys were performed at each CMAP site annually during 1989 to 1995 and again in 1999. The surveys consisted of a

mammography equipment and film processor evaluation. At each site, technologists were interviewed to ascertain the exact technique factors used for clinical imaging. These techniques were used to acquire the contrast detail and ACR phantom images used for the mammographic unit evaluation. The unit evaluation consisted of recording the exposure time, measuring patient dose and optical density (OD), and scoring the contrast detail and ACR phantoms. Film processor performance evaluation consisted of measuring film-processing contrast using the gamma plot method[35] and the $d_{max}$ under normal clinical operating conditions. All image acquisitions were done with the site's mammography unit, film processor, and clinical screen-film combination. At sites having multiple mammography units, each unit was evaluated using the common film processor at that site.

Contrast-detail (CD) images were obtained using uniform breast-equivalent (50% fibroglandular-50% fatty) materials of 2, 4, 6, and 8 cm compressed breast thicknesses imaged at each site's clinical techniques (Figure 2.1). A D-shaped uniform phantom was used, one section of which contained a 9 x 9 contrast-detail pattern for assessment of simulated low-contrast lesions (Figure 2.2).[36] Each row of the CD pattern contained 9 circular objects at a fixed level of contrast with object diameters ranging from 0.25 mm to 4.0 mm. Each of the nine different rows had a different subject contrast, ranging from 0.3% to 4.0%.

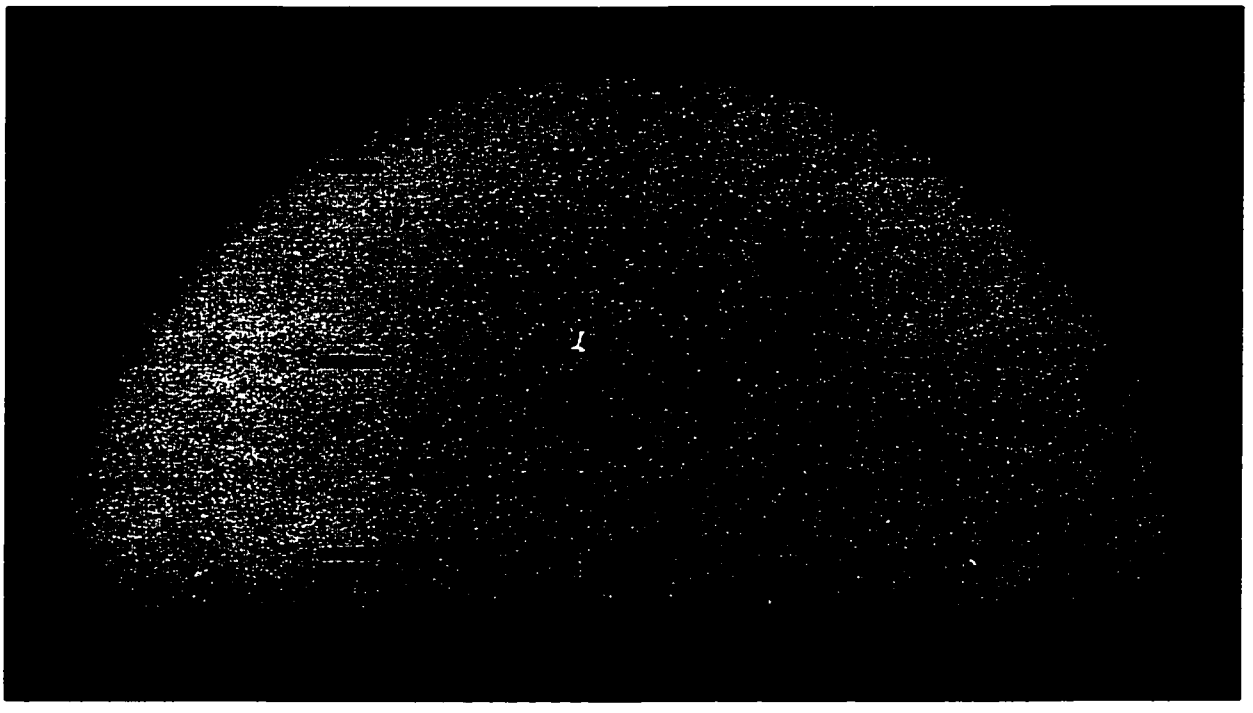

**Figure 2.1.** X-ray image of contrast-detail phantom.

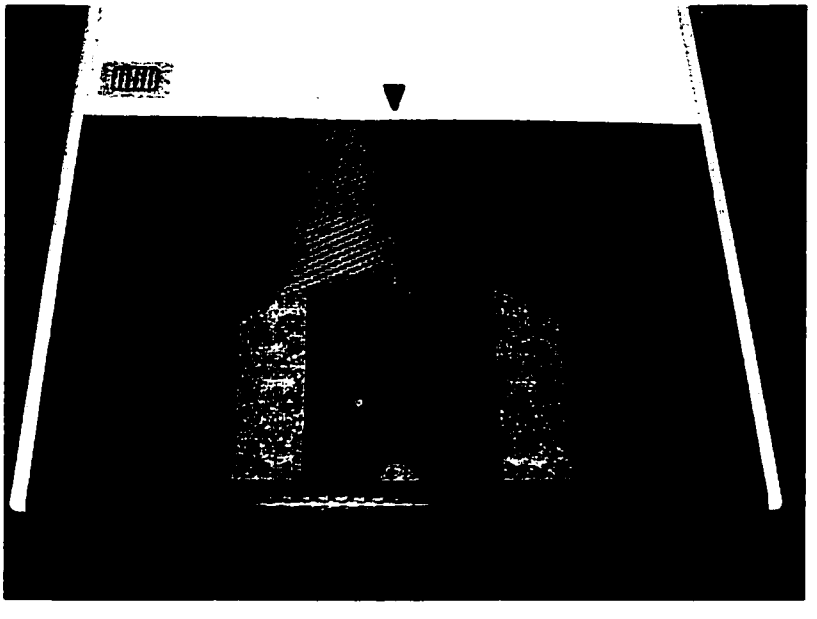

**Figure 2.2.** Setup of D-shaped contrast-detail phantom.

CD images were scored by a medical physicist under standardized viewing conditions. These included complete masking of each CD image and low ambient room lighting. Scoring of the CD phantom, starting with the highest contrast row of object, reading from the largest to smallest detectable object diameter in that row. An object was judged as "detected" if it occurred in the correct location, appeared generally round, and was more visible than artifactual "objects" occurring the in the background of the CD phantom, excluding the locations of the 91 test objects. This comparison of detected objects against artifacts in the background of the phantom, similar to the method developed for scoring the ACR mammography accreditation phantom, was used to guard against overscoring due to prior knowledge of the location of the test objects in the phantom. Once an object was deemed too faint to detect, was not generally round, or was less conspicuous than artifactual objects in the background of the phantom, counting was stopped and the number of consecutively visible objects in that row was summed. The reviewer then moved on to the next row of objects at slightly lower contrast, repeating the procedure. The CD score of each image was determined by computationally measuring the area of detected objects in CD space (Figure 2.3). The more low-contrast objects detected, the higher the CD score. If no objects were detected, the minimum score of zero would result; if all 81 objects were detected, the maximum score of 17.34 would result.

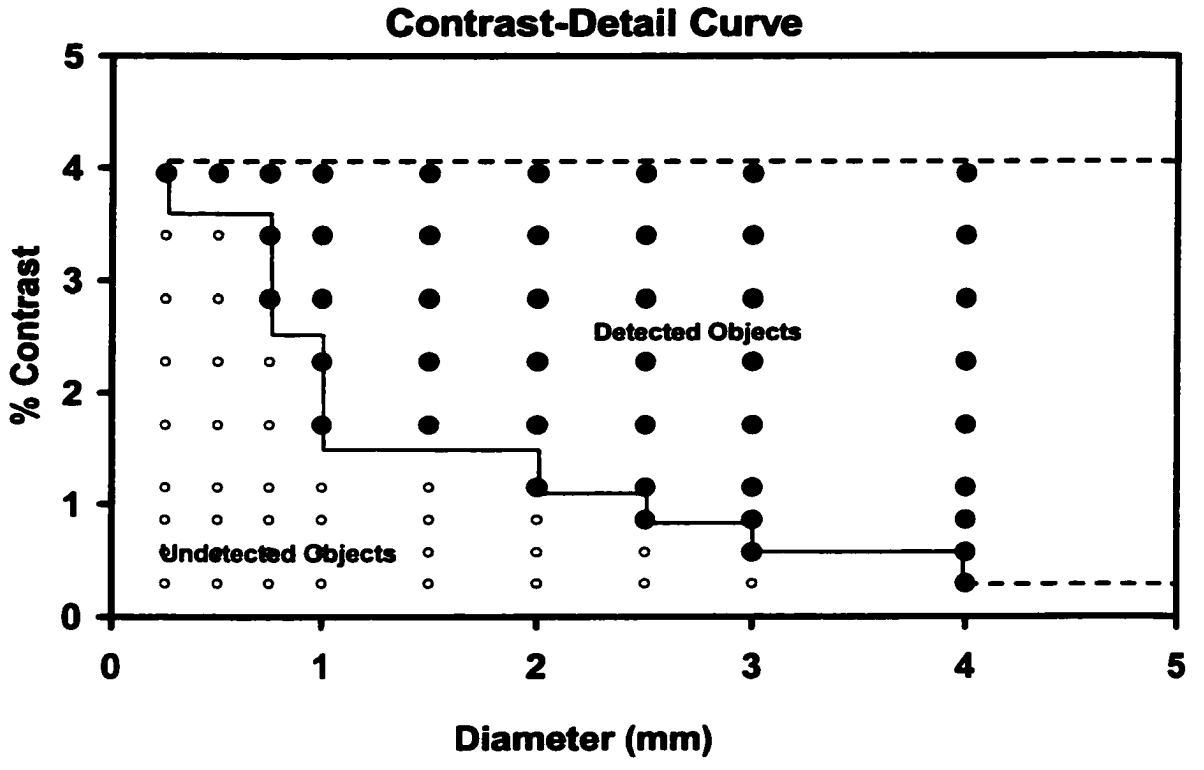


**Figure 2.3.** Schematic of contrast-detail phantom area calculation.

Optical density measurements were made for each CD phantom image at each thickness using a calibrated densitometer. The OD measurement was taken at a location approximately 2 cm from the chest wall, centered left to right.

Exposure time was calculated for each CD image by recording the mAs values directly from the unit console and dividing it by the unit's mA rating given by the manufacturer.

Average glandular dose (AGD) was measured for each CD phantom image at each individual thickness. To measure dose, the half-value layer (HVL) in millimeters of aluminum and the entrance exposure in milliRad (mR) at 50 mAs was measured. Measurements were made by placing the dosimeter 4.5 cm

above the breast support plate with the center of the chamber approximately 6 cm from the chest wall edge and centered left to right (Figures 2.4 & 2.5).

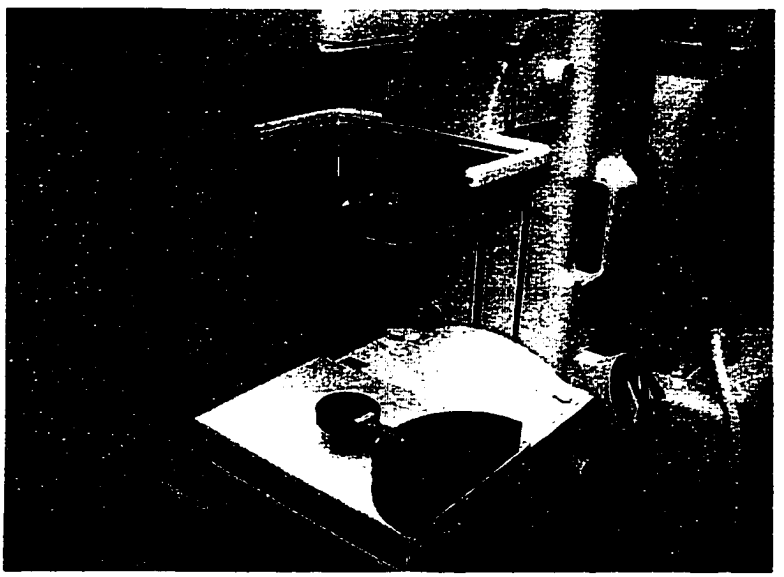

**Figure 2.4.** Half-value layer measurement setup.

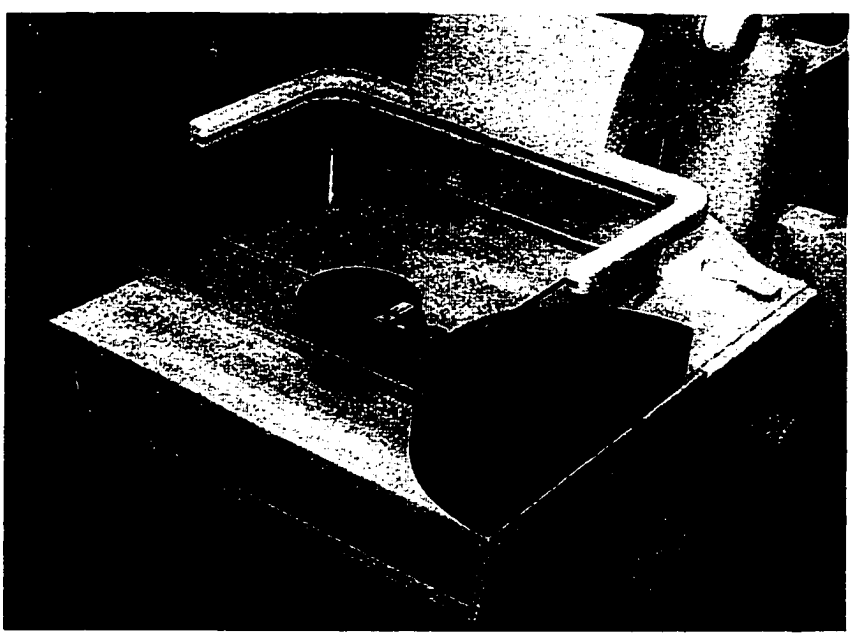

**Figure 2.5.** Entrance exposure measurement setup.

For the HVL setup, the paddle was raised as high as possible. For the entrance exposure setup, the paddle was touching the chamber, in accordance with the ACR Mammography Quality Control Manual protocol for measuring AGD.[21] HVL and entrance exposure data were used to calculate the average glandular dose using the method published by Wu, et al.[37,38]

ACR phantom images were acquired using each site's clinical technique for a 4.2 cm thick breast. All phantom images were processed in each site's clinical film processor. The ACR phantom contained three different test objects (fibers, speck groups, and masses) (Figure 2.6); scoring was performed in accordance with the 1999 version of the ACR Mammography Quality Control Manual.[21]

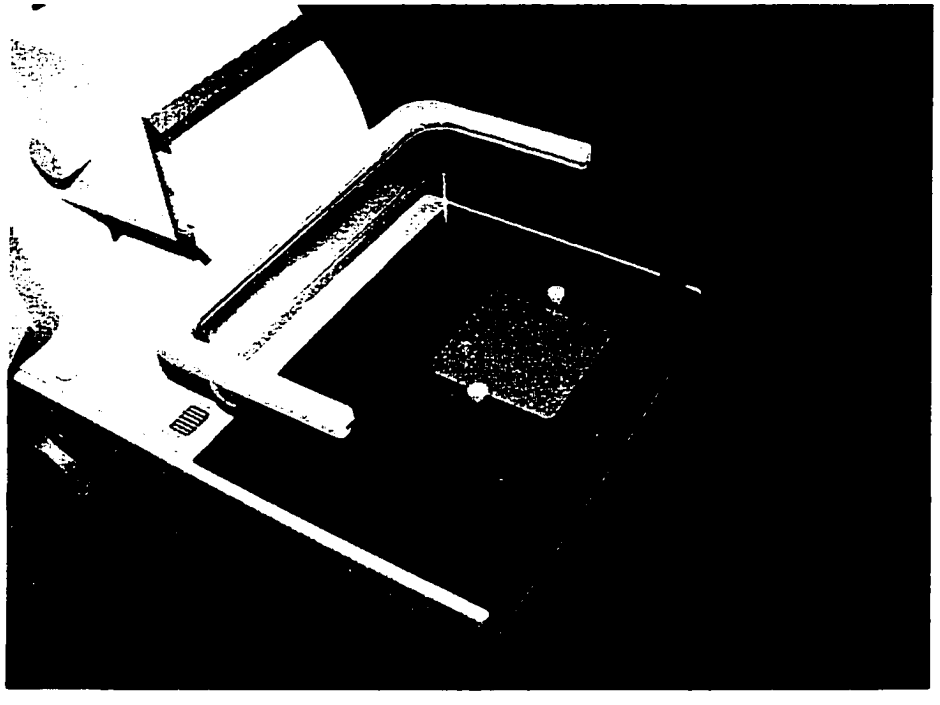

**Figure 2.6.** ACR Phantom setup.

Background OD measurements were made in the middle of the ACR phantom. Contrast OD measurements were made by subtracting the OD measurement made just outside a 4 mm acrylic disc from the OD measurement made directly in the middle of the 4 mm acrylic disc.

Exposure time was calculated for each ACR phantom image by recording the mAs values directly from the unit console and dividing it by the units mA rating given by the manufacturer.

Film processors for each site were evaluated by film sensitometry. The same 21-step sensitometer was used to expose each site's clinical film used for mammography. The sensitometry film was processed on each site's clinical film processor. All 21 step values were used to measure film contrast as the area under the gamma plot curve. Base plus fog and $D_{max}$ values were measured directly from each sensitometric strip using the same densitometer.

Comparison of results for exposure times, mean glandular doses, and CD scores between the 1989-1995 time period and 1999 were analyzed for statistical significance using the least squares random effects Laird-Ware Model (SAS Institute, Seattle, WA).

## Chapter 2. RESULTS

Results in terms of exposure times, average glandular doses, optical densities, and contrast detail scores for the 38 units tested at 25 sites in 1999 are shown in tables 2.1-2.4 and figures 2.7-2.10.

Table 2.1 shows the mean exposure time for the five different breast thicknesses. Mean exposure times were 0.16 s for 2 cm thick, 0.72 s for 4 cm thick, 1.05 s for the ACR phantom, 1.61 s for 6 cm thick, and 2.91 s for 8 cm thick breasts. The range of exposure times can be seen in Figure 2.7. For 2 cm thick breasts, exposure times ranged from 0.08 to 0.41 seconds, 0.25 to 1.16 s for 4 cm breasts, 0.44 to 1.77 s for the ACR phantom, 0.29 to 3.0 s for 6 cm breasts, and 1.19 to 5.0 s for 8 cm breasts.

**Table 2.1.** Exposure times for 5 phantom thicknesses.

| **Exposure Times (seconds) For 38 CMAP Mammography Sites in 1999** | | |
|---|---|---|
| Thickness | Mean Exposure Time | Standard Deviation |
| 2 cm | 0.16 | 0.06 |
| 4 cm | 0.72 | 0.25 |
| ACR Phantom | 1.05 | 0.33 |
| 6 cm | 1.61 | 0.58 |
| 8 cm | 2.91 | 1.10 |

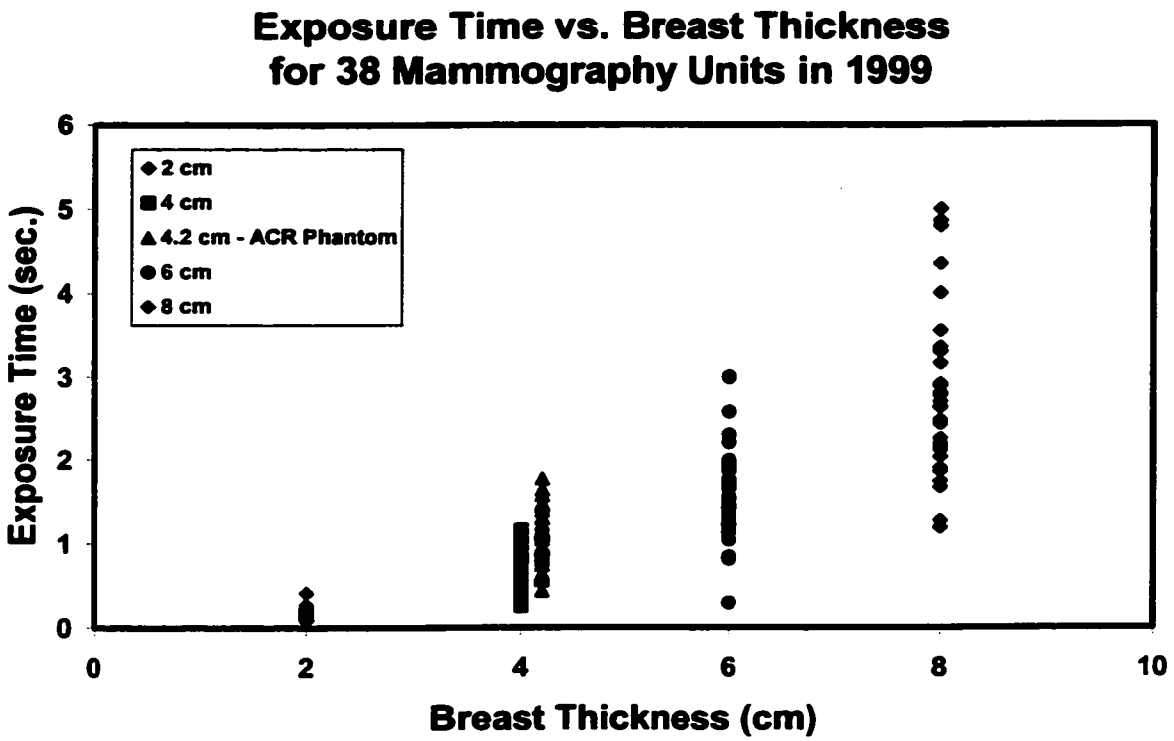


**Figure 2.7.** Exposure times versus breast thickness for 5 different phantom thicknesses.

Table 2.2 shows the average glandular dose results for the five different breast thicknesses. Mean average glandular doses were 0.43 milliGray (mGy) for 2 cm thick, 1.19 mGy for 4 cm thick, 1.68 mGy for the ACR phantom, 2.50 mGy for 6 cm thick, and 4.01 mGy for 8 cm thick breasts. The range of average glandular doses can be seen in Figure 2.8. Average glandular doses ranged from 0.22 to 0.84 mGy for 2 cm thick breasts, from 0.40 to 1.93 mGy for 4 cm breasts, from 1.01 to 2.61 mGy for the ACR phantom, from 0.57 to 4.16 mGy for 6 cm thick breasts, and from 0.59 to 6.21 mGy for 8 cm thick breasts.

**Table 2.2.** Average Glandular Doses for 5 phantom thicknesses.

| Average Glandular Dose (mGy) For 38 CMAP Mammography Sites in 1999 | | |
|---|---|---|
| Thickness | Mean Average Glandular Dose | Standard Deviation |
| 2 cm | 0.43 | 0.11 |
| 4 cm | 1.19 | 0.30 |
| ACR Phantom | 1.68 | 0.41 |
| 6 cm | 2.50 | 0.69 |
| 8 cm | 4.01 | 1.29 |

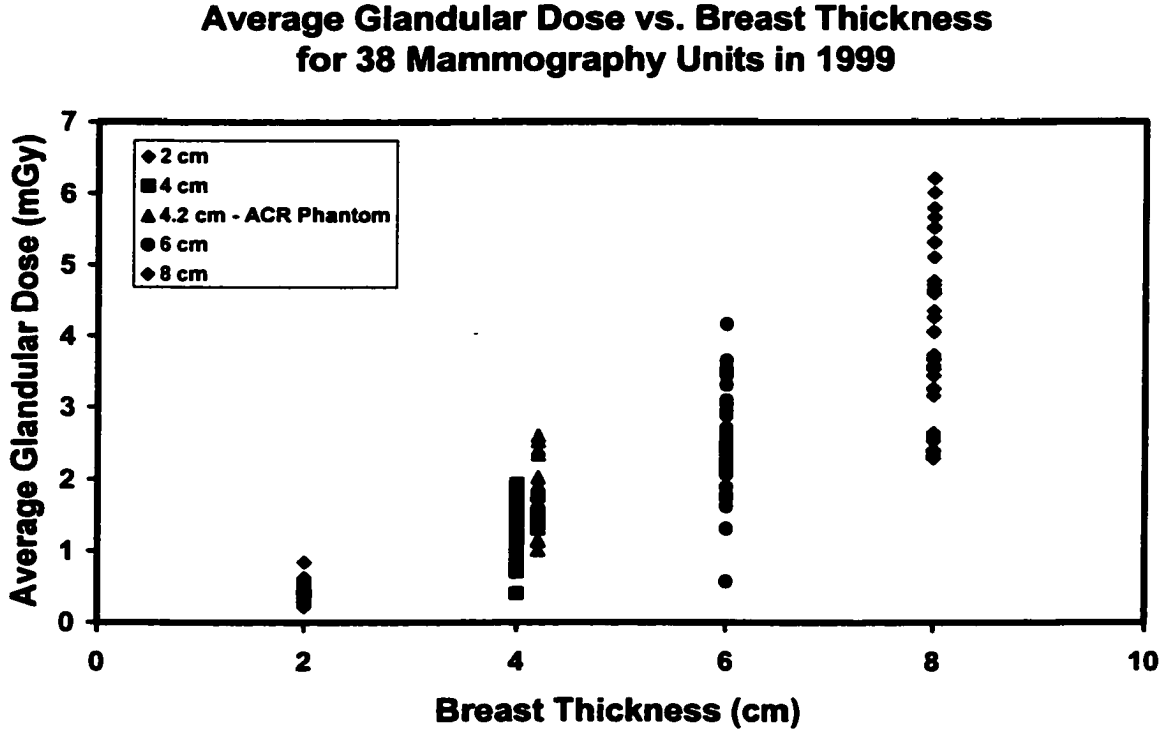


**Figure 2.8.** Average Glandular Dose versus breast thickness.

Table 2.3 shows the mean optical densities measured for the five different breast thicknesses. Mean optical densities were 1.53 for 2 cm thick breasts, 1.63 for 4 cm thick breasts, 1.56 for the ACR phantom, 1.64 for 6 cm thick breasts, and 1.55 for 8 cm thick breasts. The range of optical densities can be seen in Figure 2.9. Optical densities ranged from 0.74 to 1.96 for 2 cm thick breasts, 0.70 to 1.94 for 4 cm thick breasts, 1.14 to 1.90 for the ACR phantom, 0.61 to 2.37 for 6 cm thick breasts, and 0.59 to 2.32 for 8 cm thick breasts.

**Table 2.3.** Optical density values for 5 phantom thicknesses.

| **Optical Density** **For 38 CMAP Mammography Sites in 1999** | | |
|---|---|---|
| Thickness | Mean Optical Density | Standard Deviation |
| 2 cm | 1.53 | 0.26 |
| 4 cm | 1.63 | 0.24 |
| ACR Phantom | 1.56 | 0.16 |
| 6 cm | 1.64 | 0.31 |
| 8 cm | 1.55 | 0.44 |

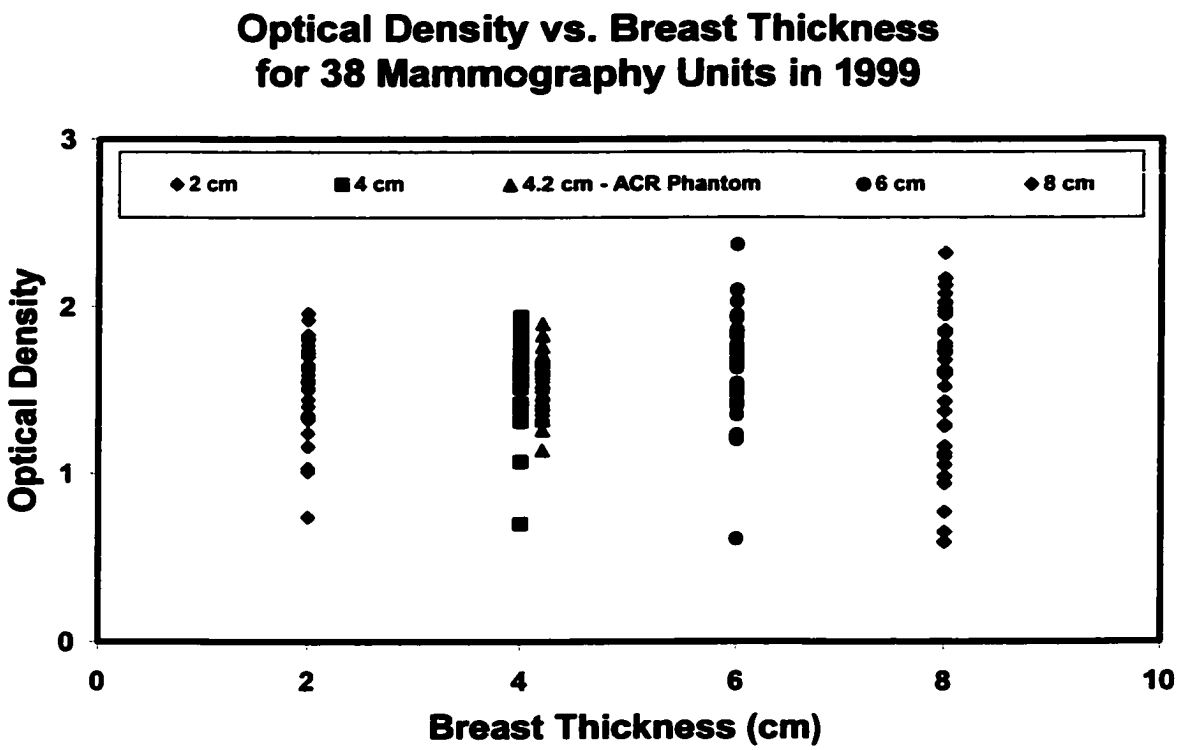


**Figure 2.9.** Optical density versus breast thickness for 5 different breast thicknesses.

Table 2.4 shows the mean contrast-detail scores for the four different breast thicknesses. Mean contrast-detail scores were 13.69 for 2 cm thick breasts, 13.35 for 4 cm thick breasts, 12.26 for 6 cm thick breasts, and 10.61 for 8 cm thick breasts. The range of contrast-detail scores can be seen in Figure 2.10. Contrast-detail scores ranged from 11.8 to 15.4 for 2 cm thick breasts, 11.1 to 14.5 for 4 cm thick breasts, 9.9 to 13.7 for 6 cm thick breasts, and 8.2 to 12.9 for 8 cm thick breasts.

**Table 2.4.** Contrast-detail scores for 4 different breast thicknesses.

| Contrast-Detail Scores For 38 CMAP Mammography Sites in 1999 | | |
|---|---|---|
| Thickness | Mean Contrast-Detail Score | Standard Deviation |
| 2 cm | 13.69 | 0.74 |
| 4 cm | 13.35 | 0.72 |
| 6 cm | 12.26 | 0.87 |
| 8 cm | 10.61 | 1.18 |

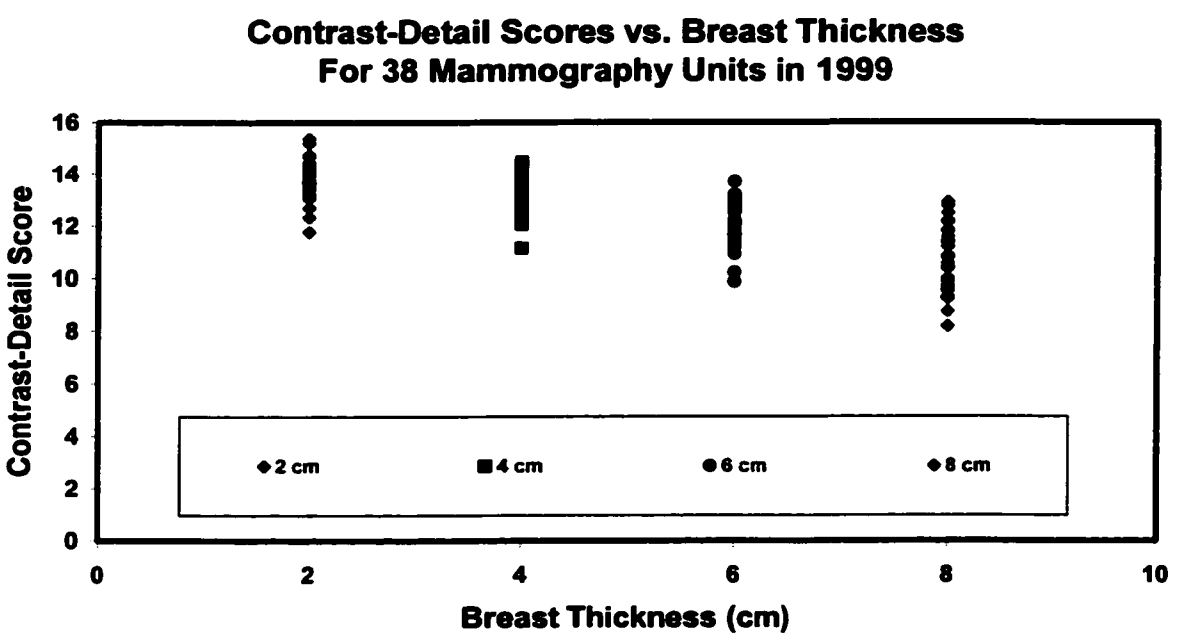


**Figure 2.10.** Contrast-detail scores for 4 different breast thicknesses.

Results comparing the 73 CMAP facilities from 1989-1995 to the 25 CMAP facilities in 1999 can be seen in Tables 2.5-2.10 and Figures 2.11-2.28.

Table 2.5 shows the results for film processor evaluation of maximum optical density and the area under the gamma plot curve, $A_g$.

**Table 2.5.** $D_{max}$ and $A_g$ scores from 1989-1995 and 1999.

| Film Processor Performance: $D_{max}$ (OD) and Contrast ($A_g$) | | | | | |
|---|---|---|---|---|---|
| | 1989-1995 | | 1999 | | p-value |
| | Least Square Mean | Standard Error | Least Square Mean | Standard Error | |
| $D_{max}$ | 3.92 | 0.03 | 4.36 | 0.07 | < 0.0001 |
| $A_g$ | 9.35 | 0.18 | 12.43 | 0.40 | < 0.0001 |

The average $D_{max}$ in 1999 (4.36) was significantly higher than the average $D_{max}$ from 1989-1995 (3.92) ($p<0.0001$). The average contrast ($A_g$) in 1999 (12.43) was also significantly higher than the average $A_g$ from 1989-1995 (9.35) ($p<0.0001$). Figures 2.11-2.13 illustrate both the variation and improvement in $D_{max}$ and $A_g$ values over the last ten years.

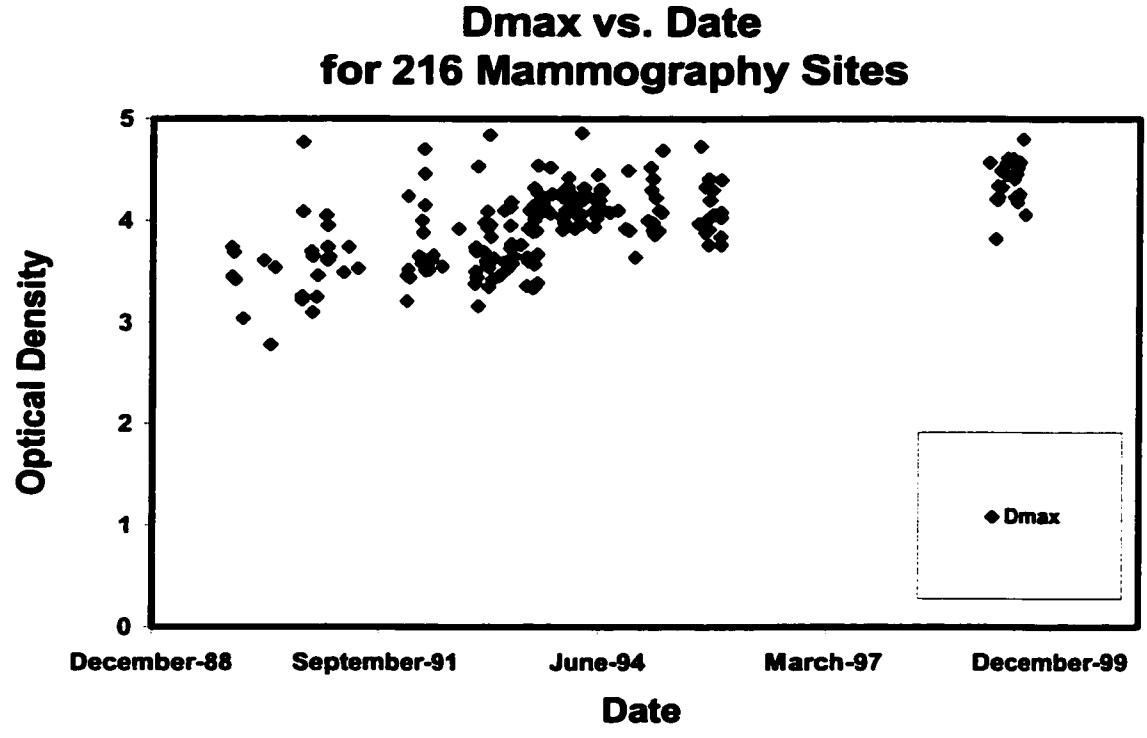


**Figure 2.11.** $D_{max}$ versus date for 216 mammography sites.

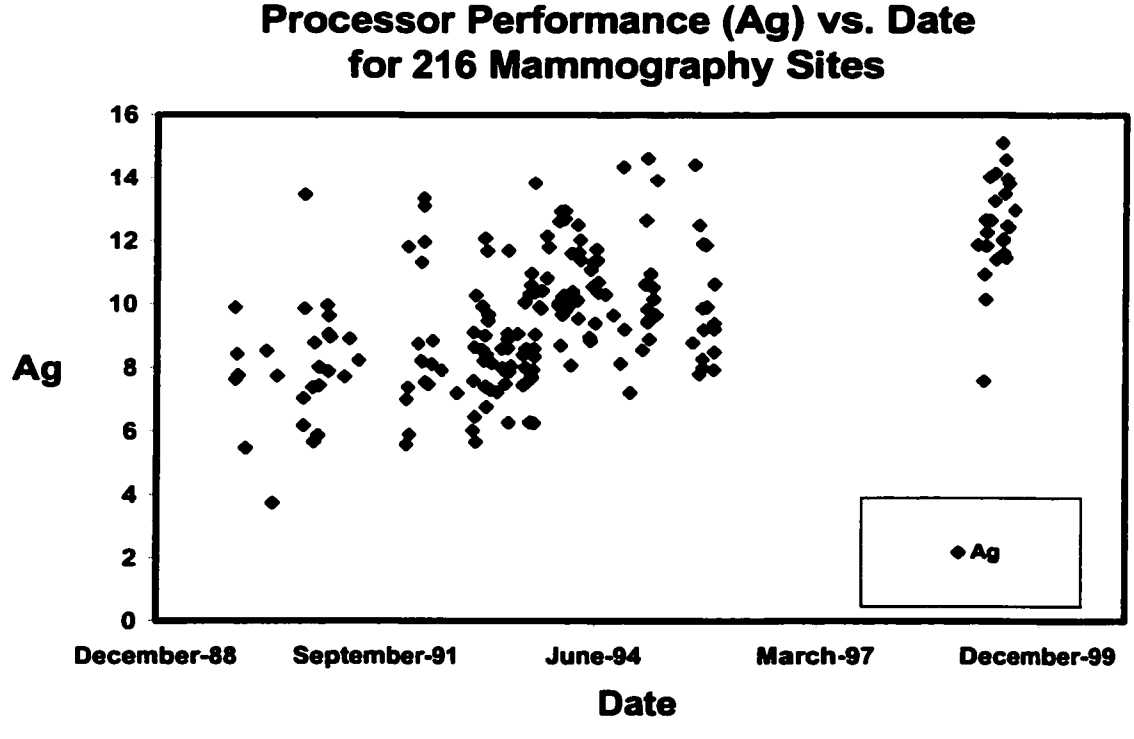


**Figure 2.12.** Ag values versus date for 216 mammography sites.

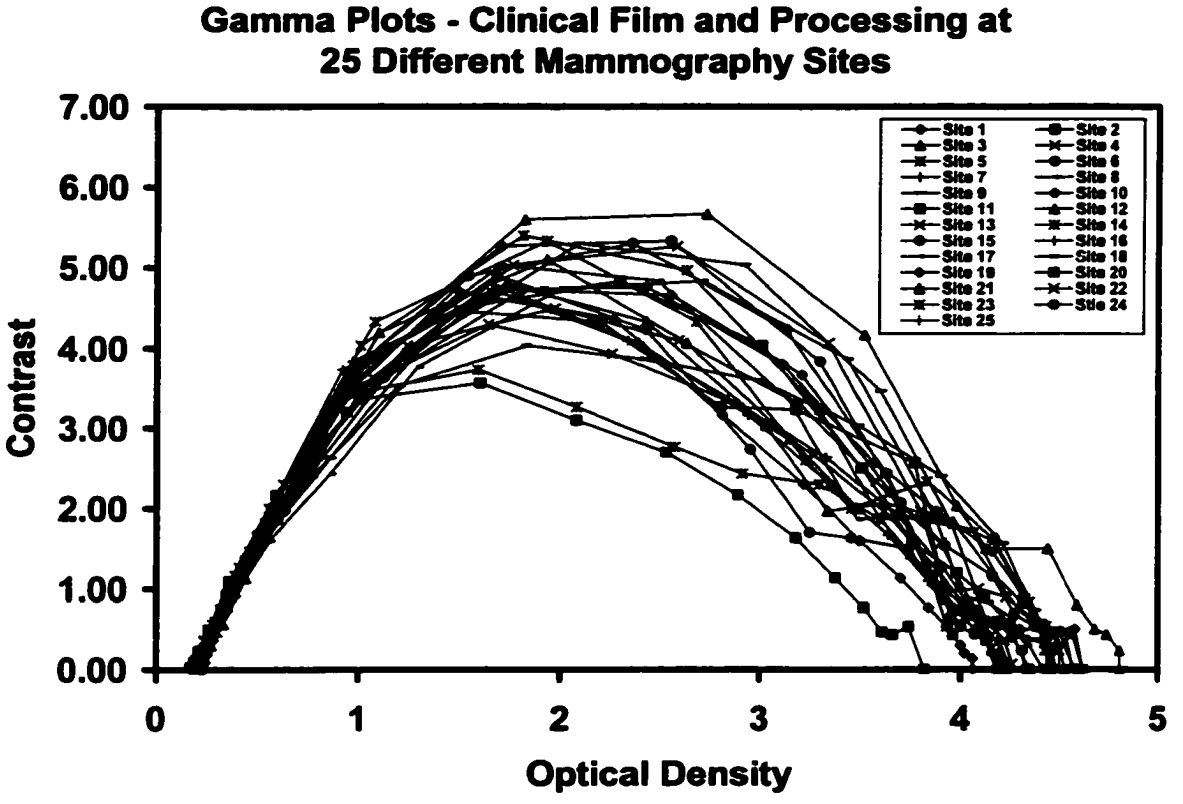


**Figure 2.13.** Gamma plots for 25 film processors at 25 mammography sites.

Table 2.6 compares ACR phantom scores from 1989-95 to those from 1999. Fiber, speck group, and mass scores all significantly improved over the ten-year period ($p<0.0001$). This can be seen in figures 2.14-2.16.

**Table 2.6.** ACR Phantom scores from 1989-1995 and 1999.

| ACR Phantom Scores | | | | | |
|---|---|---|---|---|---|
| | 1989-1995 | | 1999 | | p-value |
| | Least Square Mean | Standard Error | Least Square Mean | Standard Error | |
| Fibers | 4.37 | 0.05 | 4.82 | 0.10 | < 0.0001 |
| Speck Group | 3.31 | 0.03 | 4.03 | 0.07 | < 0.0001 |
| Masses | 3.24 | 0.04 | 3.65 | 0.08 | < 0.0001 |

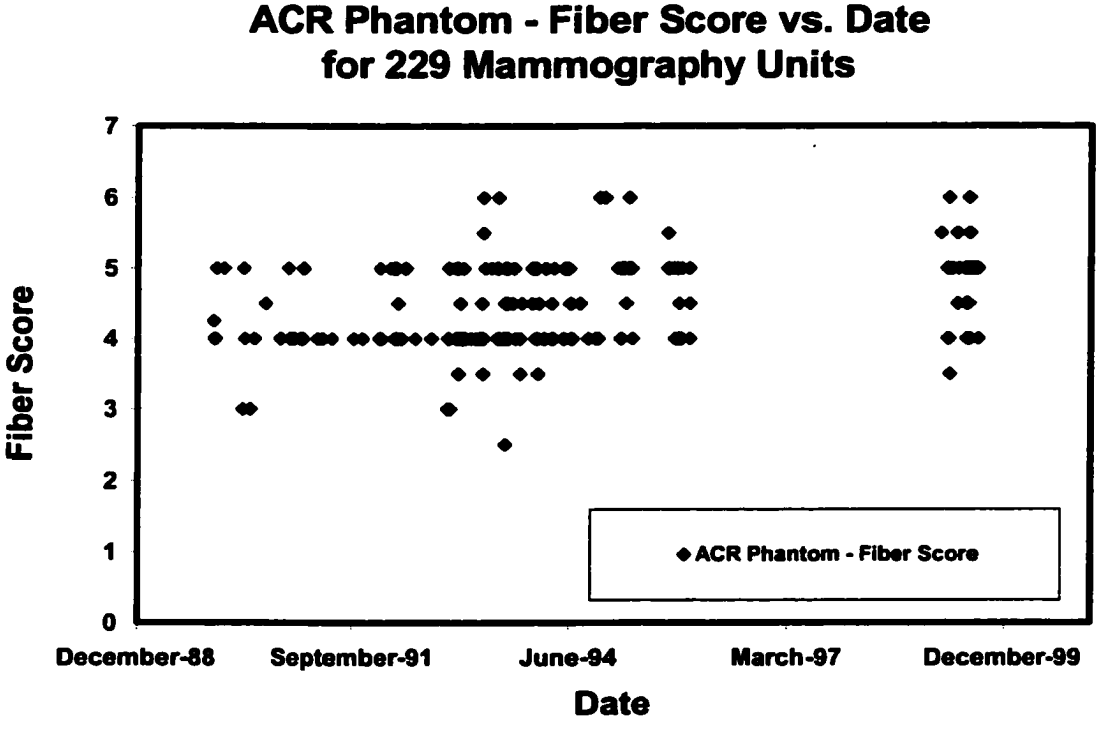


**Figure 2.14.** ACR Phantom fiber scores for 229 mammography units.

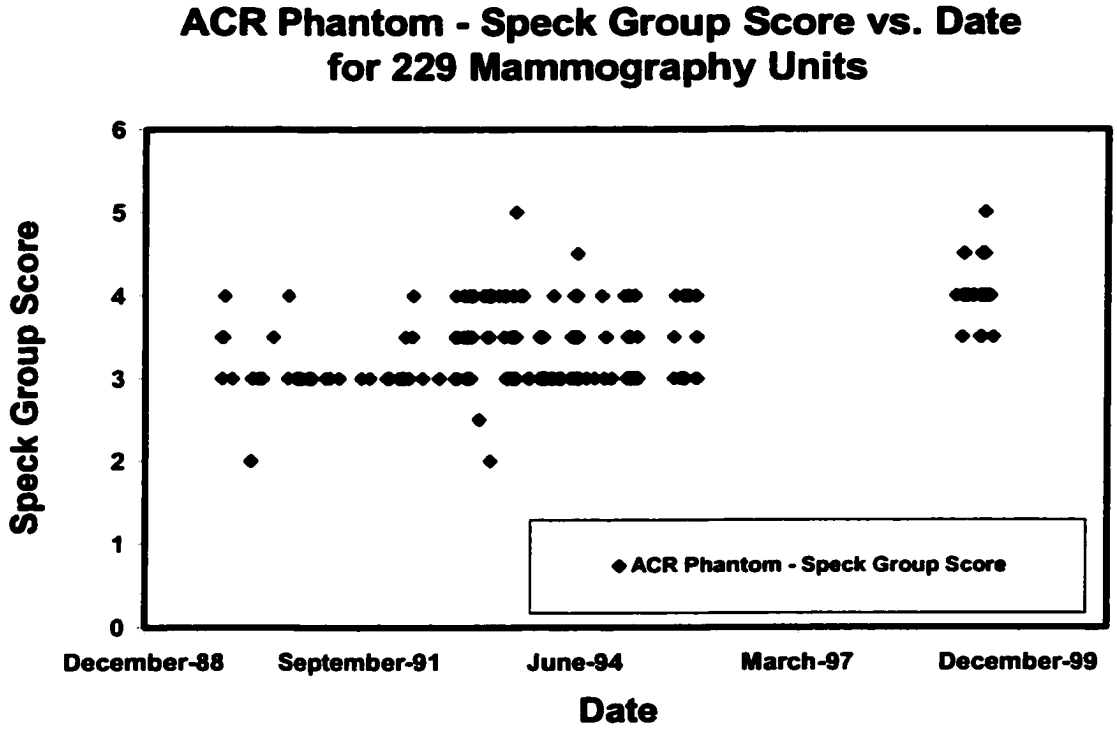


**Figure 2.15.** ACR Phantom speck group scores for 229 mammography units.

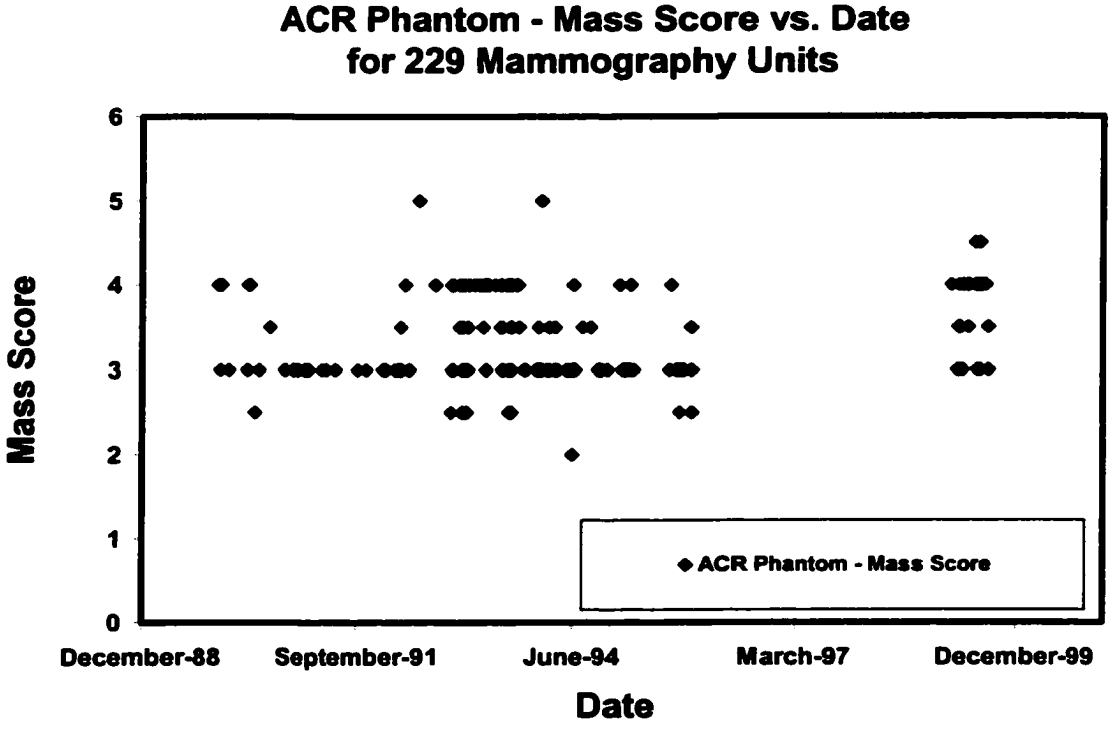


**Figure 2.16.** ACR Phantom mass scores for 229 mammography units.

Table 2.7 shows the results of the background optical density and contrast measurements from the ACR phantom from 1989-1995 and 1999. The average background optical density value of 1.34 significantly improved from 1989-1995 to 1.55 in 1999 ($p<0.0001$). The average contrast values also significantly improved from 0.40 to 0.56 ($p<0.0001$). Figures 2.17 and 2.18 illustrate the range of background and contrast OD's from the two time periods.

**Table 2.7.** Background optical density and contrast optical density for the ACR Phantom from 1989-1995 and 1999.

| ACR Phantom Optical Density (OD) | | | | | |
|---|---|---|---|---|---|
| | 1989-1995 | | 1999 | | p-value |
| | Least Square Mean OD | Standard Error | Least Square Mean OD | Standard Error | |
| Background OD | 1.34 | 0.02 | 1.55 | 0.04 | < 0.0001 |
| Contrast OD | 0.40 | 0.01 | 0.56 | 0.02 | < 0.0001 |

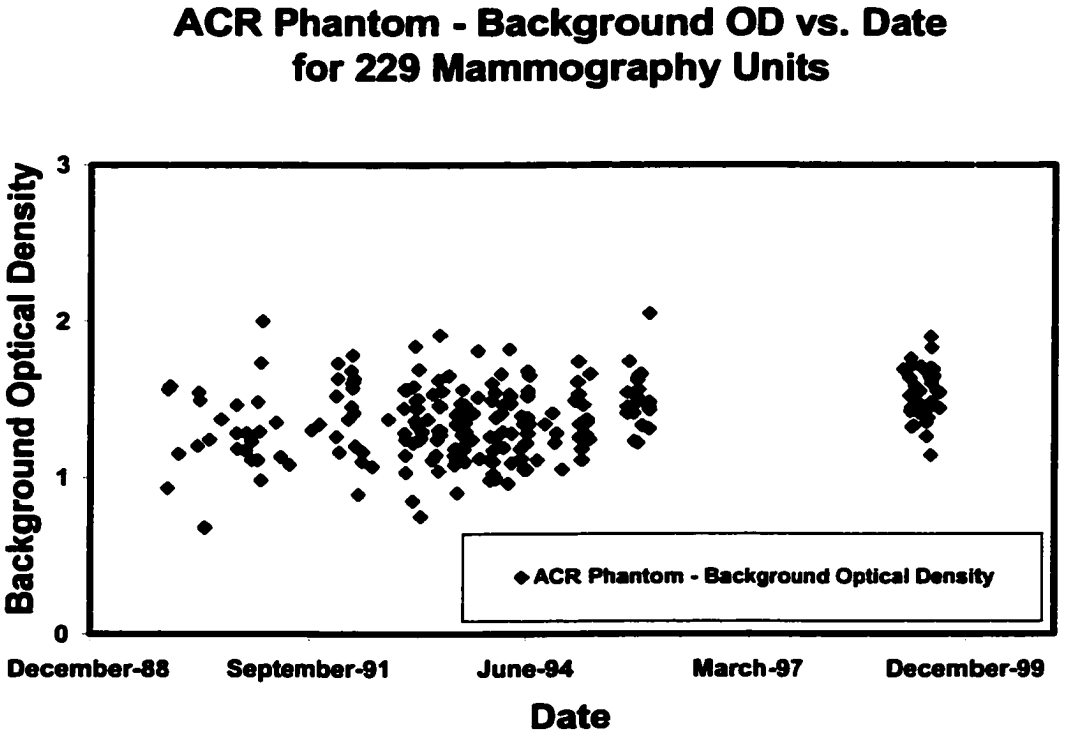


**Figure 2.17.** ACR phantom background optical density versus date for 229 mammography units.

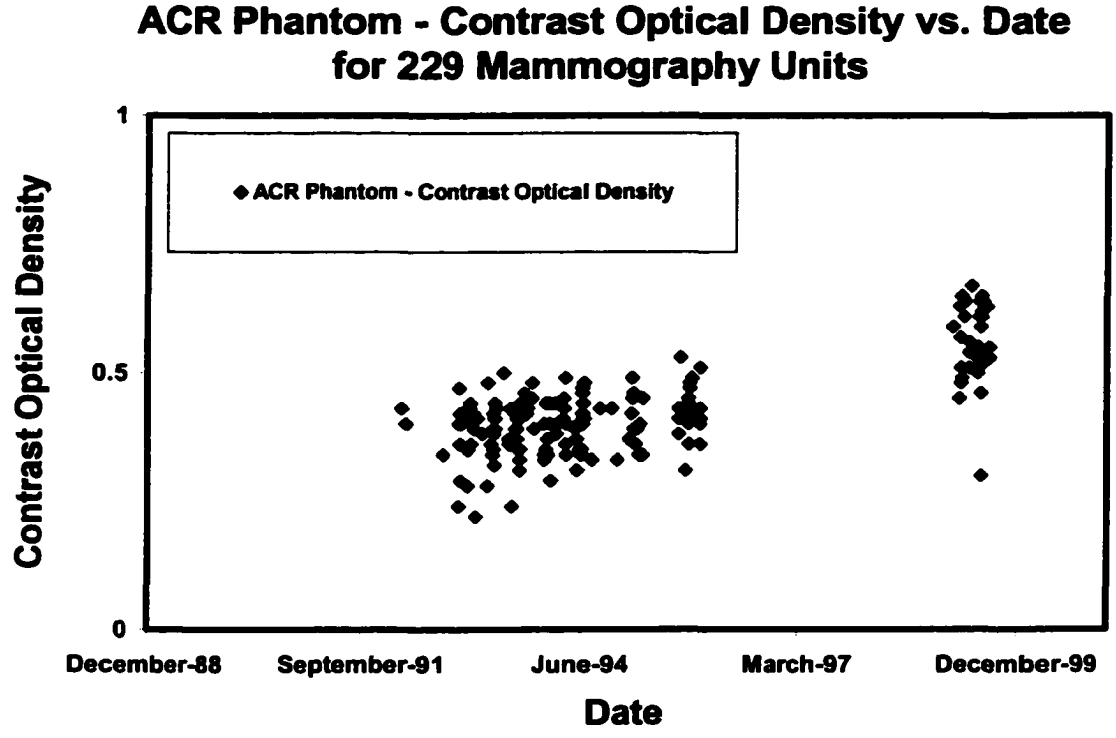


**Figure 2.18.** ACR phantom contrast optical density versus date for 229 mammography units.

Table 2.8 shows a comparison of optical density measurements for 2, 4, and 6 cm thick breast equivalent phantom images for 1989-1995 and 1999.

**Table 2.8.** Optical density measurements for 3 different phantom thicknesses from 1989-1995 and 1999.

| Uniform Breast Equivalent Phantom Optical Density (OD) | | | | | |
|---|---|---|---|---|---|
| Thickness | 1989-1995 | | 1999 | | p-value |
| | Least Square Mean OD | Standard Error | Least Square Mean OD | Standard Error | |
| 2 cm | 1.51 | 0.03 | 1.50 | 0.06 | 0.8746 |
| 4 cm | 1.39 | 0.02 | 1.61 | 0.04 | < 0.0001 |
| 6 cm | 1.24 | 0.03 | 1.63 | 0.05 | < 0.0001 |

There was no difference in optical density values for the 2 cm thick phantoms between 1989-1995 and 1999 ($p=0.8746$). For 4 and 6 cm phantoms, however, there was a significant improvement in optical density values ($p<0.0001$) between the two periods. Figures 2.19-2.21 show the results of optical density versus date for the three different breast thicknesses.

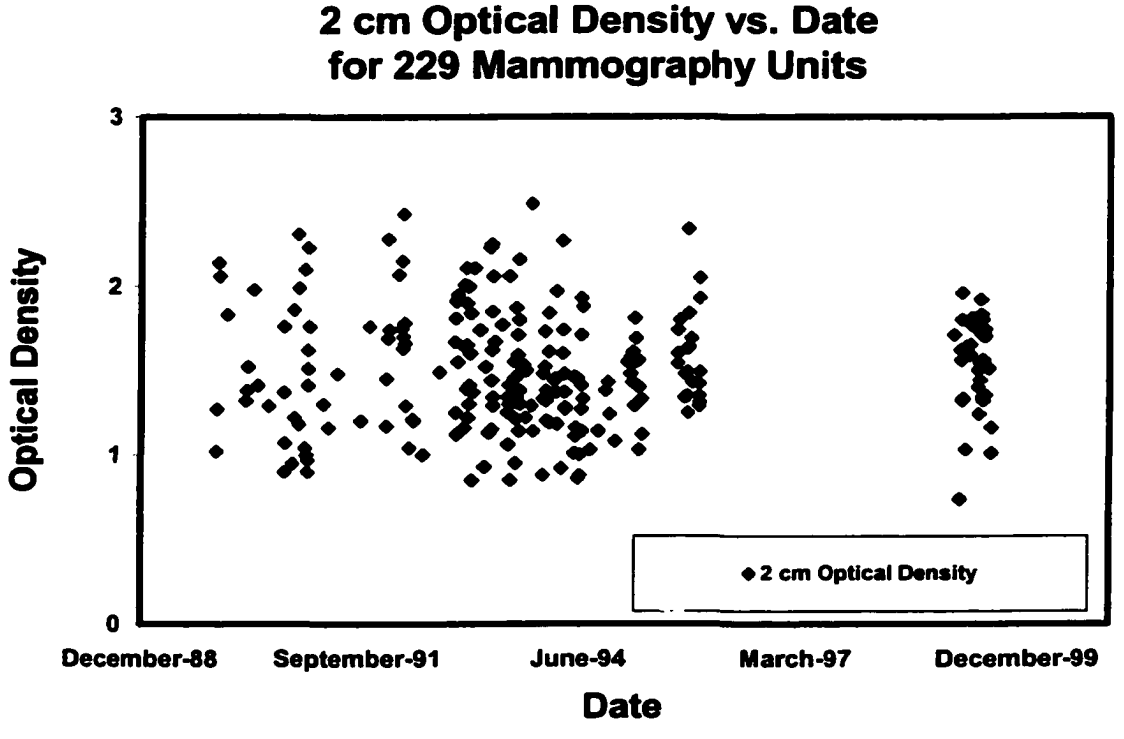


**Figure 2.19.** Optical density versus date for 2 cm thick phantom for 229 mammography units.

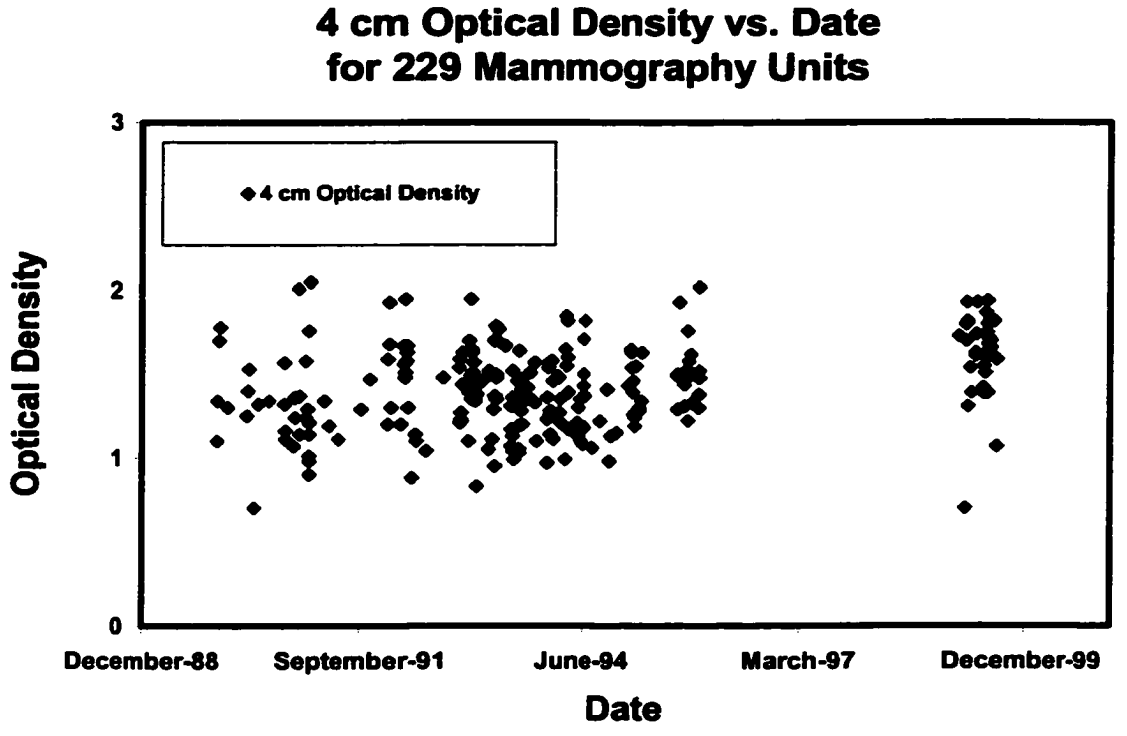


**Figure 2.20.** Optical density versus date for 4 cm thick phantom for 229 mammography units.

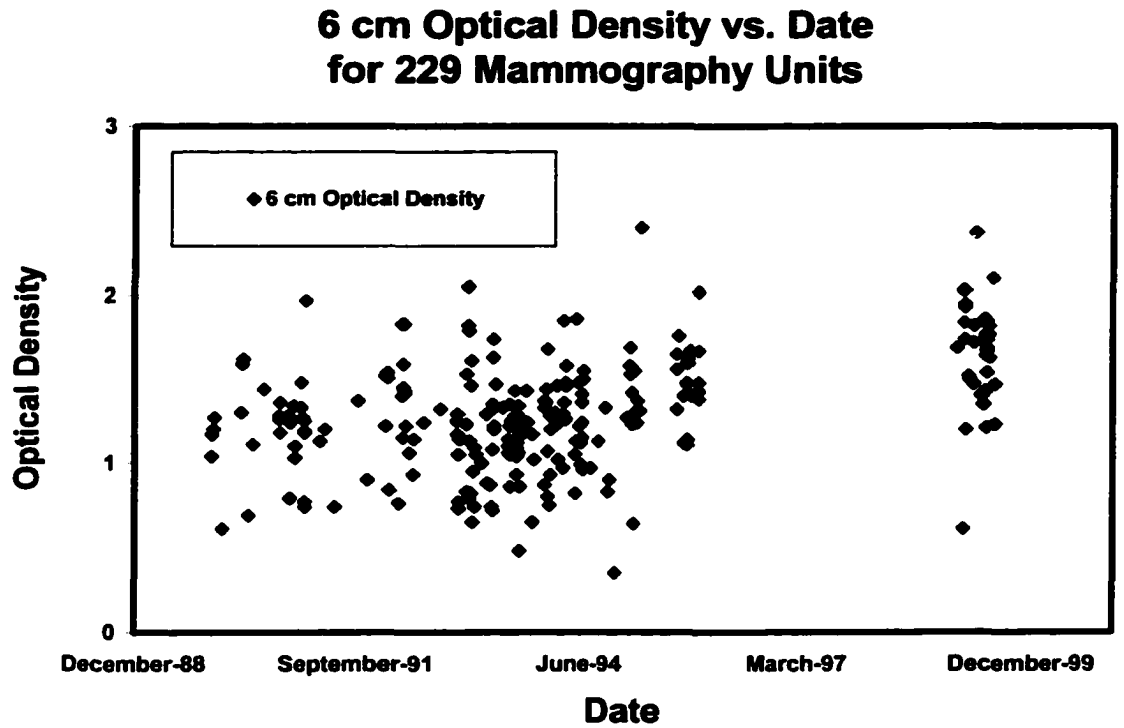


**Figure 2.21.** Optical density versus date for 6 cm thick phantom for 229 mammography units.

Table 2.9 shows a comparison of exposure times for 2, 4, and 6 cm thick breast equivalent phantom images for 1989-1995 and 1999.

**Table 2.9.** Exposure times for 3 different breast thicknesses from 1989-1995 and 1999.

| Uniform Breast Equivalent Phantom Exposure Time (sec.) | | | | | |
|---|---|---|---|---|---|
| Thickness | 1989-1995 | | 1999 | | p-value |
| | Least Square Mean | Standard Error | Least Square Mean | Standard Error | |
| 2 cm | 0.29 | 0.03 | 0.20 | 0.04 | 0.0419 |
| 4 cm | 1.03 | 0.08 | 0.74 | 0.17 | 0.1129 |
| 6 cm | 2.37 | 0.08 | 1.62 | 0.19 | 0.0003 |

For 2 cm thick breasts, the difference between exposure times of 0.29 s in 1989-1995 and 0.20 s in 1999 was barely significant (p=0.0419). For 4 cm thick breasts, exposure times did not change significantly (p=0.1129), while for 6 cm thick breasts, exposure times decreased significantly from 2.37 s to 1.62 s (p=0.0003). Figures 2.22-2.24 show the results of exposure times versus date for the three breast thicknesses

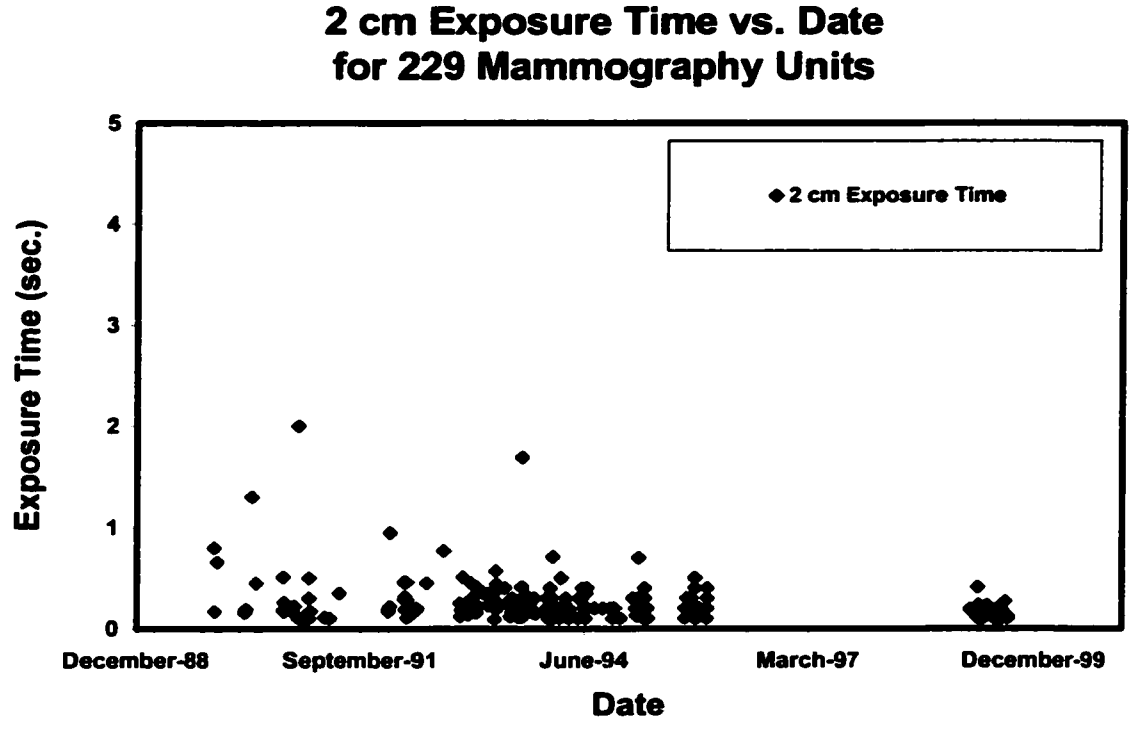


**Figure 2.22.** Exposure time versus date for 2 cm thick breast for 229 mammography units.

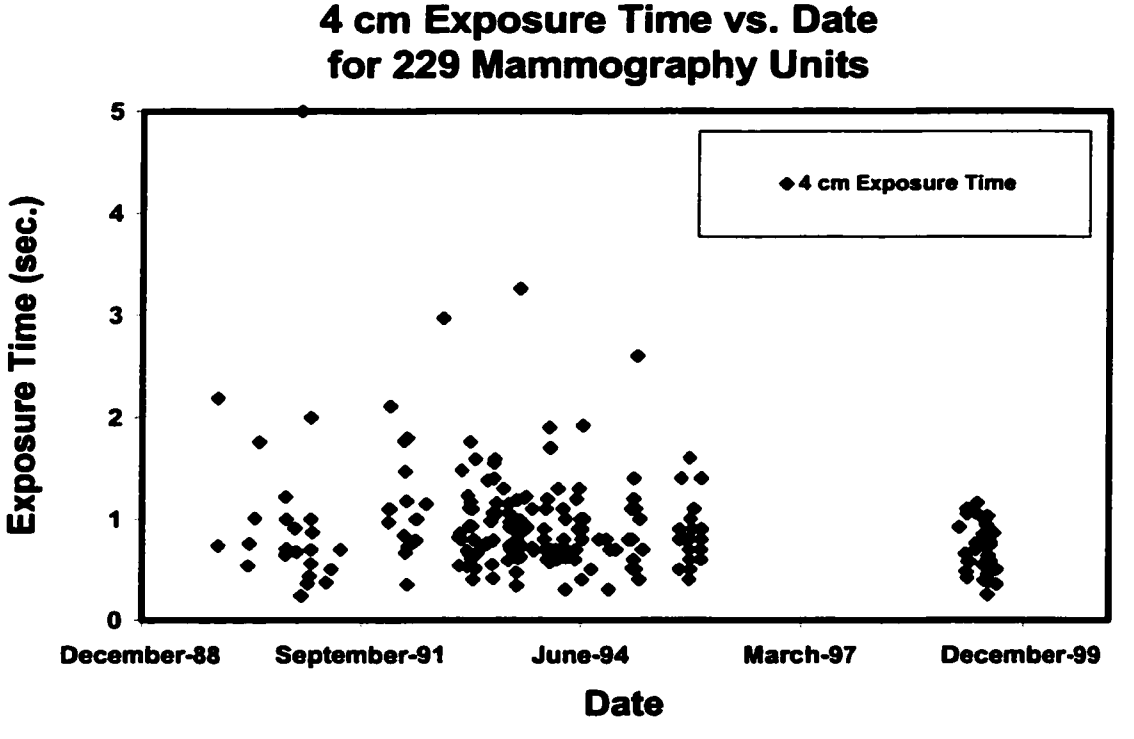


**Figure 2.23.** Exposure time versus date for 4 cm thick breast for 229 mammography units.

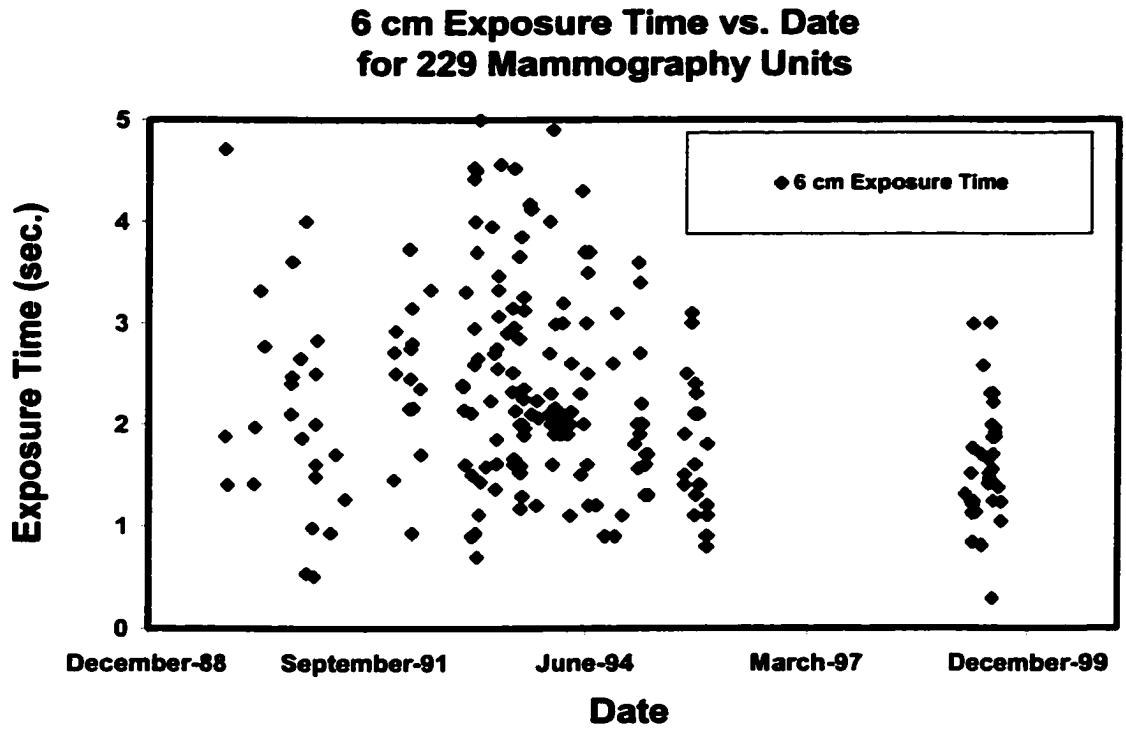


**Figure 2.24.** Exposure time versus date for 6 cm thick breast for 229 mammography units.

Table 2.10 shows the comparison of average glandular dose measurements for 1989-1995 and 1999.

**Table 2.10.** Average Glandular Doses for 5 different breast thickness from 1989-1995 and 1999.

| Average Glandular Dose (mGy) | | | | | |
|---|---|---|---|---|---|
| Thickness | 1989-1995 | | 1999 | | p-value |
| | Average Glandular Dose | Standard Deviation | Average Glandular Dose | Standard Deviation | |
| 2 cm | 0.57 | 0.36 | 0.43 | 0.11 | < 0.0001 |
| 4 cm | 1.35 | 0.43 | 1.19 | 0.30 | 0.0090 |
| ACR Phantom | 1.52 | 0.49 | 1.68 | 0.41 | 0.1636 |
| 6 cm | 3.18 | 1.20 | 2.50 | 0.69 | < 0.0001 |
| 8 cm | *** | *** | 4.01 | 1.29 | *** |

For 2 cm thick breasts, there was a significant reduction in average glandular dose from 0.57 mGy to 0.43 mGy ($p<0.0001$). For 4 cm thick breasts, there was also a significant reduction in dose from 1.35 to 1.19 mGy ($p=0.009$). However, for the ACR phantom, there was no change in dose ($p=0.1636$). For 6 cm thick breasts, there was a significant reduction in dose from 3.18 to 2.50 mGy ($p<0.0001$). Figures 2.25-2.28 illustrate the range of average glandular doses for each of the breast thickness. These figures indicate that doses measured in 1999 were more tightly grouped than in the previous six year period for each breast thickness.

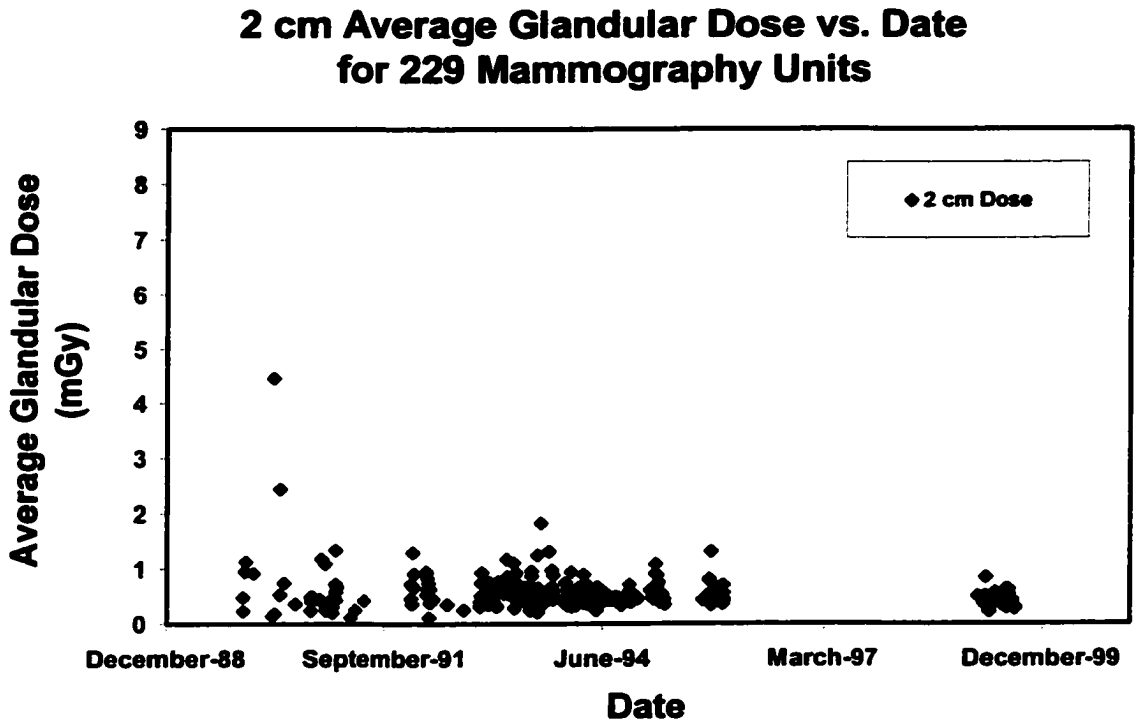


**Figure 2.25.** Average Glandular Dose for 2 cm thick breast for 229 mammography units.

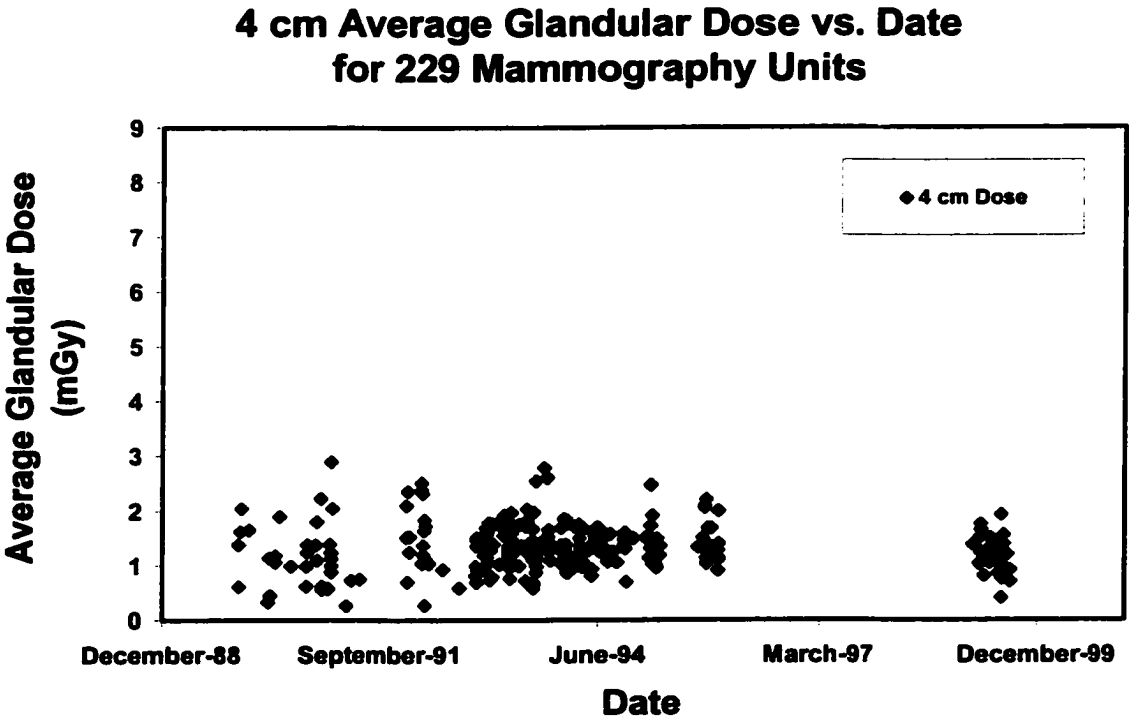


**Figure 2.26.** Average Glandular Dose for 4 cm thick breast for 229 mammography units.

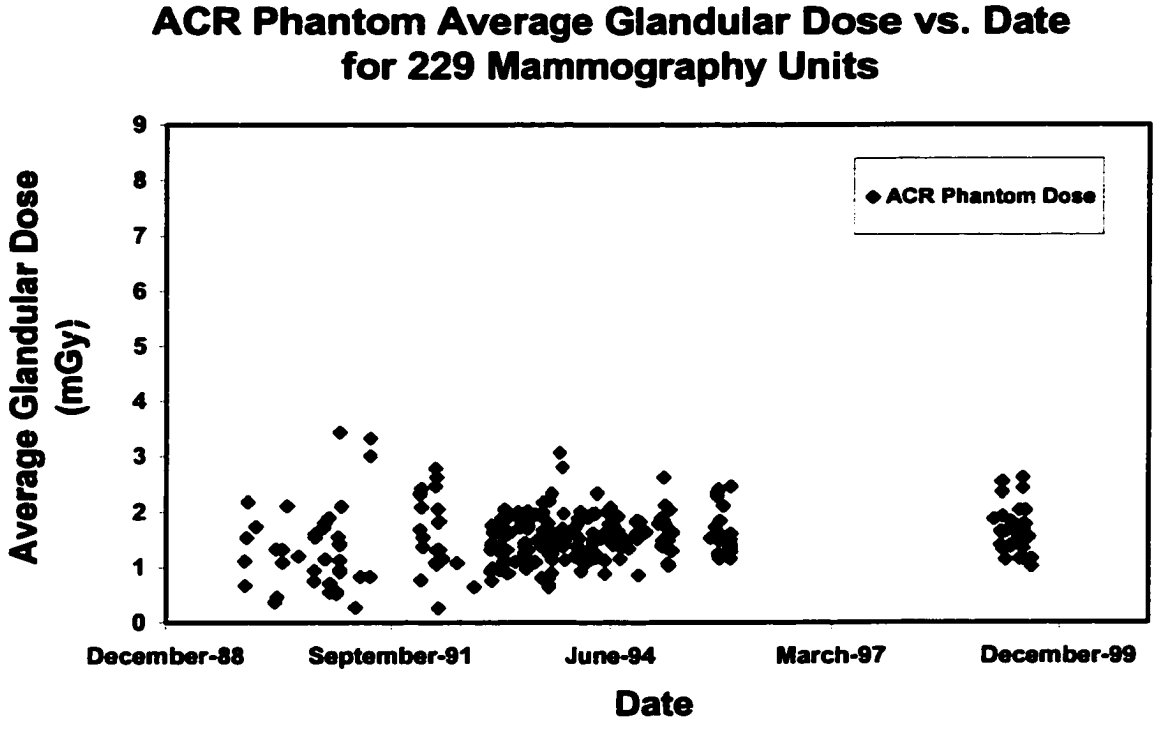


**Figure 2.27.** Average Glandular Dose for the ACR Phantom for 229 mammography units.

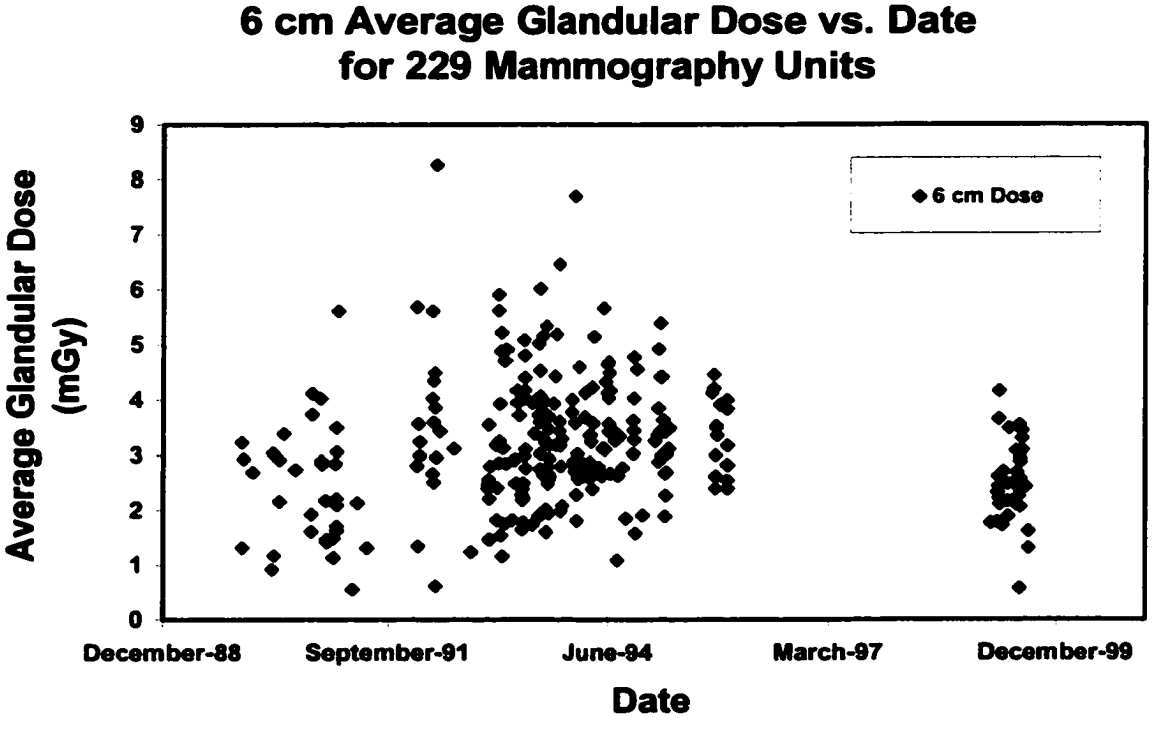


**Figure 2.28.** Average Glandular Dose for 6 cm thick breast for 229 mammography units.

Table 2.11 shows the significance of differences in variability between 1989-1995 data and 1999 data. For the ACR phantom, speck group scores, mass scores, background OD measurements, and contrast OD measurements all exhibited a significant decrease in variance between 1989-1995 and 1999. Fiber score variances were not significantly different. Exposure times for 2, 4, and 6 cm thick breasts all had significant decreases in variability between 1989-1995 and 1999. Optical densities for 2 cm thick breasts had a significant decrease in variance, while ODs for 4 and 6 cm thick breasts did not. Average glandular doses for 2, 4, and 6 cm thick breast had a significant decrease in variance, while doses for the ACR phantom did not. Film processing contrast did not have a significant change in variance between 1989-1995 and 1999 while the $d_{max}$ had a significant decrease in variance during the same time period.

**Table 2.11.** Variability results for CMAP Mammography Sites from 1989-1995 to 1999.

| Significance of Difference Between Variances<br>Comparing CMAP Mammography Sites 1989-1995 to 1999 | | |
|---|---|---|
| | | p-value |
| ACR Phantom | Fibers | 0.659 |
| | Speck Groups | 0.018 |
| | Masses | 0.013 |
| | Background OD | 0.018 |
| | Contrast OD | 0.014 |
| Exposure Times | 2 cm | < 0.0001 |
| | 4 cm | <0.0001 |
| | 6 cm | < 0.0001 |
| Optical Density | 2 cm | 0.035 |
| | 4 cm | 0.887 |
| | 6 cm | 0.906 |
| Average Glandular Dose | 2 cm | < 0.0001 |
| | 4 cm | 0.009 |
| | ACR Phantom | 0.164 |
| | 6 cm | < 0.0001 |
| Film Processors | $A_g$ | 0.391 |
| | $D_{max}$ | 0.002 |

## Chapter 2. DISCUSSION

The results of a decade of medical physics testing reveal a consistent pattern of improvement in the technical performance of mammography. Film-processing contrast, maximum film optical densities, and optical densities for the ACR phantom, and for 4 and 6 cm thick simulated breasts have increased significantly ($p < 0.0001$). Fiber, speck, and mass scores have also increased significantly, as has the radiographic contrast within the ACR phantom ($p < 0.0001$). At the same time, exposure times have decreased significantly for 2 and 4 cm thick breasts ($p < 0.05$) and mean glandular doses have decreased significantly for 2, 4, and 6 cm thick simulated breasts ($p \leq 0.009$). The decrease in breast dose from 1989-95 to 1999 is in distinction to the trend toward higher breast doses shown by the NEXT surveys between 1994-1995 and 1997.[39] That report cited the trend toward higher film optical densities as the reason for increased breast doses. The somewhat surprising and counterintuitive trends of significantly higher film optical densities along with significantly lower breast doses is a double-edged improvement in image quality brought on primarily by improvement in film and processing speed and contrast. Mammography films are achieving both higher optical densities and lower doses due to greater attention to film and film processing conditions, as indicated more directly by the trend toward significantly higher $A_g$ and $D_{max}$ values from 1989-95 compared to 1999.

Also encouraging is that the range of variability in most measured parameters decreased significantly between 1989-95 and 1999. In particular,

the decrease in variability of exposure times for all breast thicknesses ($p<0.0001$), and in dose for 2, 4, and 6 cm thicknesses ($p\leq0.009$) suggest that facilities are moving closer to standardized performance.

While these trends are statistically significant and encouraging, the more recent measurements reflect a situation that is still not perfect. 1999 data demonstrate a 3 to 5-fold range in exposure times (Figure 2.7) and average glandular doses (Figure 2.8), especially for thicker breasts. Film optical densities showed a 2 to 4-fold range at each breast thickness (Figure 2.9). For 6 cm thick breasts, 16% of units had exposure times in excess of 2 seconds. For 8 cm thick breasts, nearly ¾ of units had exposure times in excess of two seconds. These results indicate room for improvement in the current practice of mammography, in spite of the implementation of quality standards, surveys, and inspections of every mammography unit in the U.S.[40]

## Chapter 2. CONCLUSIONS

These results indicate that mammography image quality has improved significantly over the last decade. This is evidenced by significantly improved ACR phantom scores, increased ACR phantom background optical density, and increased ACR phantom contrast. Film processing has had significant improvements with increased $D_{max}$ and film contrast. For uniform breast equivalent phantoms, there were significant improvements for thicker breasts in higher optical densities and reduced exposure times. Average glandular doses

were also significantly reduced over the last decade for all thicknesses except the ACR phantom.

Despite significant improvements, however, there are still wide ranges of image quality and dose in the practice of mammography.

## Chapter 2. ACKNOWLEDGMENTS

This work was supported in part by the Lynn Sage Comprehensive Breast Center and NIH/NCI Grant # 2 U01 CA63736-06.

# CHAPTER 3

# OPTIMIZATION OF TECHNIQUE FACTORS FOR A SILICON DIODE ARRAY FULL-FIELD DIGITAL MAMMOGRAPHY SYSTEM AND COMPARISON TO SCREEN-FILM MAMMOGRAPHY WITH MATCHED MEAN GLANDULAR DOSE

## Chapter 3. INTRODUCTION

Screening mammography trials have shown that mammography has a sensitivity to breast cancer ranging from 60% to 90%, with a trend toward lower sensitivity in premenopausal women.[41,42] In an analysis of "missed" breast cancers, Bird, et.al. determined with reasonable statistical significance that missed breast cancers are more likely to occur in radiographically dense breasts.[43] It is known that breasts with higher fibroglandular density have a greater probability of masking breast cancers when they are present, due to the similar x-ray attenuation properties of glandular tissues and breast cancers. The higher the glandular content of the breast, the greater the probability that a breast cancer will be superimposed by normal glandular tissues.

The replacement of screen-film image receptors by full-field digital image receptors may increase the visibility of lesions, especially those within glandular tissues, by decoupling image acquisition and image display (Figure 3.1).

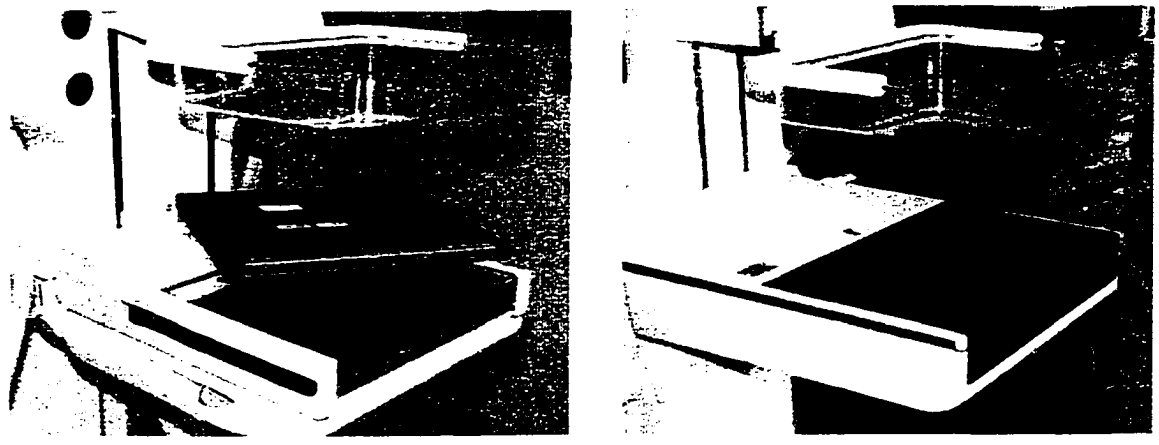

**Figure 3.1.** Screen-film and full-field digital mammography image receptors.

With digital mammography, there should be no loss of contrast within fibroglandular tissues. The effects of the characteristic curve of screen-film systems are eliminated and similar contrast resolution should exist among all breast tissues. Digital mammography systems permit user-adjustment of image display to maximize contrast resolution within specific tissues of interest. Thus, digital mammography has the potential to increase lesion visibility, especially improving the visibility of lesions in dense breasts, and the potential to decrease errors of perception and interpretation. Preliminary studies of small-field and prototype full-field digital image receptors using contrast-detail phantoms suggest that digital mammography will offer improved low contrast resolution capabilities.[44]

There are no published studies evaluating the influence of technique factors on low-contrast lesion detectibility for full-field digital mammography. However, previous work has been done to optimize spectral shape for digital mammography using a $Gd_2O_2S$ scintillating screen coupled to a solid state CCD photodetector.[45] This work found that improvements in signal-to-noise ratios can

be made by choosing different target materials for different breast thicknesses. Another study presented an energy transport model for optimizing spectral shapes for phosphor screens and illustrated methods to be used for optimizing spectral shape .[46] Another study evaluated optimized technique parameters for a slot-scanning digital mammography system and suggested that optimization can maximize image quality and that each system be individually optimized.[47] The results of these three previous studies are relevant to our study, but measurements were made on different detector types, not the cesium-iodide silicon diode array used in this study.

One published study evaluated the cesium-iodide amorphous silicon detector, along with two other digital mammography detectors, by using a "figure of merit" (FOM) as a metric for image quality.[48] In their work, FOM was defined as: FOM = $SNR^2/AGD$, where AGD is average glandular breast dose. Another metric used in the work was to measure the contrast-to-noise ratio across a slab of glandular tissue and calcified tissue relative to a uniform background. These measurements were taken for 3, 5, and 7 cm thick tissue-equivalent phantoms under manual exposures under the condition of approximately matched detector signal.

This paper determines optimized technique factors for detection of low-contrast lesions using a silicon diode array full-field digital mammography (FFDM) system. This optimization was done under the condition of matched AGD across the full range of compressed breast thicknesses. We then compare FFDM results to screen-film mammography (SFM) results at each breast

thickness. This paper differs from the previously cited paper by using detection of simulated low-contrast lesions as the detection task and performs this task under the condition of matched average glandular dose to the breast, not matched signal to the detector.

## Chapter 3. MATERIALS AND METHODS

Four contrast-detail (CD) images were acquired at 2, 4, 6, and 8 cm breast thicknesses on a SFM unit with optimized techniques using the optimization method described by Hendrick, et al, with target optical densities in the range of 1.50-1.70.[36] A D-shaped uniform CD phantom made up of 1 cm slabs of tissue-equivalent material was used, one section of which contained a 9 x 9 contrast-detail pattern for assessment of simulated low-contrast lesions (Figure 3.2). Each row of the CD pattern contained 9 circular objects at a fixed level of contrast with object diameters ranging from 0.25 mm to 4.0 mm. Each of the nine different rows had a different subject contrast, ranging from 0.3% to 4.0%.

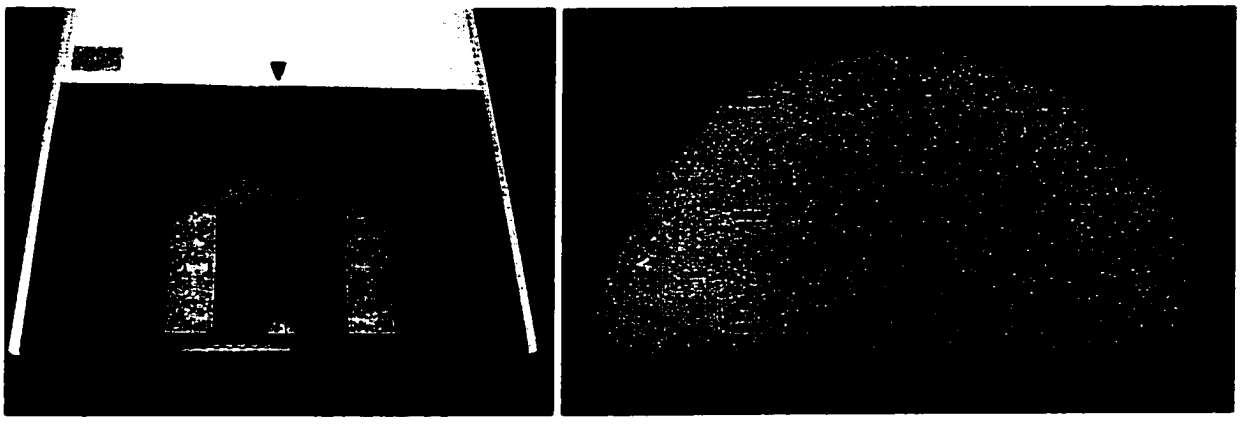

**Figure 3.2.** Contrast-detail phantom on image receptor (left) and an X-ray image of the contrast-detail phantom (right).

Technique factors were recorded for each CD image and the corresponding AGD was calculated for each phantom thickness using HVL and entrance exposure measurements made on the SFM unit (Figures 3.3 and 3.4).[37,38]

**Figure 3.3.** Half-Value Layer measurement setup.

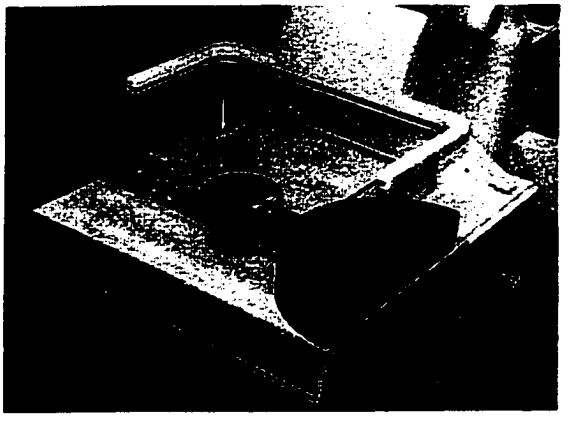

**Figure 3.4.** Entrance exposure measurement setup.

To calculate the techniques for the FFDM unit, a computer program was developed to determine the mAs value that gave equal mean glandular dose at each target-filter combination and kVp for each breast thickness. Half-value layer (HVL) and entrance exposure measurements were made on both the SFM unit and the FFDM unit at each target-filter and kVp to calculate AGD.

CD images were then acquired on the FFDM unit using manual techniques for kVps from 23-35 for Mo-Mo, 23-40 for Mo-Rh, and 25-49 for Rh-Rh under the constraint of matching the AGD for a given breast thickness. mAs values were chosen to provide the matched AGD and images were acquired at approximately every other or every third mAs step on the FFDM unit.

Screen-film CD images were scored by six readers under standardized viewing conditions. These included complete masking of each CD image and low ambient room lighting. Scoring of the CD phantom consisted of starting with the highest contrast row of object, reading from the largest to smallest detectable object diameter in that row. An object was judged as "detected" if it occurred in the correct location, appeared generally round, and was more visible than artifactual "objects" occurring in the background of the CD phantom, excluding the locations of the 81 test objects. This comparison of detected objects against artifacts in the background of the phantom, similar to the method developed for scoring the ACR mammography accreditation phantom, was used to guard against overscoring due to prior knowledge of the location of the test objects in the phantom. Once an object was deemed too faint to detect, was not generally round, or was less conspicuous than artifacts in the background of the phantom,

counting was stopped and the number of consecutively visible objects in that row was summed. The reviewer then moved on to the next row of objects at slightly lower contrast, repeating the procedure. The CD score of each image was determined by calculating the area of detected objects in CD space (Figure 3.5). The more low-contrast objects detected, the higher the CD score. If no objects were detected, a minimum score of zero would result; if all 81 objects were detected, a maximum score of 17.34 would result.

FFDM CD images were scored by the same six readers on the GE Review Workstation using the same scoring methods. CD scores were analyzed to assess trends as a function of target-filter and kVp using a linear regression model and two-sided t-tests were used to compare FFDM to SFM at each breast thickness (SAS Institute, Seattle, WA).

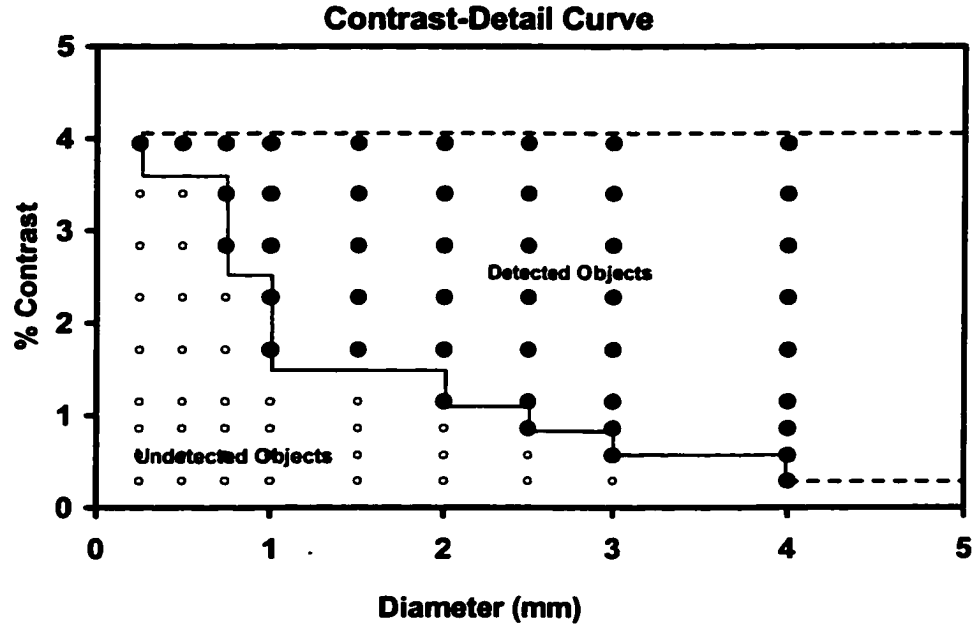


**Figure 3.5.** Schematic of contrast-detail area score calculation. The area defined by the number of detection objects determines the CD score.

## Chapter 3. RESULTS

Results of contrast-detail imaging on the screen-film unit are listed in Table 3.1. All images had optical densities in the range of 1.56 to 1. 66. These OD values are within the desired range for optimal detection of low-contrast lesions.[36]

**Table 3.1.** Optimal screen-film techniques with HVL, average glandular dose, and optical density results.

| Optimized Screen-film Techniques and Data | | | | |
|---|---|---|---|---|
| | 2 cm | 4 cm | 6 cm | 8 cm |
| Target/Filter | Mo/Mo | Mo/Mo | Mo/Rh | Rh/Rh |
| kVp | 25 | 25 | 27 | 28 |
| mAs | 16 | 85 | 168 | 283 |
| HVL (mm Al) | 0.349 | 0.349 | 0.421 | 0.432 |
| Average Glandular Dose (mGy) | 0.39 | 1.26 | 2.35 | 3.85 |
| Optical Density | 1.56 | 1.66 | 1.58 | 1.59 |

Results from the HVL measurements for the dose matching computer program are listed in Table 3.2 for both the GE DMR screen-film mammography unit and the GE Senographe 2000D full-field digital mammography unit. As expected, measured HVLs increased as kVp increased for each target-filter combination. HVL measurements were consistent between the SFM unit and FFDM unit with HVL's ranging from 0.30 to 0.43 mm Al for Mo/Mo, 0.34 to 0.50 for Mo/Rh, and 0.38 to 0.62 for Rh/Rh. Figures 3.6 and 3.7 show the results plotted as HVL versus kVp for each target-filter combination for SFM and FFDM units used in this study.

**Table 3.2.** Results from HVL measurements made on SFM and FFDM units.

| Half-Value Layer (mm Al) | | | | | | |
|---|---|---|---|---|---|---|
| | GE DMR - Film-Screen | | | GE SenoGraphe 2000D - Digital | | |
| kVp | Mo/Mo | Mo/Rh | Rh/Rh | Mo/Mo | Mo/Rh | Rh/Rh |
| 22 | 0.31 | 0.34 | | 0.30 | 0.34 | |
| 23 | 0.32 | 0.36 | | 0.31 | 0.36 | |
| 24 | 0.33 | 0.38 | | 0.33 | 0.38 | |
| 25 | 0.34 | 0.40 | 0.38 | 0.34 | 0.39 | 0.38 |
| 26 | 0.35 | 0.41 | 0.40 | 0.35 | 0.41 | 0.39 |
| 27 | 0.36 | 0.42 | 0.42 | 0.36 | 0.42 | 0.41 |
| 28 | 0.37 | 0.43 | 0.43 | 0.37 | 0.43 | 0.43 |
| 29 | 0.39 | 0.44 | 0.45 | 0.39 | 0.44 | 0.44 |
| 30 | 0.40 | 0.45 | 0.46 | 0.40 | 0.44 | 0.46 |
| 31 | 0.41 | 0.46 | 0.48 | 0.40 | 0.46 | 0.48 |
| 32 | 0.41 | 0.47 | 0.50 | 0.41 | 0.46 | 0.49 |
| 33 | 0.42 | 0.47 | 0.51 | 0.42 | 0.47 | 0.50 |
| 34 | 0.43 | 0.48 | 0.52 | 0.42 | 0.48 | 0.51 |
| 35 | 0.43 | 0.48 | 0.53 | 0.43 | 0.48 | 0.53 |
| 36 | | 0.49 | 0.54 | | 0.48 | 0.54 |
| 37 | | 0.49 | 0.55 | | 0.49 | 0.54 |
| 38 | | 0.49 | 0.55 | | 0.49 | 0.55 |
| 39 | | 0.50 | 0.56 | | 0.50 | 0.56 |
| 40 | | | 0.57 | | 0.50 | 0.56 |
| 41 | | | 0.57 | | | 0.57 |
| 42 | | | 0.58 | | | 0.57 |
| 43 | | | 0.58 | | | 0.58 |
| 44 | | | 0.59 | | | 0.58 |
| 45 | | | 0.59 | | | 0.59 |
| 46 | | | 0.60 | | | 0.60 |
| 47 | | | 0.61 | | | 0.61 |
| 48 | | | 0.62 | | | 0.61 |
| 49 | | | | | | 0.62 |

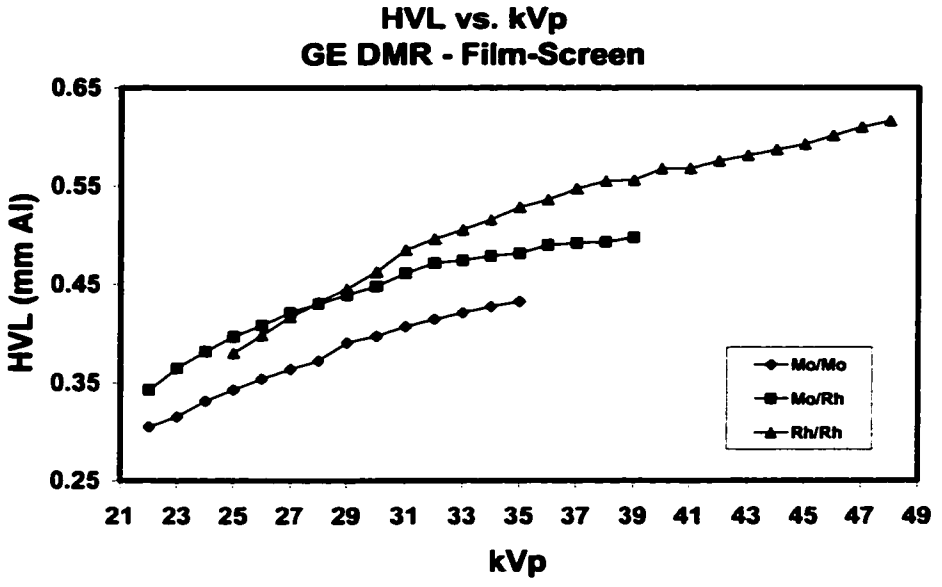


**Figure 3.6.** HVL vs. kVp results for the GE DMR screen-film unit.

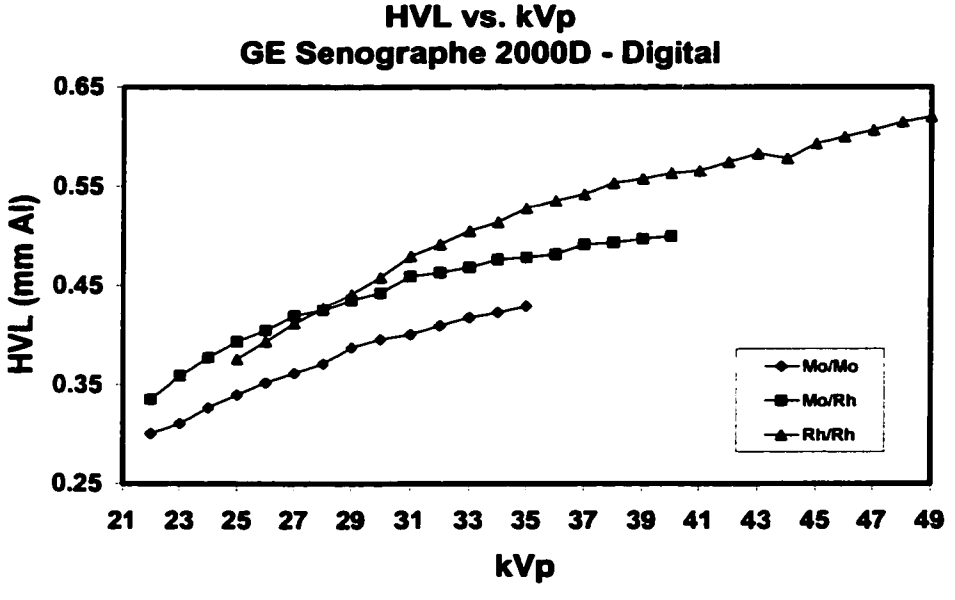


**Figure 3.7.** HVL vs. kVp results for the GE Senographe 2000D full-field digital mammography unit.

Results from exposure output measurements used in the dose matching program are listed in Table 3.3 for both the GE DMR screen-film unit and the GE Senographe 2000D full-field digital mammography unit. As expected, output in terms of mR/mAs rose as kVp increased for each target-filter combination. Output measurements were approximately consistent between the SFM unit and FFDM unit ranging from 5.0 to 22.4 mR/mAs for Mo/Mo, 3.8 to 25.0 mR/mAs for Mo/Rh, and 6.6 to 38.8 mR/mAs for Rh/Rh across the range of kVp values. Figures 3.8 and 3.9 show the results plotted as entrance exposure versus kVp for each target-filter combination for the SFM and FFDM units.

**Table 3.3.** Results from exposure output measurements made on the GE DMR screen-film unit and GE Senographe 2000D full-field digital unit.

| Entrance Exposure (mR/mAs) At 4.5 cm Breast Thickness | | | | | | |
|---|---|---|---|---|---|---|
| | GE DMR - Film-Screen | | | GE SenoGraphe 2000D - Digital | | |
| kVp | Mo/Mo | Mo/Rh | Rh/Rh | Mo/Mo | Mo/Rh | Rh/Rh |
| 22 | 5.4 | 4.2 | | 5.0 | 3.8 | |
| 23 | 6.3 | 5.0 | | 5.9 | 4.6 | |
| 24 | 7.3 | 5.9 | | 6.9 | 5.5 | |
| 25 | 8.4 | 6.8 | 6.9 | 8.0 | 6.4 | 6.6 |
| 26 | 9.6 | 7.9 | 7.8 | 9.1 | 7.4 | 7.5 |
| 27 | 10.8 | 8.9 | 8.8 | 10.3 | 8.4 | 8.5 |
| 28 | 12.1 | 10.1 | 9.9 | 11.6 | 9.5 | 9.6 |
| 29 | 13.5 | 11.3 | 11.0 | 12.9 | 10.7 | 10.6 |
| 30 | 14.8 | 12.5 | 12.1 | 14.2 | 11.8 | 11.8 |
| 31 | 16.3 | 13.7 | 13.3 | 15.6 | 13.0 | 12.9 |
| 32 | 17.7 | 14.9 | 14.5 | 17.0 | 14.2 | 14.1 |
| 33 | 19.2 | 16.2 | 15.8 | 18.5 | 15.5 | 15.4 |
| 34 | 20.8 | 17.6 | 17.0 | 20.0 | 16.8 | 16.6 |
| 35 | 22.4 | 18.9 | 18.4 | 21.5 | 18.1 | 18.0 |
| 36 | | 20.3 | 19.7 | | 19.4 | 19.3 |
| 37 | | 21.8 | 21.1 | | 20.8 | 20.7 |
| 38 | | 23.2 | 22.5 | | 22.2 | 22.1 |
| 39 | | 24.7 | 24.0 | | 23.6 | 23.5 |
| 40 | | | 25.4 | | 25.0 | 24.9 |
| 41 | | | 26.9 | | | 26.4 |
| 42 | | | 28.4 | | | 27.9 |
| 43 | | | 29.9 | | | 29.4 |
| 44 | | | 31.5 | | | 31.0 |
| 45 | | | 32.9 | | | 32.5 |
| 46 | | | 34.5 | | | 33.9 |
| 47 | | | 36.1 | | | 35.6 |
| 48 | | | 37.7 | | | 37.2 |
| 49 | | | | | | 38.8 |

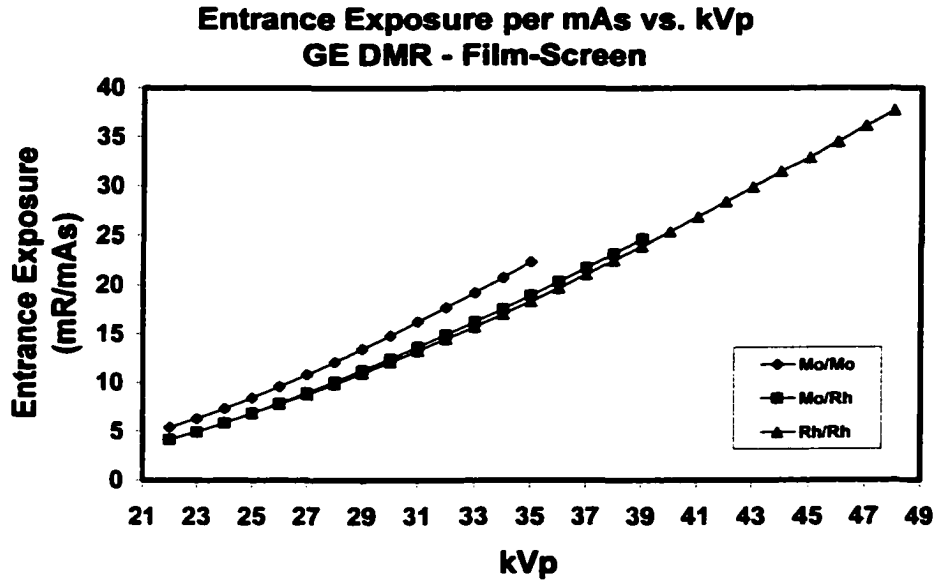


**Figure 3.8.** Exposure output vs. kVp results for the GE DMR screen-film unit.

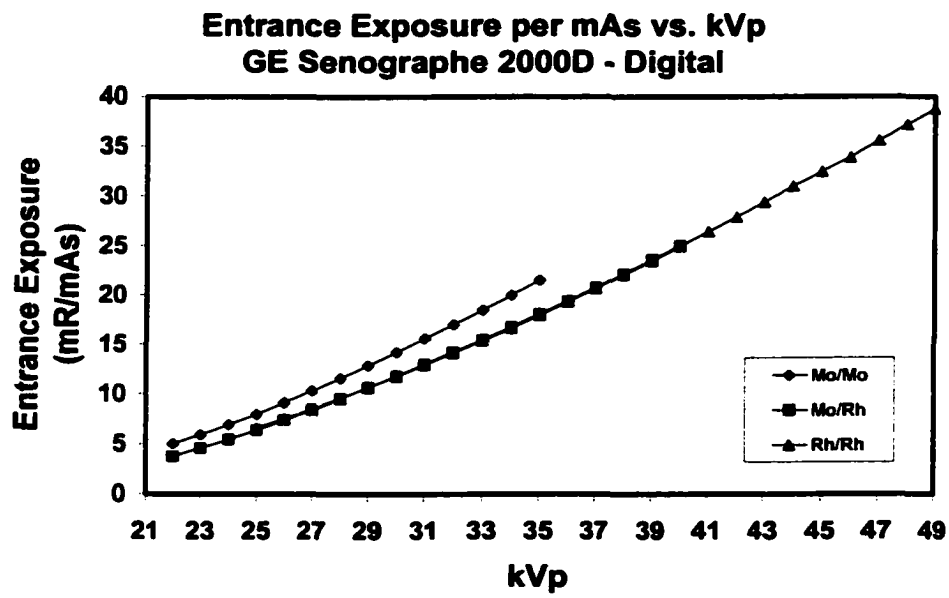


**Figure 3.9.** Exposure output vs. kVp results for the GE Senographe 2000D full-field digital mammography unit.

Results of contrast-detail scores and SNR measurements can be seen in Tables 3.4-3.7 and Figures 3.10-3.17. Table 3.4 shows contrast-detail results of imaging a 2 cm thick breast for both SFM and FFDM. Figure 3.10 shows CD results plotted versus kVp. For the digital mammography system, the highest CD scores occurred at the lowest possible kVp settings for each target-filter combination. The optimum digital mammography CD score for each of the 3 target-filters (13.45-13.71) was virtually identical to the optimized screen-film CD score (13.75) for 2 cm thick breasts. Figure 3.11 shows the SNR vs kVp for each target-filter combination in digital mammography. The significance of trends in CD scores and SNR values is discussed at the end of this results section.

**Table 3.4.** Contrast-detail phantom image results for 2 cm breast thickness.

| Contrast-Detail Phantom Imaging Results | | | | | | |
|---|---|---|---|---|---|---|
| 2 cm Breast Thickness | | | | | | |
| Average Glandular Dose = 0.39 mGy | | | | | | |
| Modality | Technique | | | SNR | Contrast Detail Score | |
| | Target/Filter | kVp | mAs | | Mean | Standard Deviation |
| Screen-film | Mo/Mo | 25 | 16 | *** | 13.75 | 0.68 |
| Digital | Mo/Mo | 23 | 25 | 69.27 | 13.45 | 0.69 |
| | Mo/Mo | 26 | 14 | 65.93 | 13.38 | 0.60 |
| | Mo/Mo | 30 | 8 | 57.07 | 13.09 | 0.43 |
| | Mo/Mo | 34 | 5 | 68.93 | 12.15 | 0.66 |
| | Mo/Rh | 23 | 28 | 74.94 | 13.66 | 0.62 |
| | Mo/Rh | 26 | 16 | 73.34 | 12.65 | 0.97 |
| | Mo/Rh | 30 | 9 | 63.99 | 12.26 | 0.76 |
| | Mo/Rh | 35 | 5 | 74.98 | 12.73 | 0.44 |
| | Mo/Rh | 40 | 4 | 78.77 | 12.02 | 1.04 |
| | Rh/Rh | 25 | 18 | 76.27 | 13.71 | 0.58 |
| | Rh/Rh | 29 | 10 | 70.15 | 12.73 | 0.78 |
| | Rh/Rh | 33 | 6 | 71.43 | 11.98 | 0.73 |
| | Rh/Rh | 37 | 4 | 84.14 | 12.14 | 1.22 |

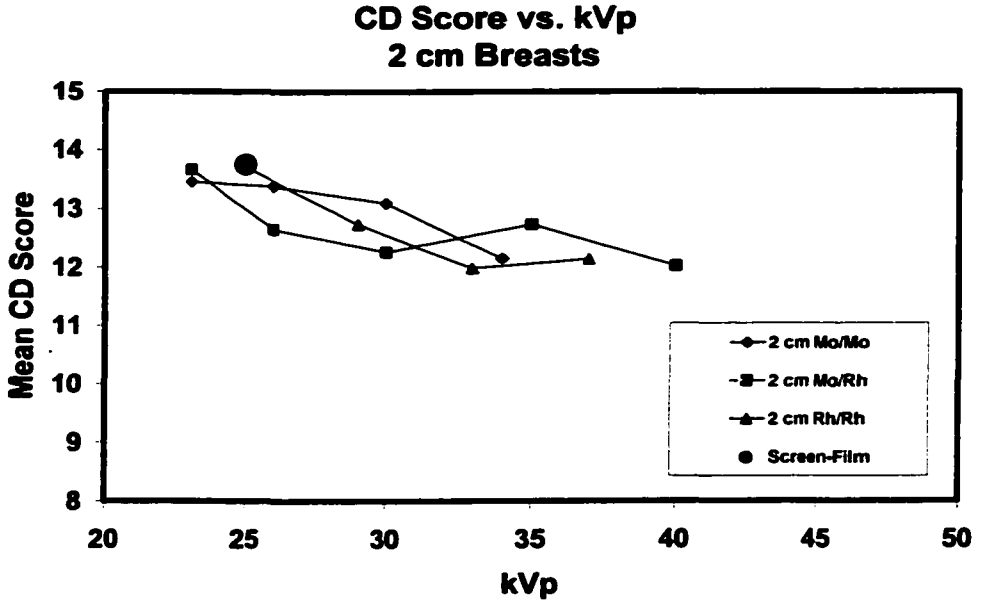


**Figure 3.10.** CD score versus kVp for 2 cm breast thickness.

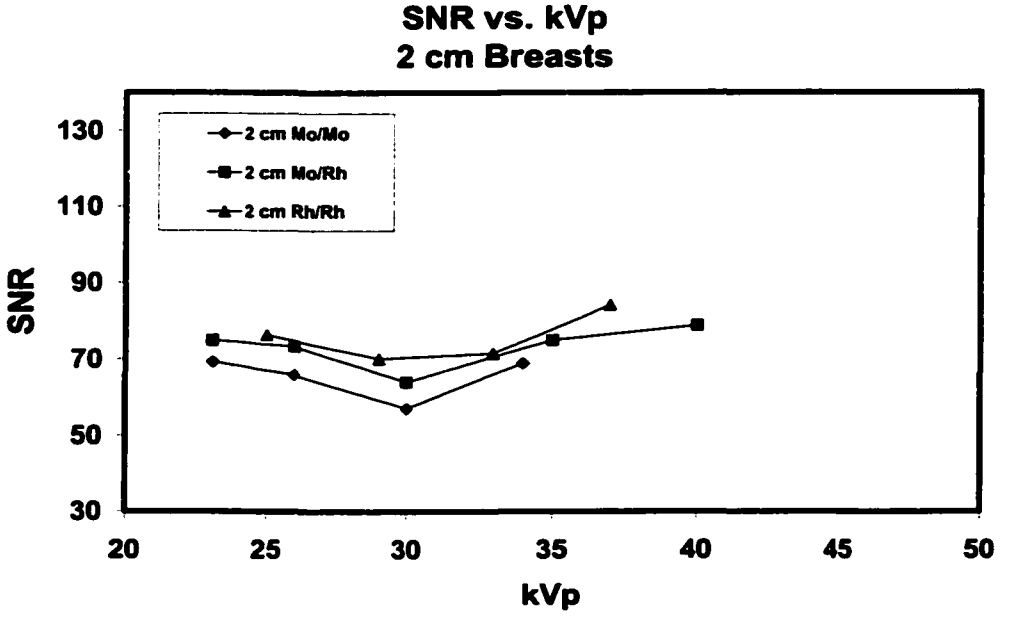


**Figure 3.11.** SNR versus kVp for 2 cm breast thickness.

Table 3.5 shows CD results for the 4 cm thick breast using both SFM and FFDM. Figure 3.12 shows the results of the digital mammography CD scores plotted versus kVp. Most digital CD scores exceeded the optimized screen-film CD score for 4 cm thick breasts. Figure 3.13 shows the results of the SNR values versus kVp for 4 cm thick breasts, demonstrating higher SNRs for higher kVps with each target-filter combination.

**Table 3.5.** Contrast-Detail phantom image results for 4 cm breast thickness.

| Contrast-Detail Phantom Imaging Results | | | | | | |
|---|---|---|---|---|---|---|
| 4 cm Breast Thickness | | | | | | |
| Average Glandular Dose = 1.26 mGy | | | | | | |
| Modality | Technique | | | SNR | Contrast Detail Score | |
| | Target/Filter | kVp | mAs | | Mean | Standard Deviation |
| Film-Screen | Mo/Mo | 25 | 85 | *** | 12.83 | 0.62 |
| Digital | Mo/Mo | 22 | 160 | 65.17 | 13.63 | 0.72 |
| | Mo/Mo | 24 | 110 | 72.15 | 14.20 | 0.89 |
| | Mo/Mo | 28 | 56 | 75.17 | 13.99 | 0.64 |
| | Mo/Mo | 31 | 40 | 82.66 | 13.57 | 0.88 |
| | Mo/Mo | 34 | 28 | 83.16 | 13.12 | 1.31 |
| | Mo/Rh | 23 | 140 | 77.02 | 14.10 | 0.91 |
| | Mo/Rh | 26 | 80 | 83.84 | 13.68 | 0.78 |
| | Mo/Rh | 30 | 45 | 85.78 | 13.59 | 1.20 |
| | Mo/Rh | 35 | 28 | 90.40 | 14.38 | 0.80 |
| | Mo/Rh | 39 | 20 | 92.86 | 13.21 | 0.94 |
| | Rh/Rh | 26 | 80 | 88.17 | 14.00 | 1.10 |
| | Rh/Rh | 29 | 50 | 91.67 | 14.36 | 0.66 |
| | Rh/Rh | 34 | 28 | 91.73 | 13.74 | 0.62 |
| | Rh/Rh | 38 | 20 | 101.41 | 13.81 | 0.65 |
| | Rh/Rh | 43 | 14 | 107.42 | 13.27 | 0.82 |
| | Rh/Rh | 49 | 9 | 112.92 | 12.25 | 0.73 |

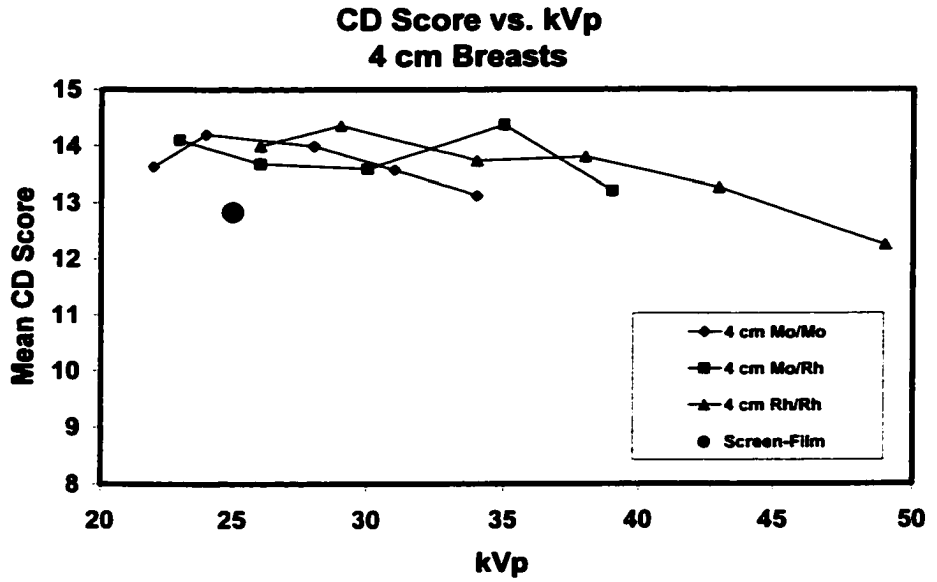


**Figure 3.12.** CD score versus kVp for 4 cm breast thickness.

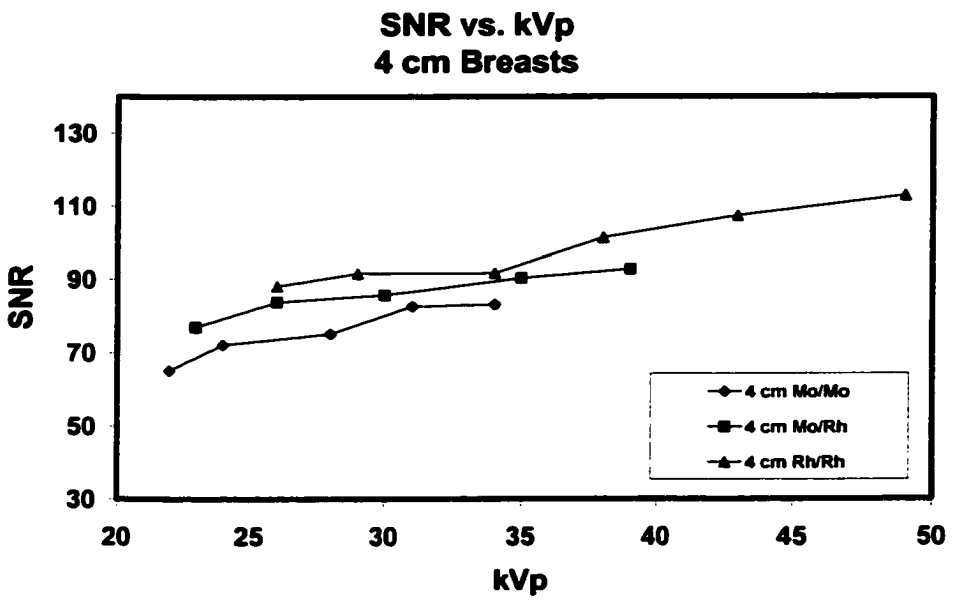


**Figure 3.13.** SNR versus kVp for 4 cm breast thickness.

Table 3.6 shows CD results for 6 cm thick breasts using both SFM and FFDM. Figure 3.14 shows CD results plotted versus kVp. All digital CD scores exceeded the optimized screen-film CD score for 6 cm thick breasts. Figure 3.15 shows SNR results versus kVp for 6 cm thick breasts, demonstrating a strong linear dependence of SNR values on kVp values for digital mammography.

**Table 3.6.** Contrast-Detail phantom image results for 6 cm breast thickness.

| Contrast-Detail Phantom Imaging Results | | | | | | |
|---|---|---|---|---|---|---|
| 6 cm Breast Thickness | | | | | | |
| Average Glandular Dose = 2.35 mGy | | | | | | |
| Modality | Technique | | | SNR | Contrast Detail Score | |
| | Target/Filter | kVp | mAs | | Mean | Standard Deviation |
| Screen-film | Mo/Rh | 27 | 168 | *** | 11.28 | 0.48 |
| Digital | Mo/Mo | 22 | 450 | 42.02 | 11.76 | 0.77 |
| | Mo/Mo | 24 | 280 | 49.40 | 12.27 | 0.75 |
| | Mo/Mo | 26 | 200 | 52.66 | 12.50 | 0.42 |
| | Mo/Mo | 29 | 125 | 57.34 | 12.21 | 0.74 |
| | Mo/Mo | 31 | 100 | 68.22 | 12.22 | 0.34 |
| | Mo/Mo | 33 | 80 | 66.43 | 11.77 | 0.93 |
| | Mo/Mo | 35 | 63 | 73.85 | 11.87 | 0.67 |
| | Mo/Rh | 22 | 500 | 53.20 | 12.34 | 0.59 |
| | Mo/Rh | 25 | 250 | 56.29 | 12.45 | 0.43 |
| | Mo/Rh | 27 | 180 | 65.79 | 12.71 | 0.45 |
| | Mo/Rh | 30 | 125 | 70.73 | 12.66 | 0.81 |
| | Mo/Rh | 34 | 80 | 77.54 | 12.66 | 0.68 |
| | Mo/Rh | 36 | 63 | 79.79 | 12.71 | 0.71 |
| | Mo/Rh | 40 | 45 | 92.25 | 12.37 | 0.43 |
| | Rh/Rh | 26 | 200 | 74.68 | 13.23 | 0.51 |
| | Rh/Rh | 28 | 140 | 77.74 | 12.81 | 0.62 |
| | Rh/Rh | 30 | 110 | 81.98 | 13.31 | 0.40 |
| | Rh/Rh | 32 | 80 | 82.90 | 12.85 | 0.75 |
| | Rh/Rh | 35 | 63 | 89.73 | 13.23 | 0.74 |
| | Rh/Rh | 38 | 56 | 100.16 | 12.81 | 0.55 |
| | Rh/Rh | 41 | 40 | 104.72 | 12.87 | 0.34 |
| | Rh/Rh | 44 | 32 | 113.60 | 12.87 | 0.80 |
| | Rh/Rh | 46 | 28 | 118.83 | 12.99 | 0.31 |
| | Rh/Rh | 49 | 22.5 | 117.18 | 12.92 | 0.55 |

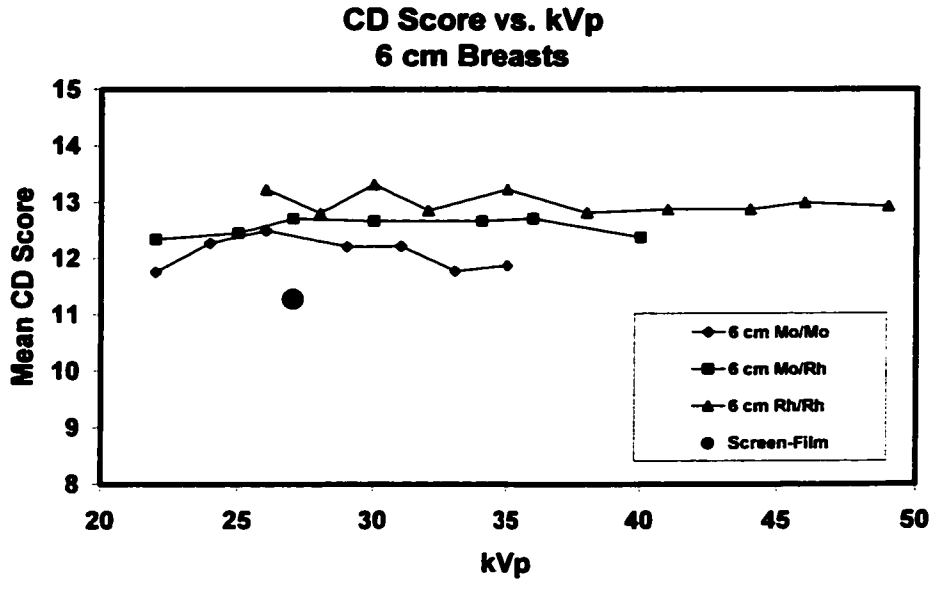


**Figure 3.14.** CD score versus kVp for 6 cm breast thickness.

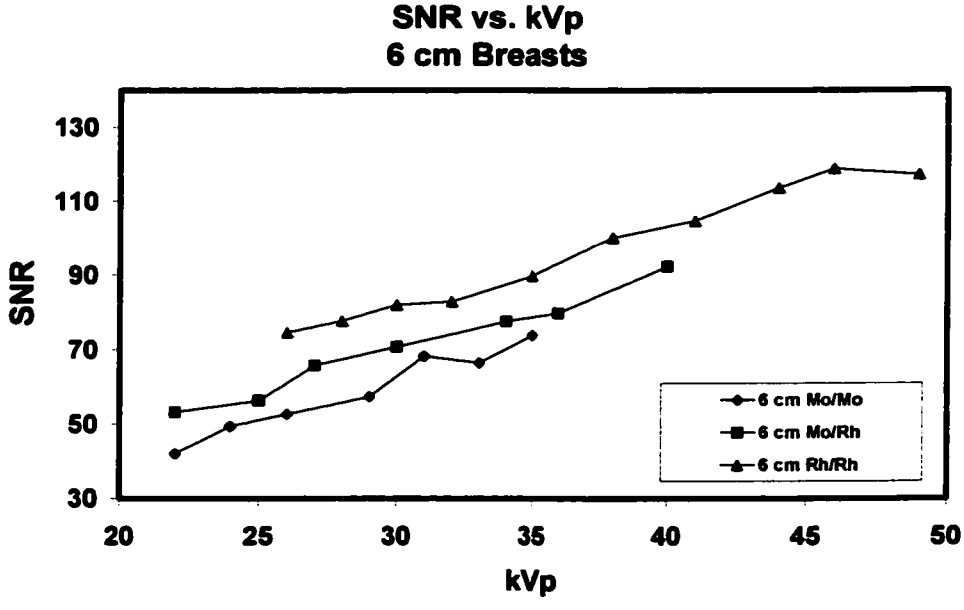


**Figure 3.15.** SNR versus kVp for 6 cm breast thickness.

Table 3.7 shows CD and SNR results for 8 cm thick breasts using both SFM and FFDM. Figure 3.16 shows the results of the CD scores plotted versus kVp for 8 cm thick breasts. CD scores for both FFDM using Rh-Rh and Mo-Rh target-filters were superior to those for SFM at this breast thickness. The highest CD scores for digital occurred with Rh-Rh, regardless of the kVp selected. Figure 3.17 shows SNR results versus kVp for 8 cm thick breasts, demonstrating a strong linear dependence of SNR on kVp under the condition of matched breast dose.

**Table 3.7.** Contrast-Detail phantom image results for 8 cm breast thickness.

| Contrast-Detail Phantom Imaging Results | | | | | | |
|---|---|---|---|---|---|---|
| 8 cm Breast Thickness | | | | | | |
| Average Glandular Dose = 3.85 mGy | | | | | | |
| Modality | Technique | | | SNR | Contrast Detail Score | |
| | Target/Filter | kVp | mAs | | Mean | Standard Deviation |
| Screen-film | Rh/Rh | 28 | 283 | *** | 9.48 | 0.94 |
| Digital | Mo/Mo | 24 | 600 | 39.49 | 8.28 | 1.54 |
| | Mo/Mo | 27 | 360 | 41.97 | 9.25 | 1.23 |
| | Mo/Mo | 30 | 225 | 50.95 | 8.80 | 1.08 |
| | Mo/Mo | 33 | 160 | 6071 | 9.68 | 0.91 |
| | Mo/Mo | 35 | 140 | 68.73 | 10.02 | 0.95 |
| | Mo/Rh | 24 | 600 | 45.04 | 10.52 | 1.01 |
| | Mo/Rh | 27 | 360 | 50.00 | 10.82 | 2.04 |
| | Mo/Rh | 29 | 288 | 58.00 | 10.87 | 0.99 |
| | Mo/Rh | 32 | 200 | 64.14 | 10.62 | 1.22 |
| | Mo/Rh | 34 | 160 | 69.02 | 9.82 | 0.84 |
| | Mo/Rh | 37 | 125 | 77.74 | 11.75 | 0.85 |
| | Mo/Rh | 40 | 90 | 84.04 | 10.30 | 0.62 |
| | Rh/Rh | 25 | 500 | 57.51 | 11.55 | 0.73 |
| | Rh/Rh | 29 | 250 | 68.44 | 11.78 | 0.50 |
| | Rh/Rh | 34 | 140 | 80.84 | 12.19 | 1.20 |
| | Rh/Rh | 36 | 110 | 84.79 | 12.22 | 1.04 |
| | Rh/Rh | 39 | 90 | 98.75 | 12.46 | 0.62 |
| | Rh/Rh | 43 | 71 | 111.97 | 12.57 | 0.65 |
| | Rh/Rh | 46 | 56 | 119.36 | 12.85 | 0.29 |
| | Rh/Rh | 49 | 45 | 121.87 | 12.22 | 0.84 |

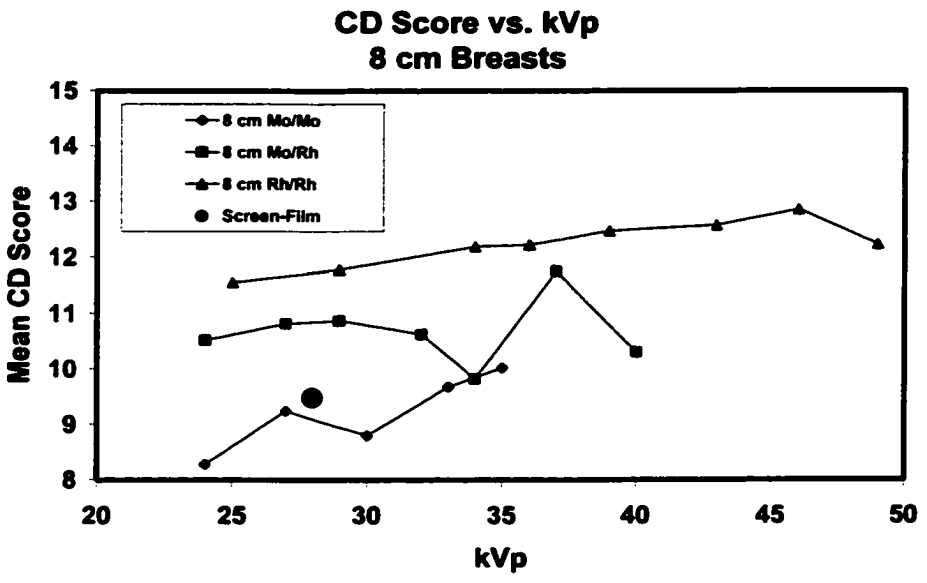


**Figure 3.16.** CD score versus kVp for 8 cm breast thickness.

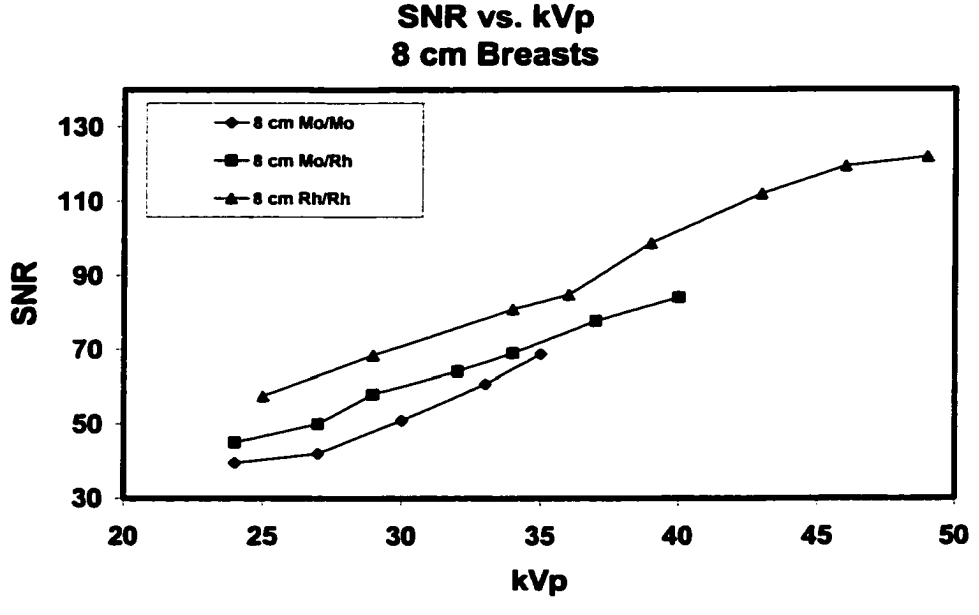


**Figure 3.17.** SNR versus kVp for 8 cm breast thickness.

Optimal digital CD scores are compared to those for SFM in Table 3.8. Trends in CD scores versus kVp at each breast thickness and target-filter combination are shown in Table 3.9. Trends in SNR values versus kVp at each breast thickness and target-filter combination are shown in Table 3.10.

For 2 cm thick breasts, there was no statistical distinction between SFM and optimum FFDM CD scores. Table 3.10 indicates that CD scores tended to drop as kVp increased for each target-filter material for 2 cm breasts, but the trend to lower CD scores at higher kVp values was not statistically significant. Table 3.11 indicates that there was no statistically significant trend in SNR values as a function of kVp for 2 cm breasts.

For 4 cm breasts, optimal FFDM CD scores occurred at 24 kVp for Mo-Mo (14.20), 35 kVp for Mo-Rh (14.38), and 29 kVp for Rh-Rh (14.36). The optimal FFDM CD scores for each target-filter was superior to the SFM CD score ($p \leq 0.013$). The trend toward a lower CD score at higher kVp values was observed in the 4 cm data, but as Table 3.9 indicates, the trend was statistically significant only for the Rh-Rh target material ($p = 0.012$). As Table 3.10 indicates, the trend toward higher SNR values as kVp increased was statistically significant for 4 cm thick breasts for each target-filter material ($p < 0.01$).

**Table 3.8.** Mean CD score comparison.

| Mean CD Score Comparison Under Optimized Techniques | | | |
|---|---|---|---|
| | Screen-Film | Optimal Digital | |
| Breast Thickness | Mean CD Score | Mean CD Score | P-value |
| 2 cm | 13.75 | 13.45 | 0.47 |
| 4 cm | 12.83 | 14.20 | 0.013 |
| 6 cm | 11.8 | 13.3 | < 0.0001 |
| 8 cm | 9.48 | 12.9 | < 0.0001 |

For 6 cm breasts, optimum FFDM CD scores occurred for Rh-Rh at 30 kVp and were significantly higher than the SFM CD score (13.3 vs. 11.8, $p<0.0001$). In fact, for 6 cm thick breasts, all FFDM CD scores were higher than the SFM CD score (Figure 3.14). Table 3.9 indicates that there was no statistically significant trend in CD scores versus mAs for 6 cm breasts for any target-filter combination. Figure 3.15 and Table 3.10 indicate that there was a statistically significant increase in SNR for increasing kVp for each target-filter combination $p < 0.0001$).

For 8 cm breasts, optimum FFDM CD scores occurred for Rh-Rh at 46 kVp and were significantly higher than SFM CD scores (12.9 vs. 9.48, $p<0.0001$). In general, CD scores for Rh-Rh were higher than those for Mo-Mo or Mo-Rh at this breast thickness. For Mo-Mo and Rh-Rh, FFDM CD scores increased significantly as kVp increased ($p < 0.05$). For 8 cm thick breasts with all target-filter materials, SNR values increased significantly as kVp increased ($p < 0.005$).

**Table 3.9.** Statistical significance of trends in CD scores versus kVp at each breast thickness and target-filter combination.

| Trend Results For Contrast-Detail Scores Versus kVp | | | | |
|---|---|---|---|---|
| Breast Thickness | Target/Filter | Mean Value | R-Square | Trend p-value |
| 2 cm | Mo/Mo | 13.0 | 0.855 | 0.0752 |
| | Mo/Rh | 12.7 | 0.576 | 0.1369 |
| | Rh/Rh | 12.6 | 0.813 | 0.0985 |
| 4 cm | Mo/Mo | 13.7 | 0.440 | 0.2221 |
| | Mo/Rh | 13.8 | 0.119 | 0.5691 |
| | Rh/Rh | 13.6 | 0.824 | 0.0123 |
| 6 cm | Mo/Mo | 12.1 | 0.068 | 0.5710 |
| | Mo/Rh | 12.6 | 0.045 | 0.6496 |
| | Rh/Rh | 13.0 | 0.147 | 0.2735 |
| 8 cm | Mo/Mo | 9.21 | 0.793 | 0.0428 |
| | Mo/Rh | 10.7 | 0.001 | 0.9453 |
| | Rh/Rh | 12.2 | 0.677 | 0.0121 |

**Table 3.10.** Statistical significance of trends in SNR values versus kVp at each breast thickness and target-filter combination.

| Trend Results For SNR Versus kVp | | | | |
|---|---|---|---|---|
| Breast Thickness | Target/Filter | Mean Value | R-Square | Trend p-value |
| 2 cm | Mo/Mo | 65.3 | 0.037 | 0.8071 |
| | Mo/Rh | 73.2 | 0.118 | 0.5718 |
| | Rh/Rh | 75.5 | 0.258 | 0.4929 |
| 4 cm | Mo/Mo | 75.5 | 0.927 | 0.0086 |
| | Mo/Rh | 86.0 | 0.939 | 0.0065 |
| | Rh/Rh | 98.9 | 0.951 | 0.0009 |
| 6 cm | Mo/Mo | 58.6 | 0.961 | < 0.0001 |
| | Mo/Rh | 70.8 | 0.979 | < 0.0001 |
| | Rh/Rh | 96.2 | 0.977 | < 0.0001 |
| 8 cm | Mo/Mo | 52.4 | 0.959 | 0.0035 |
| | Mo/Rh | 64.0 | 0.994 | < 0.0001 |
| | Rh/Rh | 92.9 | 0.987 | < 0.0001 |

## Chapter 3. DISCUSSION

Low-contrast detection in screen-film mammography was shown to be optimized by selecting Mo-Mo target-filter combinations for thin to intermediate breasts (under 5 cm) and by selecting Rh-Rh for thick breasts (over 7 cm).[36] With those target-filters, low-contrast detection has been shown to be maximized by picking the lowest kVp that keeps exposure times adequately short (under 2 seconds) for a given breast thickness.[49]

It might be expected that optimization of technique factors in digital mammography would follow similar trends. The use of cesium-iodide as the scintiallation material in digital mammography, instead of gadolinium oxysulfite as used in screen-film mammography, complicates the issue. The two materials have different x-ray attenuation properties and different energy dependences of those attenuation properties. The only way to ensure that technique factors are optimized for detection of low-contrast lesions in digital mammography is to conduct experiments that replicate the clinical situation as closely as possible using the digital detector of interest. That has been done in this study.

Our results indicate that with a CsI scintillator and amorphous silicon detector, it is reasonable to maximize tissue contrast by using a softer x-ray beam (Mo-Mo target-filter and relatively low kVp) for thin breasts. Results comparing digital to screen-film mammography for thin breasts, however, indicate that digital should not be expected to yield superior low-contrast detection to screen-film mammography.

For thick breasts (> 5 cm thick) on the other hand, low-contrast detection is maximized in digital mammography by selecting a harder x-ray beam (Rh-Rh target-filter and kVp values up to 46). This results from the combined effect of decreased breast absorption (and therefore decreased breast dose) for higher energy x-rays in thicker breasts and higher SNR per unit dose for higher energy x-rays.

Our results indicate that technique selection for digital mammography at intermediate breast thicknesses is insensitive to the target-filter and kVp selected. Low-contrast lesion detection showed no clear trends in terms of target-filter or kVp selection for 4 and 6 cm thick breasts, even though SNR increased significantly as kVp increased for each target-filter combination at these intermediate breast thicknesses. This indicates that higher SNR as kVp increases is approximately counterbalanced by the effect of decreased tissue contrast as kVp increases.

Our results can be compared to the results of Williams, et.al., who used different experimental techniques to determine optimal beam spectra for digital mammography.[48] For the GE system, their calculated FOM was approximately constant as a function of kVp for all phantom thicknesses and target-filter combinations. Moreover, the FOM showed no distinction among the 3 different target-filter combinations for 3 cm thick breasts. For 7 cm thick breasts, the FOM indicated preference for Rh-Rh target-filter, but not kVp preference. Their SNR (actually contrast-to-noise ratio) metric indicated that the lowest kVps for each breast thickness yielded the highest SNR. This is because under the condition

of fixed detector signal, SNR decreases due to decreased contrast between target and background tissues as kVp increases. Their SNR calculations suggest that the Mo-Mo target-filter combination (and low kVp) is preferable for 3 cm thick breasts. Their SNR calculations, however, find no distinction among the three target-filter combinations for thicker (7 cm thick) breasts. In short, they get different conclusions depending on whether they use SNR or FOM as their criteria for technique selection.

Our CD results indicate that Mo-Mo and low kVp are preferable for thin breasts, while Rh-Rh and high kVp are preferable for thick breasts.

## Chapter 3. CONCLUSIONS

These results indicate that low-contrast lesion detection was optimized for FFDM under the constraint that MGD was kept constant by using a softer x-ray beam for thin breasts and a harder x-ray beam for thick breasts. Under this constraint, FFDM CD scores were superior to SFM CD scores for all but the thinnest breasts. Under the constraint of constant dose for each breast thickness, a statistically significant trend toward higher signal-to-noise ratios measured by the digital detector at higher kVp values was observed for all but the thinnest breasts.

## Chapter 3. ACKNOWLEDGMENTS

This work was supported in part by the Lynn Sage Comprehensive Breast Center and U.S. Army Medical Research and Materiel Command Award Number: DAMD17 –99-1-9144.

# CHAPTER 4

# PERFORMANCE COMPARISON OF FULL-FIELD DIGITAL MAMMOGRAPHY TO SCREEN-FILM MAMMOGRAPHY IN CLINICAL PRACTICE

## Chapter 4. INTRODUCTION

The first full-field digital mammography system was approved for clinical use by the U.S. Food and Drug Administration on January 28, 2000. During the first year of introduction, approximately 50 full-field digital mammography systems (Senographe 2000D, GE Medical Systems, Wakesha, WI) were installed for clinical use in the U.S. A similar number of FFDM units were installed outside the U.S., primarily in Europe.

While screen-film image receptors have a limited range of acceptable breast dose that is constrained by the requirement of getting adequate optical densities on the processed film, digital mammography has no similar constraint on breast doses. In fact, digital detectors are typically linear over 4-5 decades of exposure to the detector. This opens up the possibility of breast doses from digital mammography that are much higher or much lower than those from screen-film mammography. It also opens up the possibility that image quality on digital may differ from that in screen-film mammography, either due to inherent detector sensitivity differences or due to user-selection of different doses to the breast.[50,51]

During the course of the last year, we have served as MQSA-qualified medical physicists in acceptance testing 18 full-field digital mammography units. During the past 2 years, we have been involved in conducting annual performance evaluations of 38 screen-film units through the Colorado Mammography Advocacy Project (CMAP).[31] During these evaluations of both digital and screen-film units, measurements were made to assess the performance of these clinical systems under automatic exposure control conditions using clinical techniques. In addition to the ACR phantom, breast-equivalent phantoms of 2, 4, 6, and 8 cm thickness have been used to measure exposure times, mean glandular doses, and image quality as assessed by the same contrast-detail pattern for each unit at each breast thickness.[36]

This paper compares acceptance testing of 18 of the first digital mammography systems introduced into clinical practice to annual review of 38 screen-film mammography systems.

## Chapter 4. MATERIALS AND METHODS

Uniform breast-equivalent (50% fibroglandular-50% fatty) materials of 2, 4, 6, and 8 cm compressed breast thicknesses were imaged using each site's clinical techniques. A D-shaped uniform phantom was used, one section of which contained a 9 x 9 contrast-detail pattern for assessment of simulated low-contrast lesions (Figure 4.1).[36] Each row of the CD pattern contained 9 circular objects at a fixed level of contrast with object diameters ranging from 0.25 mm to 4.0 mm. Each of the nine different rows had a different subject contrast, ranging

from 0.3% to 4.0%. In addition, the ACR mammography phantom was used to simulate a 4.5-cm thick compressed breast with test objects of fibers, specks, and masses, as previously described.[21]

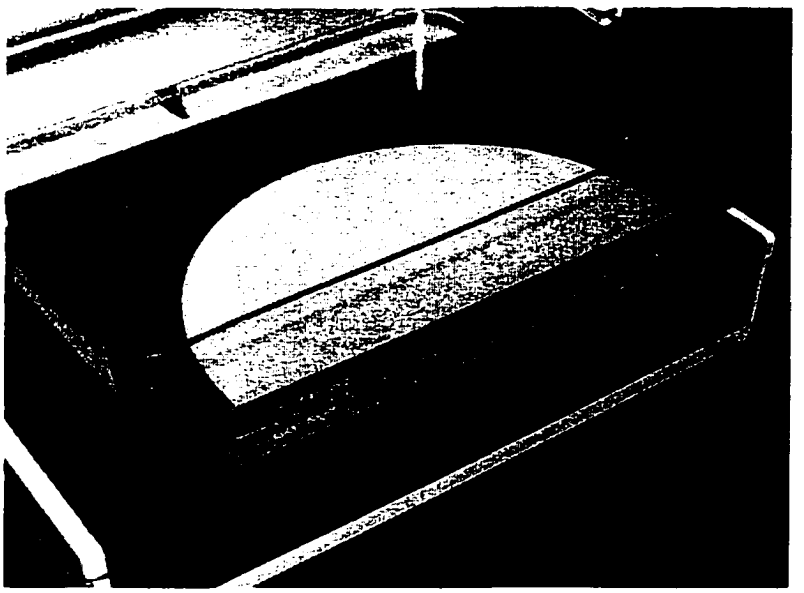

**Figure 4.1.** Contrast-detail phantom.

Automatic exposure control (AEC) was used on 38 screen-film units and compared to the AEC performance of 18 GE Senographe 2000D full-field digital mammography systems. The Senographe 2000D system employs a cesium iodide scintillator coupled to an amorphous silicon diode array.[38] The array has 1920 x 2304 array elements uniformly distributed over a 19.2 x 23.0 cm field of view, each detector element being 100 microns on a side.

The GE Senographe 2000D system can function in one of three AEC (or AOP, for automated optimization of parameters) modes: AOP contrast (CNT), AOP standard (STD), or AOP dose (DOS) mode. In each of these AOP modes, a 14 x 15 cm area of the detector centered left-to-right and near the chest wall of

the full detector is designated as the AOP sensor on the Senographe 2000D system (Figure 4.2).

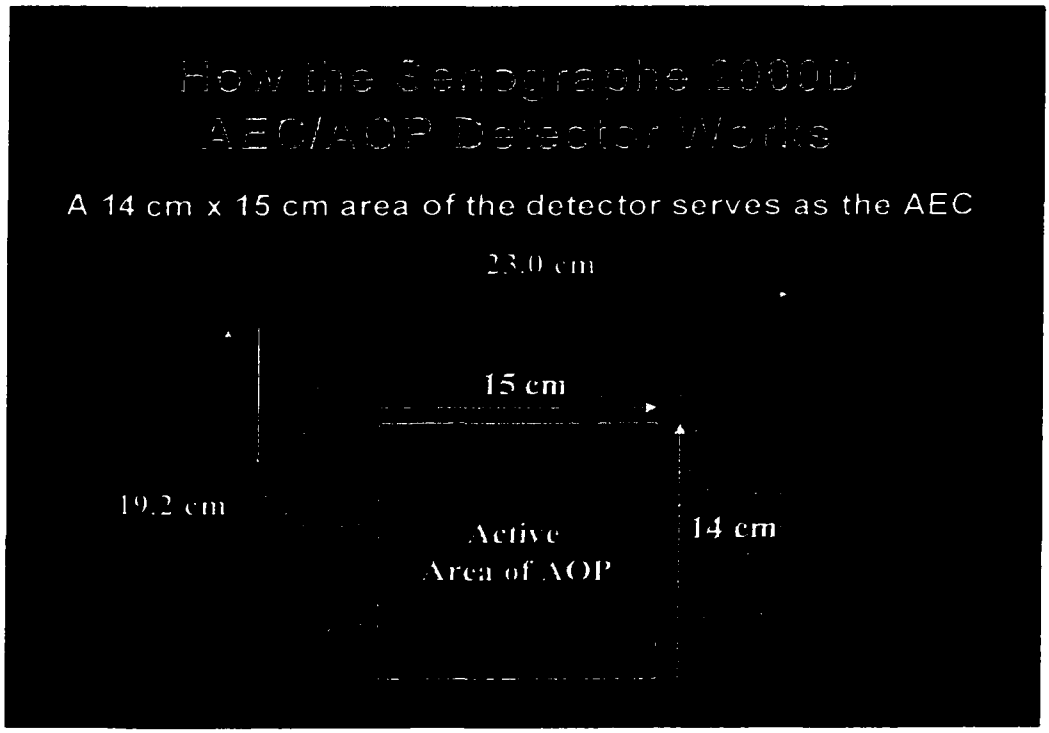


**Figure 4.2.** Schematic of Senographe 2000D AOP System.

During a 15 millisecond pre-exposure, the system takes a preliminary measurement that is used to select the target material (molybdenum or rhodium), filtration material (molybdenum or rhodium), and peak kilovoltage (kVp) setting. During the pre-exposure, the system also selects a 1 x 1 cm sub-region of the 14 x 15 cm AOP detector area that serves as the active AEC sensor during the exposure that follows. The system selects the specific 1 x 1 cm sub-region that records the lowest signal during pre-exposure. The full exposure is terminated when the selected 1 x 1 cm region records an adequate

signal, thereby helping to ensure adequate signal and signal-to-noise ratio to the entire image.

Results for exposure times, mean glandular doses, and CD scores between modalities and among FFDM modes were analyzed for statistical significance using analysis of variance methods (SAS Institute, Seattle, WA). t-tests were used to analyze differences among means and Satterthwaite tests were used to analyze differences in the variances between modalities.

## Chapter 4. RESULTS

Results in terms of exposure times, average glandular doses, and contrast detail scores are shown in Table 4.1 and Figures 4.3-4.5.

**Table 4.1.** Comparison of exposure times, mean glandular doses, and contrast-detail scores for screen-film and digital mammography in each AOP mode at each breast thickness.

| | Screen-film Mammography | Digital Mammography | | |
|---|---|---|---|---|
| | Clinical Technique | AOP Contrast | AOP Standard | AOP Dose |
| **Exposure Time (seconds)** | | | | |
| **2 cm** | 0.16 | 0.24 | 0.19 | 0.16 |
| **4 cm** | 0.72 | 0.85 | 0.54 | 0.49 |
| **6 cm** | 1.61 | 1.09 | 0.79 | 0.74 |
| **8 cm** | 2.91 | 1.69 | 1.69 | 1.70 |
| **Average Glandular Dose (mGy)** | | | | |
| **2 cm** | 0.43 | 0.57 | 0.53 | 0.52 |
| **4 cm** | 1.19 | 1.47 | 1.28 | 1.06 |
| **6 cm** | 2.50 | 1.66 | 1.51 | 1.48 |
| **8 cm** | 4.01 | 3.04 | 3.05 | 3.06 |
| **Contrast-Detail Score** | | | | |
| **2 cm** | 13.7 | 15.4 | 15.2 | 15.2 |
| **4 cm** | 13.4 | 14.6 | 14.3 | 14.1 |
| **6 cm** | 12.3 | 13.0 | 12.9 | 12.8 |
| **8 cm** | 10.6 | 11.8 | 11.9 | 11.9 |

Figure 4.3 demonstrates that exposure times for digital units were within the range of those for screen-film units for 2, 4, and 4.5 cm breast thicknesses, but were shorter on average for digital mammography than for screen-film mammography for 6 and 8 cm thick compressed breasts, regardless of the AOP mode used for digital ($p<0.0001$).

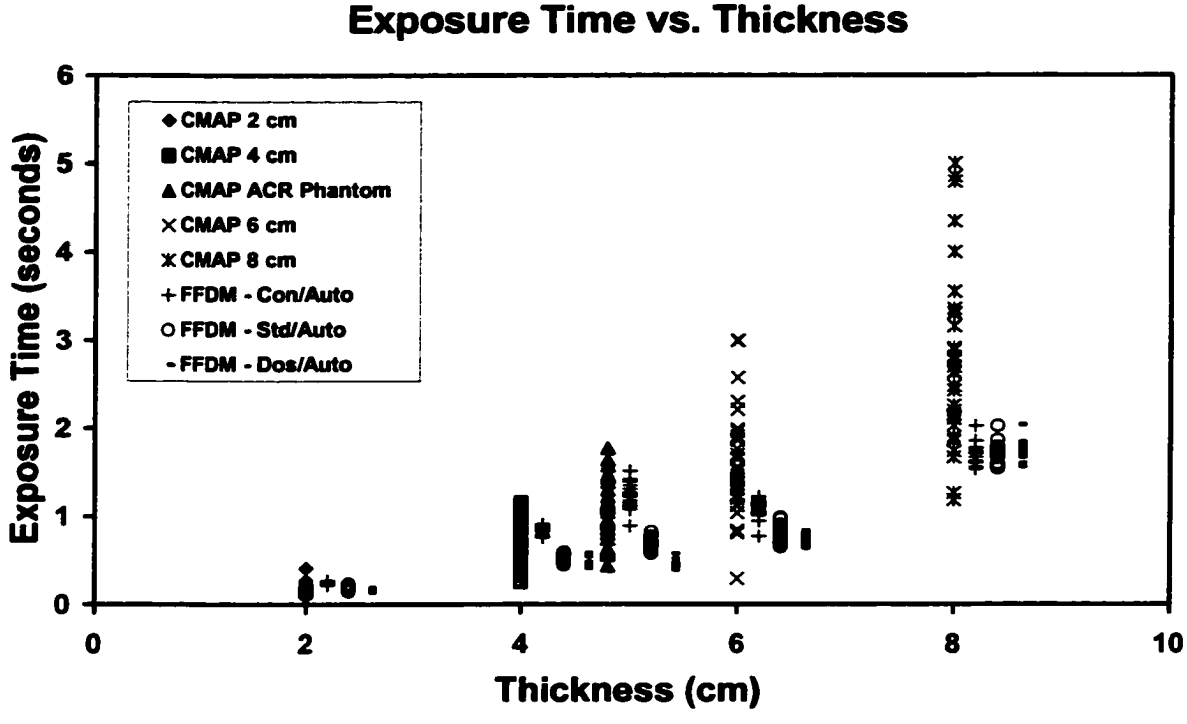


**Figure 4.3.** Exposure time versus compressed breast thickness for 38 screen-film units and 18 digital mammography units in each AOP exposure mode.

Comparison of digital mammography exposure times using different AOP modes indicated that AOP mode selection made a significant difference in exposure times between contrast mode and the other two modes for 2, 4, 4.5, and 6 cm breasts ($p<0.001$), but made no difference for 8 cm breasts ($p>0.9$).

Only for 4.5 cm simulated breasts was there a statistical distinction in exposure times between standard and dose modes ($p<0.001$). The variance in exposure times across all digital mammography units, regardless of AOP mode, was significantly lower than the variance in exposure times across all screen-film units for 2, 4, 6, and 8 cm thick simulated breasts ($p<0.0001$).

Figure 4.4 demonstrates that for 2 cm breasts, mean glandular doses with digital were significantly higher than doses for screen-film, regardless of the digital mode used ($p<0.0001$).

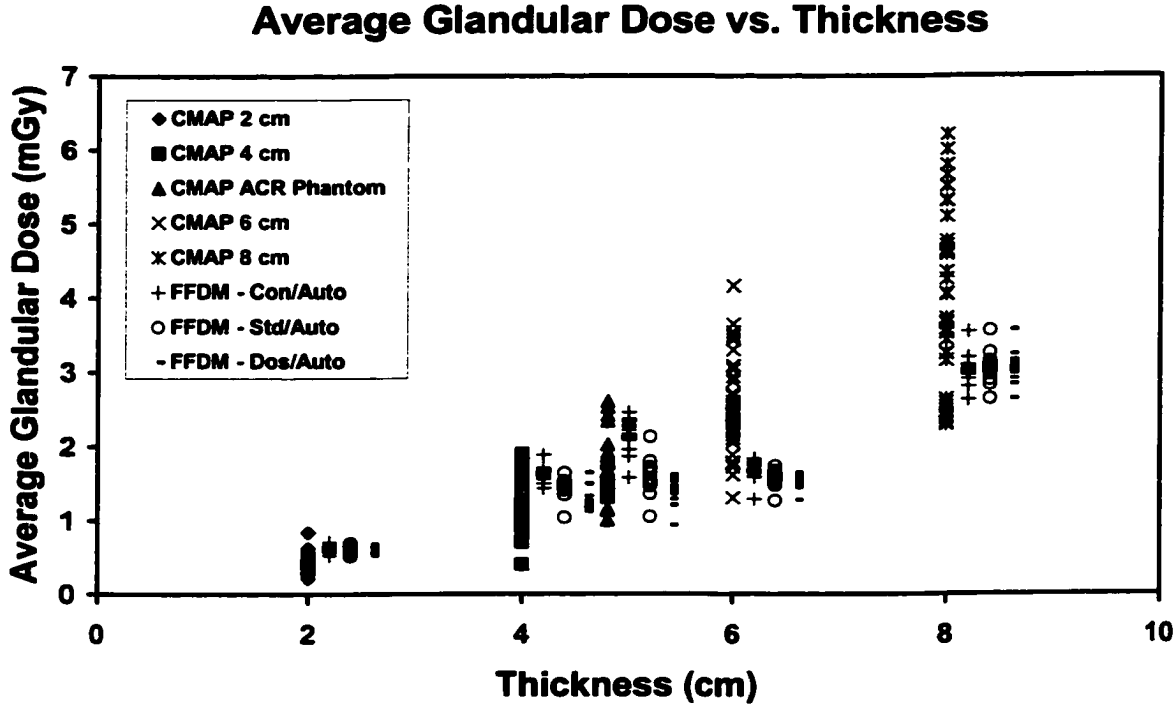


**Figure 4.4.** Average glandular dose versus compressed breast thickness for 38 screen-film units and 18 digital mammography units in each AOP exposure mode.

For 4 cm breasts and the ACR phantom, digital doses in AOP contrast mode were significantly higher than screen-film doses ($p<0.004$), while in AOP standard and dose modes, digital doses were significantly lower than screen-film doses ($p<0.001$). For 6 and 8 cm breasts, digital doses were significantly lower than screen-film, regardless of AOP mode selected ($p<0.0001$). Comparison of breast doses for different digital AOP modes indicated that AOP contrast had significantly higher breast dose than the other two AOP modes for 2-6 cm thick breasts ($p<0.03$). No significant difference in dose was observed between standard and dose modes for 2-6 cm breasts and no difference was found among any mode for 8 cm thick breasts ($p>0.9$). The variance in breast doses from digital mammography for each AOP mode was significantly lower than the variance in breast doses for screen-film mammography for 2, 4, 6, and 8 cm thick simulated breasts ($p<0.0001$).

Figure 4.5 demonstrates contrast-detail scores for both screen-film and digital mammography for 2, 4, 6, and 8 cm breast thicknesses. Results of contrast-detail experiments indicate that for each breast thickness, digital mammography provided better low-contrast lesion detection than screen-film mammography, independent of the AOP mode selected ($p<0.0001$ for 2, 4, and 8 cm, and $p<0.012$ for 6 cm thick breasts). Comparison of digital mammography contrast-detail scores indicated that selection of AOP mode had no significant effect on low-contrast lesion detection for any breast thickness. The variance in contrast-detail scores for digital from each AOP mode was lower than the

variance of contrast-detail scores from screen-film mammography ($p<0.08$ for all comparisons, $p<0.05$ for 9 of 12 comparisons).

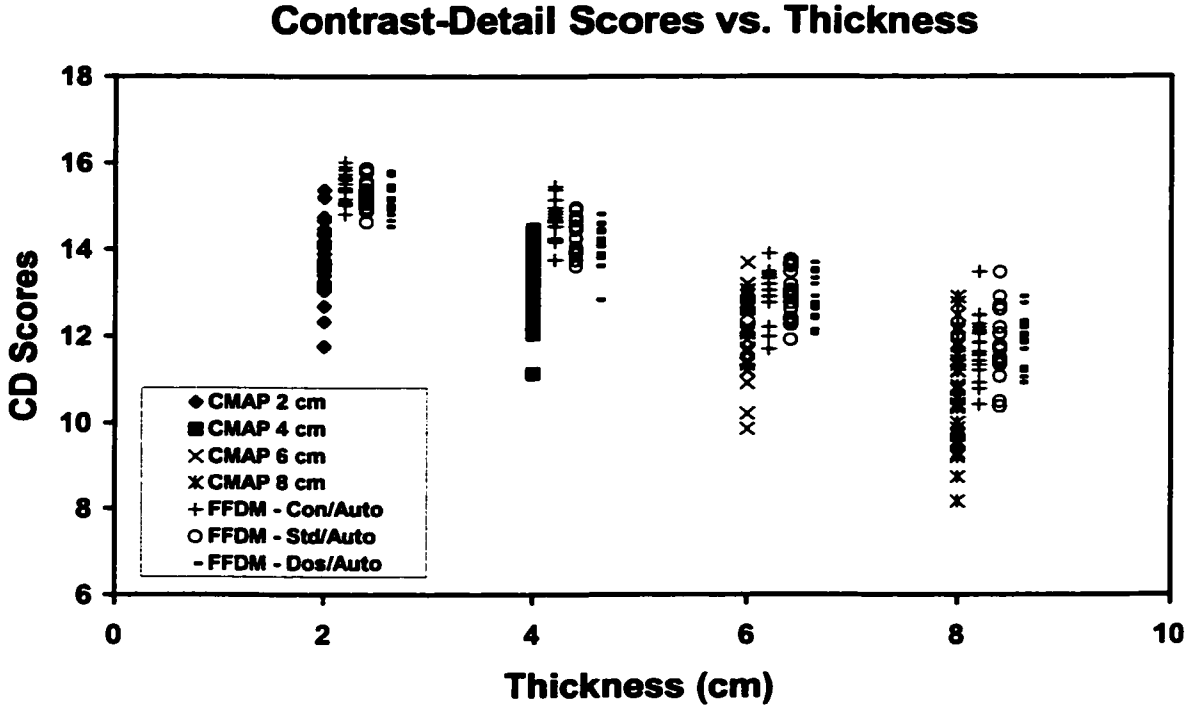


**Figure 4.5.** Contrast detail scores versus compressed breast thickness for 38 screen-film units and 18 digital mammography units in each AOP exposure mode.

Figure 4.6 shows signal-to-noise ratios from digital mammography for 2, 4, 6, and 8 cm breast thicknesses. SNR fell, on average, as breast thickness increased ($p<0.001$). For each breast thickness, measured SNR values had no significant dependence on the digital AOP mode selected ($p>0.2$). For 2 cm AOP-DOS mode, one digital unit had a distinctly lower SNR that the rest (Figure 6). That low SNR value was the result of the unit selecting a higher kVp than

other units for a 2 cm thick breast (28 kVp), resulting in an extremely short exposure time (0.14 s). This led to the presence of residual grid lines in the image, which increased the standard deviation of the signal and decreased the SNR in the resultant image.

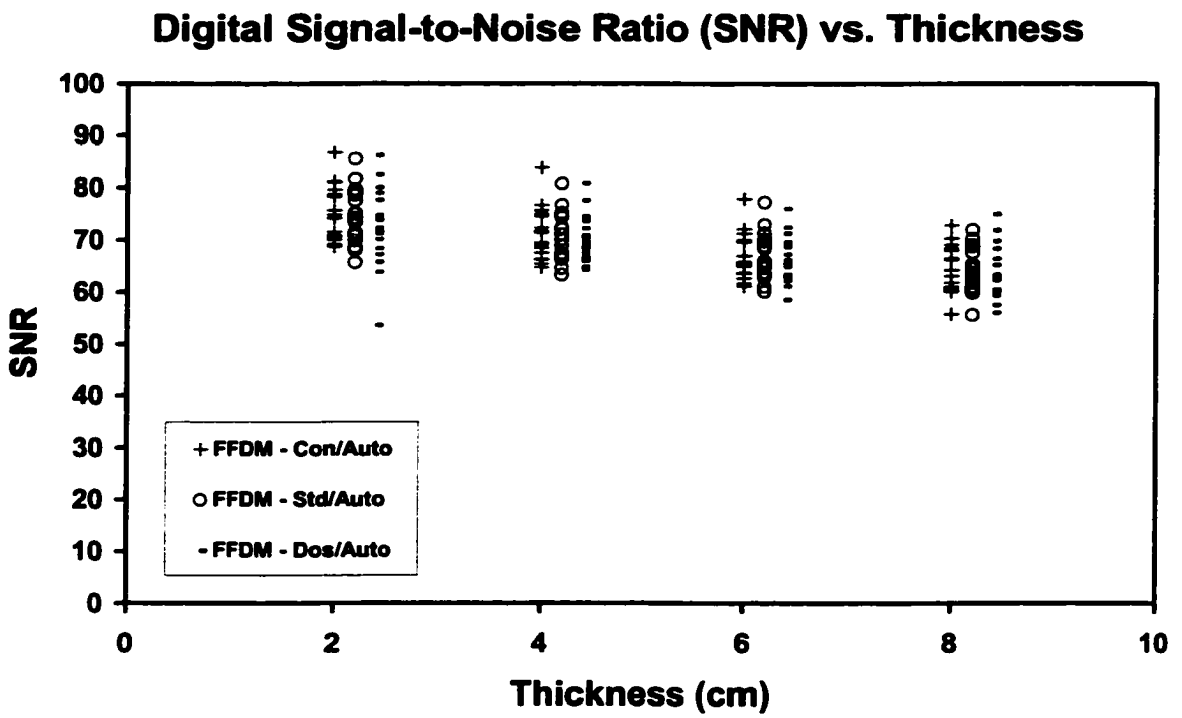


**Figure 4.6.** Signal-to-noise ratios measured at 2, 4, 6,and 8 cm thick compressed breast thicknesses in each AOP mode for 18 digital mammography units.

Finally, Table 4.2 shows typical technique factors and mean exposure results for the 38 screen-film units and the 18 digital mammography units (in AOP standard mode) included in the testing.

**Table 4.2.** Comparison of typical technique factors selected by screen-film and digital mammography systems, along with resulting mean exposure, dose, and image quality measurements.

| | Screen-film Mammography | | | | | Digital Mammography (AOP – Standard Mode) | | | | |
|---|---|---|---|---|---|---|---|---|---|---|
| | 2 cm | 4 cm | ACR Phantom | 6 cm | 8 cm | 2 cm | 4 cm | ACR Phantom | 6 cm | 8 cm |
| Target | Mo | Mo | Mo | Mo | Mo | Mo | Mo | Mo | Rh | Rh |
| Filter | Mo | Mo | Mo | Mo | Mo | Mo | Mo | Rh | Rh | Rh |
| kVp | 25 | 25 | 25 | 28 | 30 | 26 | 28 | 28 | 31 | 32 |
| mAs | 16 | 72 | 102 | 156 | 278 | 19 | 55 | 68 | 59 | 127 |
| Exposure Time (seconds) | 0.16 | 0.72 | 1.05 | 1.61 | 2.91 | 0.19 | 0.54 | 0.70 | 0.79 | 1.69 |
| HVL (mm Al) | 0.33 | 0.33 | 0.34 | 0.38 | 0.41 | 0.35 | 0.37 | 0.44 | 0.48 | 0.49 |
| Average Glandular Dose (mGy) | 0.43 | 1.19 | 1.68 | 2.50 | 4.01 | 0.53 | 1.28 | 1.50 | 1.51 | 3.05 |
| Optical Density | 1.53 | 1.63 | 1.56 | 1.64 | 1.55 | ** | ** | ** | ** | ** |
| Contrast-Detail Scores | 13.7 | 13.4 | ** | 12.3 | 10.6 | 15.2 | 14.3 | ** | 12.9 | 11.9 |
| SNR | ** | ** | ** | ** | ** | 74 | 71 | ** | 67 | 64 |

## Chapter 4. DISCUSSION

Results comparing exposure times and mean glandular doses for digital and screen-film mammography allay some possible concerns about the performance of digital mammography. For thicker breasts, where longer exposure times and higher breast doses are a potential concern, digital mammography performed better than screen-film mammography. Even for 8 cm breasts, where 82% of screen-film units yielded exposure times over 2 seconds (mean exposure time: 2.9 s), digital mammography consistently produced exposure times under 2 seconds (mean exposure time: 1.7 s). This reduction in exposure time is important in reducing motion artifacts on mammograms.

For 8 cm thick breasts, mean glandular doses averaged 3.05 mGy for AOP-STD mode digital and 4.11 mGy for screen-film; 81% of screen-film units had doses higher than 3.05 mGy. At the same time, contrast-detail scores were higher for digital (mean CD score: 11.9) than for screen-film (mean CD score: 10.6) for 8 cm thick breasts.

Table 4.2 illustrates the main reason for shorter exposure times and lower breast doses for thicker breasts on digital mammography. The table indicates that the digital AOP-STD mode picked a more penetrating beam quality for each breast thickness, with the difference increasing as breast thickness increased. For example, for 6 cm breasts, the mean half-value layer (HVL) selected by screen-film systems was 0.38 mm of aluminum, compared to a mean HVL of 0.48 mm of aluminum for digital. The price that might be paid for a harder x-ray beam is lower subject contract and image contrast. The effect of lower image

contrast in digital mammography is offset by the higher detector signal and signal-to-noise ratio for the harder x-ray beam, due to the projection of more visible light photons per x-ray absorbed in the digital detector, plus the ability to adjust display window width to enhance contrast in the displayed digital image. As the results for thicker breasts indicate, the use of a harder x-ray beam reduces exposure time and breast dose without compromising low-contrast lesion detection.

Our results indicate that digital mammography had significantly reduced variances in exposure times and mean glandular doses, along with reduced variance in contrast-detail scores, compared to screen-film mammography at each breast thickness. Factors in the greater variability of screen-film image receptor sensitivities are the variability of system speed caused by the use of different screen-film combinations, different resultant film optical densities (ODs), and different film processing conditions. For example, among the 38 screen-film units, film ODs for the ACR phantom ranged from 1.14 to 1.90 and for 6 cm breast equivalent material from 0.61 to 2.37. The high degree of variability among mammography film processing systems has been well documented.[35,52] Digital detectors eliminate target OD variability and processing variability, substituting the variability of detector sensitivity in its place.

The measured variability of digital detector AEC performance was considerably lower than for screen-film image receptors. One mitigating factor is that all digital mammography data presented here was for initial acceptance of digital systems. Subsequent surveys of digital mammography equipment will be

needed to see if the trend of reduced variability in exposure time, mean glandular dose, and contrast-detail scores will continue as the installed base of digital mammography systems ages and as other manufacturers enter the digital mammography marketplace.

## Chapter 4. CONCLUSIONS

Digital mammography systems had similar exposure times and breast doses to screen-film mammography for thin to intermediate breasts, but resulted in shorter exposure times and lower mean glandular doses, on average, for thicker breasts. For all breast thicknesses, digital mammography had better detection of low-contrast simulated lesions, on average, than screen-film mammography. Digital mammography also demonstrated less variance than screen-film mammography in exposure times, mean glandular doses, and contrast-detail scores. These results indicate that clinical use of digital mammography may improve image quality for equal or lower breast doses, while providing tighter control over exposures and image quality than screen-film mammography.

## Chapter 4. ACKNOWLEDGMENTS

This work was supported in part by the Lynn Sage Comprehensive Breast Center.

## REFERENCES


1. Salomon A. Beitrage zur pathologie und klinik der mammacarcinome. Arch Klin Chir 1913; 101: 573-668.

2. Leborgne RA. Diagnosis of Tumors of the Breast by Simple Roentgenology. American Journal of Roentgenology and Radium Therapy. 1951; 65:1-11.

3. Leborgne RA. The Breast in Roentgen Diagnosis. Montevideo, Uruguay: Impresora Uruguaya, 1953.

4. Egan RL. Experience with mammography in a tumor institution: evaluation of 1000 cases. Radiology. 1960; 75: 894-900.

5. Gros CM. Methodologie: Symposium Sur Le Sein. Journal of Radiol Electrol Med Nucl. 1967; 48:638-655.

6. Sickles EA, Doi K, Genant HK. Magnification Film Mammography: Image Quality and Clinical Studies. Radiology. 1977; 125: 69-76.

7. Haus AG, Paulus DD, Dodd GD, Coward RW, Bencomo J. Magnification Mammography: Evaluation of Screen-Film and Xeroradiographic Techniques. Radiology. 1979; 133: 223-226.

8. Price JL, Butler, PD. The Reduction of Radiation and Exposure Time in Mammography. British Journal of Radiology. 1970; 43:251-255.

9. Ostrum BJ, Becker W; Israd HJ. Low-Dose Mammography. Radiology. 1973; 109:323-326.

10. Weiss JP, Wayrynen RE. Imaging System for Low-Dose Mammography. Journal of Applied Photographic Engineering. 1976; 2:7-10.

11. Buchanan RA, Finkelstein SI, Wickersheim KA. X-ray Exposure Reduction Using Rare Earth Oxysulfide Intensifying Screens. Radiology. 1976; 118: 183-188.

12. Haus AG. Technologic Improvements in Screen-Film Mammography. Radiology. 1990; 174;628-637.

13. Conway BJ, McCrohan JL, Reuter FG, Suleiman OH. Mammography in the 80s. Radiology. 1990; 177:335-339.

14. Mees CE, James TH. The Theory of the Photographic Process. New York: Macmillan, 1966.

15. Russell HD. Rapid Processing of X-ray Film. Photographic Science and Engineering. 1959; 3:32-34.

16. Reuter FG. Preliminary Report: NEXT-85. In: National Conference on Radiation Control: Proceedings of the 18th Annual Conference of Radiation Control Program Directors. CRCPD Publication 86-2. Charlseton, W. Va: CRCPD 1986; 111-120.

17. Galkin BM, Feig SA, Muir HD. The Technical Quality of Mammography in Centers Participating in a Regional Breast Cancer Awareness Program. Radiographics 1988; 8:133-145.

18. McLelland R. Gray JE, McCrohan J, et al: ACR Mammography Quality Control Manuals. Reston, VA., American College of Radiology. 1990.

19. American College of Radiology. Mammography Quality Control. Reston, VA: American College of Radiolgoy; 1992.

20. American College of Radiology. Mammography Quality Control Manual – Revised Edition, 1994. Reston, VA: American College of Radiolgoy; 1994.

21. American College of Radiology. Mammography Quality Control Manual. Reston, VA: American College of Radiolgoy; 1999.

22. Mammography Facilities-Requirements for Accrediting Bodies and Quality Standards and Certification Requirements; Part VII. Interim Rules, 21 CFR Part 900. Federal Register. 1993

23. Quality Mammography Stands; Final Rule. Part II. 21 CFR Part 16 and 900. Federal Register. 1997

24. National Council on Radiation Protection and Measurements. Mammography – A User's Guide. Report No. 85. 1986.

25. Bassett LW, Hendrick RE, Bassford TL, et al. Quality Determinants of Mammography. Clinical Practice Guideline No. 13. AHCPR Publication No. 95-0632. Rockville, MD: Agency for Health Care Policy and Research, Public Health Service, U.S. Department of Health and Human Services. October 1994.

26. Lewin JM, Hendrick RE, D'Orsi CJ, et al. Comparison of Full-Field Digital Mammography with Screen-Film Mammography for Cancer Detection: Results of 4,945 Paired Examinations. Radiology. 2001; 218:873-880

27. Gold HR. The Evolution of Mammography. Radiologic Clinics of North America: Breast Imaging. Lawrence W. Bassett, ed., Philadelphia: WB Saunders Co., Volume 30, Number 1, p. 1-19, 1992.

28. Bassett LW, Gold RH, Kimme-Smith C. History of the Technical Development of Mammography. RSNA AAPM Syllabus on Technical Aspects of Breast Imaging. Third Edition. 1994.

29. Houn F, Elliott ML, McCrohan JL. The Mammography Quality Standards Act of 1992. Radiologic Clinics of North America: Breast Imagin. Philadelphia: WB Saunders Co., Volume 33, Number 6, p. 1059-1065. 1995.

30. Hendrick RE. Quality Assurance in Mammography. Radiologic Clinics of North America: Breast Imaging. Lawrence W. Bassett, ed., Philadelphia: WB Saunders Co., Volume 30, Number 1, p. 243-255, 1992.

31. Hendrick RE, Chrvala CA, Plott CA, Wilcox-Buchalla P, Jessop N, Cutter GA. Improvement in Mammography Quality Control, 1987-1995. Radiology 207: 663-668,1998.

32. ACR Standards for the Performance of Screening Mammography, American College of Radiology, 1990.

33. Hendrick RE, Bassett LW, Botsco MA, Butler PA, Dodd GD, et. Al., Mammography Quality Control Manual. American College of Radiology. First Edition 1990.

34. United States Federal Register. Mammography facilities: requirements for accrediting bodies and quality standards and certification requirements. No. 243, December 21, 1993; 58: 67558-67572.

35. Hendrick RE, Berns EA. Optimizing the selection of film and film processing in screen-film imaging. In Advances in Film Processing Systems, Technology, and Quality Control in Medical Imaging. Arthur G. Haus, ed. Madison, WI: Medical Physics Publishing, p. 115-128, 2001.

36. Hendrick RE, Berns EA. Optimizing techniques in screen-film mammography. In Radiologic Clinics of North America: Breast Imaging.Stephen A. Feig, ed., Philadelphia: WB Saunders Co., Volume 38, Number 4, p. 701-718, 2000.

37. Wu X, Gingold EL, Barnes GT, Tucker DM. Normalized average glandular dose in molybdenum target-rhodium filter and rhodium target-rhodium filter mammography. Radiology. 1994; 193:83-89.

38. Sobol WT, Wu X. Parameterization of mammography normalized average glandular dose tables. Medical Physics 24 (4), April 1997.

39. Suleiman OH, Spelic DC, McCrohan JL, Symonds GR, Houn F. Mammography in the 1990s: The United States and Canada. Radiology. 1999; 210:345-351.

40. Hendrick RE. Standardization of image quality and dose in mammography. Radiology 174: 648-654; 1990.

41. Fletcher SW, Black W, Harris R, Rimer BK, Shapiro. Report of the International Workshop of Screening for Breast Cancer. JNCI 1993; 85:1644-56.

42. Elwood JM, Cox B, Richardson AK. The effectiveness of breast cancer screening by mammography in younger women. Online Journal Curr Clin Trials 1993; 1:32-227.

43. Bird RE, Wallace TW, Yankaskas BC. Analysis of cancers missed at screening mammography. Radiology 1992; 184:613-7.

44. Nishsikawa RM, Mawdsley GE, Fenster A, Yaffe MJ. Scanned-projection digital mammography. Med Phys 1987; 14:717-727.

45. Fahrig R. Yaffe MJ. Optimization of spectral shape in digital mammography: dependence on anode material, breast thickness, and lesion type. Medical Physics. 21(9): 1473-81, 1994 Sep.

46. Fahrig R. Yaffe MJ. A model for optimization of spectral shape in digital mammography. Medical Physics. 21(9):1473-81, 1994 Sep.

47. Court LE. Speller R. A multiparameter optimization of digital mammography. Physics in Medicine & Biology. 40(11): 1841-61, 1995 Nov.

48. Williams MB, More MJ, Venkatakkrishnan V, et al. Beam Optimization for Digital Mammography. IWDM 5th International Workshop on Digital Mammography. Medical Physics Publishing . 2001. p. 108-119.

49. Hendrick RE, Berns EB. Optimizing Mammographic Techniques. RSNA AAPM syllabus on technological innovation in breast imaging - 1999.

50. Vedantham S, Karellas A, Suryanarayanan S, Albagli D, Han S, Tkaczyk E, Landberg CE, Opsahl-Ong B, Granfors PR, Levis I, D'Orsi CJ, Hendrick RE. Full-breast digital mammography with an amorphous silicon-based flat panel detector: physical characteristics of a clinical prototype. Medical Physics 27: 558-567, 2000.

51. Lewin JM, Hendrick RE, D'Orsi CJ, Isaacs PK, Moss LJ, et.al. Comparison of full-field digital mammography with screen-film mammography for cancer detection: results of 4,945 paired examinations. Radiology 2001; 218: 873-880.

52. Haus AG, Jaskulski SM. The basics of film processing in medical imaging. Madison, WI: Medical Physics Publishing Co., 1997.